Regulated expression of

Down Syndrome Cell Adhesion Molecule

controls precise synaptic targeting

by

Vedrana Cvetkovska

Integrated Program in Neuroscience

McGill University, Montréal

April, 2014

A thesis submitted to McGill University in partial fulfilment of the requirements

of the degree of Doctor of Philosophy

Abstract

Neurons are organized in functional circuits to allow an organism to perform complex behaviors. The mechanisms that dictate self-assembly of hard-wired neuronal circuits during development are still poorly understood. How are neurons able to distinguish correct from incorrect synaptic targets when they are faced with thousands of possible partners? To address this question, my dissertation explores the molecular mechanisms that regulate synaptic specificity in a hard-wired neuronal circuit of the model organism *Drosophila melanogaster*. I describe a method that allows combined structural and functional analysis of axonal targeting in single identifiable sensory neurons. This method is used to demonstrate that elevated levels of Down Syndrome Cell Adhesion Molecule, due to gene triplication or due to loss of regulation by Fragile X Mental Retardation Protein, perturbs the fine-scale connectivity of single sensory neurons and results in impaired circuit function and behavioral response to sensory stimuli. Single cell analysis of identified sensory neurons also allows for determining the molecular wiring code of a neuron. Using an RNA interference screen for genes involved in axonal targeting, I identified Teneurin-m as a cell surface receptor required for proper axonal branch targeting. I characterized stereotyped miswiring that occurs due to loss of Teneurin-m expression and the behavioral consequences of these synaptic targeting errors. The experiments presented here support the model that tightly regulated expression of genetically-encoded wiring instructions in the form of cell surface molecules determine the precise connectivity of single neurons in hard-wired circuits. Advancing our knowledge of the basic mechanisms of neural circuit formation may help us understand how genetic variation contributes to altered neuronal connectivity in human neurodevelopmental disorders.

Résumé

Les neurones sont organisés en circuits fonctionnels pour permettre aux organismes d'effectuer des comportements complexes. Cependant, les mécanismes qui gouvernent l'assemblée des circuits neuronaux durant le développement sont à ce jour peu compris. Comment les neurones peuvent-ils faire la distinction entre une cible synaptique adéquate et inadéquate lorsqu'ils font face à des milliers de partenaires synaptiques potentiels? Pour répondre à cette question, ma dissertation explore les mécanismes moléculaires qui régulent la spécificité synaptique des circuits neuronaux de l'organisme modèle *Drosophila melanogaster*. J'y décris un modèle à l'aide de neurones sensoriels identifiés qui permet l'analyse combinée structurelle et fonctionnelle de l'embranchement axonal ciblé. Cette méthode est utilisée pour démontrer qu'un niveau élevé de Down Syndrome Cell Adhesion Molecule (Dscam), qui peut être le résultat de trois copies du gène Dscam ou de la perte de régulation par le Fragile X Mental Retardation Protein, perturbe la connectivité de fins embranchements neuronaux sensoriels et résulte en une déficience des circuits fonctionnels ainsi qu'en réponses comportementales non appropriées lors de la stimulation sensorielle. L'analyse combinée structurale et fonctionnelle de cellule identifiée permet aussi d'établir le code d'embranchement moléculaire de neurones. En utilisant de criblage par ARN interférent pour des gènes qui régulent un embranchement axonal ciblé, j'y identifie Teneurin-m comme un récepteur de surface cellulaire nécessaire pour l'embranchement axonal ciblé. J'y caractérise les défauts de connexion stéréotypés qui surviennent lors de la perte d'expression de Teneurin-m et les conséquences comportementales de ces erreurs de ciblage synaptiques. Les expériences présentées dans cette dissertation supportent un modèle qui régule de façon fiable l'expression d'instructions d'embranchement

génétiquement encodées, c'est-à-dire que les molécules en surface des cellules déterminent la connectivité précise de neurones à l'intérieur des circuits d'embranchement. L'avancement de nos connaissances sur les mécanismes de base de formation des circuits neuronaux pourrait nous aider à comprendre comment la variation génétique contribue à la connectivité neuronale altérée lors de désordres humains neuro-développementaux.

Acknowledgements

My career accomplishments and science education would not have resulted in this thesis if not for my graduate supervisor Dr. Brian Chen, who guided me through this adventure. My gratitude also goes to my advisory committee members Dr. Don van Meyel and Dr. Keith Murai for their continuous help and encouragement.

I would like to thank all my colleagues at the Centre for Research in Neuroscience, especially for their patience when I was a fresh grad student in a new lab borrowing their equipment and using their microscopes. Many thanks to members of the van Meyel and Rao labs for sharing fly stocks and genetics advice. I am also thankful to Ariane Gagnon for helping me with the translation of the abstract.

Having spent many days, nights and weekends in the Chen lab, it would not have been such a positive experience if not for past and present members of the lab. Many people come to mind, but I would like to especially acknowledge Alexa Hibbert for being a great friend and co-author, and Dr. Farida Emran for providing a wealth of practical help and a drive to accomplish more.

A special thank you goes to one of my best friends, partner in crime, and co-author Ibrahim Kays, who shared a lot more than his enzyme aliquots with me.

My gratitude for funding my studies goes to the Integrated Program in Neuroscience, the Research Institute of the McGill University Health Centre, and to the Sievers family for their generous contribution.

To my parents Biljana and Cvetan, and my sisters Marina and Sara, and my feline companion Hiro, for your unconditional love and support I dedicate this thesis to you.

Contribution of authors

This thesis is presented in a manuscript-based format in accordance with the guidelines from McGill University Graduate and Postdoctoral Studies. It comprises original work from two published manuscripts and one that is in preparation.

A modified version of **Chapter 1 section 1.6** and **Chapter 2** has been published as:

Kays I*, **Cvetkovska V***, Chen BE (2014) Structural and functional analysis of single sensory neurons in *Drosophila melanogaster* using lipophilic dye labeling and behavior for hard-wired neural connectivity analysis. *Nature Protocols.* 9: 1-14.

Brian E. Chen supervised the project. Ibrahim Kays and Vedrana Cvetkovska contributed equally to this work. Specifically, dye filling experiments were performed by I. Kays and V. Cvetkovska. Behavioral experiments were performed by V. Cvetkovska. Data analysis was performed by I. Kays and V. Cvetkovska. The figures were made by V. Cvetkovska with assistance from I. Kays and suggestions from B.E. Chen. The manuscript text was written by B. E. Chen, I. Kays and V. Cvetkovska.

A modified version of **Chapter 3** has been published as:

Cvetkovska V*, Hibbert AD*, Emran F, Chen BE (2013) Overexpression of Down Syndrome Cell Adhesion Molecule impairs precise synaptic targeting. *Nature Neuroscience*, 16: 677-682.

Brian E. Chen designed the experiments and supervised the project. Vedrana Cvetkovska and Alexa D. Hibbert contributed equally to this work**.** V. Cvetkovska, A.D. Hibbert and Farida Emran performed the experiments. Specifically, immunoprecipitation and Western blots were performed by V. Cvetkovska and F. Emran. Cryosections and fluorescent in situ hybridization were performed by F. Emran, immunohistochemistry was performed by V. Cvetkovska. Dye filling experiments were performed by V. Cvetkovska and A.D. Hibbert. Behavioral experiments were performed by V. Cvetkovska. qPCR was performed by Tsung-Jung Lin, who also helped prepare pyrosequencing samples. Pyrosequencing was performed with assistance from Alfredo Staffa from the Génome Québec Massively Parallel Sequencing Unit. Data analysis was performed by V. Cvetkovska, A.D. Hibbert and B.E. Chen. The figures were made by V. Cvetkovska and B.E. Chen. The manuscript text was written by V. Cvetkovska, F. Emran and B.E. Chen.

A modified version of **Chapter 4** is in preparation for publication:

Cvetkovska V, Chen BE (2014) Teneurin-m regulates precise synaptic targeting in *Drosophila* mechanosensory neurons, *in preparation*

Vedrana Cvetkovska and Brian E. Chen designed the experiments. V. Cvetkovska collected and analyzed all the data. V. Cvetkovska drafted a version of the manuscript.

Table of contents

List of figures

Chapter 3

Chapter 4

List of abbreviations

Acj6	abnormal chemosensory jump 6
aDc	anterior dorsocentral
ANOVA	analysis of variance
aNp	anterior notopleural
aPa	anterior postalar
aSa	anterior supraalar
aSc	anterior scutellar
BAC	bacterial artificial chromosome
brat	brain tumor
CO_2	carbon dioxide
CNS	central nervous system
CT	cycle threshold
ddH_2O	double distilled water
DiD	1,1′-dioctadecyl-3,3,3′,3′-tetramethylindodicarbocyanine, 4-chlorobenzenesulfonate salt
DiI	1,1′-dioctadecyl-3,3,3′,3′-tetramethylindocarbocyanine perchlorate
DiO	3,3′-dioctadecyloxacarbocyanine perchlorate
DMF	dimethylformamide
Dscam	Down Syndrome Cell Adhesion Protein
Dscam-L1	Down Syndrome Cell Adhesion Protein-Like1
dsRNA	double stranded ribonucleic acid
Dock	dreadlocks
dSema1a	*Drosophila* Semaphorin 1a

dSema2a	*Drosophila* Semaphorin 2a
dSema5c	*Drosophila* Semaphorin 5c
EGF	Epidermal growth factor
ELAV	embryonic lethal abnormal vision
Fas2	Fasciclin2
Fas3	Fasciclin3
Fmr1	Fragile X Mental Retardation 1
FMRP	Fragile X Mental Retardation Protein
Hu	humoral
IP	immunoprecipitation
LRRTM	leucine-rich repeat transmembrane neuronal
mRNA	messenger ribonucleic acid
MARCM	Mosaic analysis with a repressible cell marker
MBD1	methyl CpG binding domain protein 1
Pak1	p21 protein-activated kinase 1
PBS	phosphate buffered saline
PCR	polymerase chain reaction
pDc	posterior dorsocentral
Pea3	polyoma enhancer activator 3
PKA	protein kinase A
PlexA	PlexinA
PlexB	PlexinB
pNp	posterior notopleural
pPa	posterior postalar
Ps	presutral

pSa	posterior supraalar
pSc	posterior scutellar
Repo	reversed polarity
RNA	ribonucleic acid
RNAi	ribonucleic acid interference
Rp49	Ribosomal protein 49
RT-PCR	reverse transcription- polymerase chain reaction
Sema6A	Semaphorin 6A
Sema3E	Semaphorin 3E
SH3	Src-homology 3
Ten-m	Teneurin major
Ten-a	Teneurin accessory
UAS	upstream activating sequence
YD	tyrosine-aspartate
Zic-1	Zic family member 1

Chapter 1

Mechanisms of synaptic specificity:

relevant background and thesis introduction

1.1 Abstract

Billions of neurons in the human brain form hundreds of trillions of synaptic connections to organize the brain into functional circuits. The precision with which such organization is achieved during brain development is a longstanding puzzle in neuroscience. Many circuits self-assemble without the necessity of coordinated neuronal activity, which suggests that cell-specific wiring instructions are encoded in the genome. This chapter summarizes important findings on the mechanisms of synaptic target selection, focusing on the role of cell surface molecules and the utility of hard-wired circuits in the study of neuronal wiring.

1.2 Molecular mechanisms of synaptic specificity

The incredible precision with which synaptic connections are made between neurons to form a functional circuit is conceptually challenging to grasp. During development neurons form selective contacts with synaptic partners when they may be faced with billions of potential choices. It is thought that the controlled expression of genes encoding neural wiring molecules underlies precise circuit formation. Synaptic targeting was first described by Roger Sperry's chemo-affinity hypothesis, which states that the chemical affinity between a specific receptor on one neuron and its corresponding ligand on a second neuron determines the specificity of the connection formed by the two cells (Sperry, 1963). In this model the expression of these instructive molecules in individual neurons must be tightly regulated both temporally and spatially to ensure proper circuit development. Furthermore, sufficient molecular specificity must be encoded to impart neurons and axons with a distinct identity to allow them to find their precise synaptic partners. The specificity requirement raises an important consideration that

Sperry himself recognized early on: there is a statistical improbability that ~20,000 protein-coding genes in the human genome could individually tag a billion neurons, let alone trillions of synapses. Therefore, it is generally accepted that several mechanisms must exist concomitantly to faithfully wire a brain.

The contributions of guidepost cells, cellular scaffolds, and activity-dependent circuit development are outside the scope of this dissertation, and details can be found elsewhere (Palka et al., 1992; Chotard and Salecker, 2004; Katz and Shatz, 1996). The concept of electrical activity shaping neural connectivity during development was demonstrated in seminal work by David Hubel and Torsten Wiesel, showing that early postnatal visual experience shapes ocular dominance column organization in the cat visual cortex (Hubel and Wiesel, 1965; 1970). Prior to sensory experience, spontaneous neural activity in the retina and visual cortex of cat, rodent, and primate embryos contributes to early visual circuit refinement (Katz, 1993; Katz and Shatz, 1996; Blankenship and Feller, 2010). In these activity-dependent systems it is thought that activity-independent molecular cues produce a preliminary imprecise wiring pattern, while spontaneous and experience-driven activity refines the circuit by strengthening appropriate connections and eliminating inappropriate ones. This plasticity of synaptic connections persists throughout life and enables complex and adaptive behaviors such as learning and memory (Kolb and Whishaw, 1998). Nevertheless, while flexibility is generally advantageous, many systems must form extremely precise invariant connections, such as reflex behaviors, and must therefore assemble without activity-dependent mechanisms (see section 1.5 below).

Synaptic targeting is a term that encompasses several levels of decision-making by a neuron (**Figure 1.1**) (Williams et al., 2010). First, a neuron must target its neuronal processes into a general target area. Some examples are the growth of axons to a specific brain region, or

the convergence of inputs into defined layers or laminae. Many brain structures have a laminar organization and neuronal processes of distinct sub-populations of neurons can terminate into specific layers while bypassing others. Once a neuronal process reaches a general target area, it must make choices to contact specific neurons depending on the circuit required. Finally, upon target recognition a decision is made whether to form a functional synapse. The chemo-affinity hypothesis proposes that a major mechanism for how neurons can distinguish between a correct and incorrect synaptic target is through the specific interactions between cell surface receptors (Yamagata et al., 2003; Shen, 2004; Shen and Scheiffele, 2010). In the next section I will describe some of the evidence that cell surface receptors of several classes can instruct synaptic specificity and that they could address the requirements of highly specific recognition and diversity.

1.3 Cell surface receptors in synaptic target recognition

The primary function of neurons is processing of information. Therefore they must be able to sense their environment, communicate and organize with other cells. Neurons use cell surface receptors to perform numerous functions, such as receiving neurochemical signals, sensing molecular cues for guidance of growing axons, fasciculation into nerve bundles and tracts, formation of stable contacts with other neurons and glia, and assuring the integrity of synapses (Shapiro et al., 2007). The most investigated candidates for synaptic target selection have been cell surface molecules that mediate cell adhesion and axon guidance molecules that affect targeting through the cytoskeleton.

Cell adhesion molecules

Cell adhesion is a basic property of all cells. Processes such as cell migration and tissue organization depend on interactions between proteins coating cell surfaces and the external environment (Gumbiner, 1996). Neurons use cell adhesion for versatile functions in nearly all stages of development. For example during axon guidance, neuronal cell adhesion molecules guide growing axons through interactions with the extracellular matrix, promote axon growth, and regulate the bundling or fasciculation of axons (Chiba and Keshishian, 1996; Kamiguchi, 2007). Because of their ability to form highly specific interactions homo- and heterophilically many studies have investigated cell adhesion molecules as targeting molecules.

Cell adhesion molecules belong to numerous families and classes however they all share a general structure. They are transmembrane proteins that bind their ligands through specialized extracellular domains, and engage in downstream signaling on their intracellular side (Shapiro et al., 2007). For initial target recognition cells could present and receive the same signal to inform them of contacting a correct target. In this scenario homophilic binding between like proteins could represent a simple model of achieving specificity, and in fact homophilic matching between cell adhesion molecules belonging to the immunoglobulin superfamily, the cadherin family and leucine-rich repeat cell adhesion proteins, has been shown in vertebrate and invertebrate systems. For example, laminar targeting in the chick retina is regulated by matching immunoglobulin cell surface molecules. The retina has a layered organization with two synaptic layers, the outer and inner plexiform layer. The inner plexiform layer is further divided into sublaminae, where subsets of interneurons synapse with retinal ganglion cells. It has been shown that correct inner plexiform layer targeting involves the homophilic binding of immunoglobulin Dscam, Dscam-L1, Sidekick-1, Sidekick-2 and contactin proteins expressed in non-overlapping

subsets of interneurons and retinal ganglion cells (Yamagata and Sanes, 2008; Yamagata et al., 2002; Yamagata and Sanes, 2012). Depletion of these immunoglobulin receptors resulted in inappropriate extensions into other laminae, and ectopic expression was sufficient to redirect cells into areas that express the receptor (Yamagata and Sanes, 2008; Yamagata et al., 2002; Yamagata and Sanes, 2012). Synaptic targeting involving cell adhesion has also been extensively studied in the *Drosophila* visual system. In contrast to interneuron connections in the vertebrate retina, *Drosophila* photoreceptor neurons project directly from the compound eye into the central nervous system (CNS), where they synapse into distinct areas in the lamina and medulla layers of the optic lobe. Here, homophilic binding of N-cadherin, the related protocadherin Flamingo, and leucine-rich repeat protein Capricious regulate the correct targeting of R1-R6 photoreceptor neurons in the lamina and R7 and R8 photoreceptor neurons in layers of the medulla (Lee et al., 2001; Nern et al., 2008; Lee et al., 2003; Senti et al., 2003; Shinza-Kameda et al., 2006). Thus, it appears that matching the expression of cell adhesion molecules in axons and target areas is a common mechanism across different organisms; however, it is not clear whether there is an underlying reason why a particular system may choose to use an immunoglobulin versus a cadherin or leucine-rich repeat axon-target matching code.

Matching partner neurons via cell adhesion brings the two membranes in very close proximity, and stable cell adhesion is also involved in synaptogenesis (Kohmura et al., 1998; Song et al., 1999). However not every physical contact between two neurons results in a synapse. It is not clear whether initial target recognition and synapse formation could be mediated by the same proteins. One synaptogenic binding pair is formed by the neurexin and neuroligin families of cell adhesion molecules (Nguyen and Sudhof, 1997). Heterophilic binding of the extracellular domains of these proteins sends bidirectional signals that induce clustering of presynaptic

machinery on the neurexin side and postsynaptic machinery on the neuroligin side, even when ectopically expressed in non-neuronal cells (Scheiffele et al., 2000; Graf et al., 2004). Although synaptogenesis is most likely their primary role, it is worth noting that neurexins and neuroligins fulfill several criteria that could implicate them in target selection. For example, neurexins also bind other cell adhesion molecules, such as the leucine-rich repeat LRRTM proteins which compete with neuroligins for neurexin binding (Ko et al., 2009; de Wit et al., 2009; Siddiqui et al., 2010). Interestingly, LRRTMs are not expressed uniformly in all brain regions and are sometimes excluded from specific layers (Lauren et al., 2003). Along with the extensive alternative splicing of neurexins (see section 1.6 below), preferential ligand interactions could also potentially confer specificity. Despite these suggestions, there is currently no evidence for neurexins and their ligands being involved in synaptic targeting.

Guidance cues and secreted molecules

During the 1990s much of the attention in the neural development field was focused on the molecular biology of axon guidance (reviewed in: Tessier-Lavigne and Goodman, 1996; Huber et al., 2003). As a result, many structurally distinct proteins have been shown to direct axon guidance by providing either attractive or repulsive signals to the growing axon. In general, interaction between a receptor and a ligand induces downstream signaling cascades that result in rearrangement of the cytoskeleton to polarize the growth of the axon either towards or away from the ligand (Huber et al., 2003). In addition to directing axonal growth across long distances, this mechanism seems to be well suited for restricting axons to more defined target areas. Some of the earliest evidence for molecules involved in targeting of axons to appropriate targets came

from loss- and gain-of-function experiments of guidance cues in the formation of neuromuscular connections in *Drosophila* embryos. These studies suggested that a proper balance between attractive and repulsive cues instructs motor axons to target to appropriate muscles, as a combination of secreted molecular gradients and cell adhesion molecules, namely attractive Netrin, Fas2 and Fas3, and repulsive dSema2 and Connectin signals (Winberg et al., 1998; Chiba et al., 1995; Mitchell et al., 1996; Matthes et al., 1995; Nose et al., 1994). This concept of balanced attractive and repulsive forces was favored at the time however it failed to explain how multiple molecules with redundant functions can impart specificity to the targeting of individual cells (Tessier-Lavigne and Goodman 1996).

Nevertheless, evidence from several other systems has supported the idea that guidance molecules can instruct axons to correct target regions. For example in the mouse hippocampus, laminar targeting of several types of projections is impaired in animals that lack Netrin1, and in animals that lack Plexin-A2 and Plexin-A4 receptors due to loss of repulsion from their ligand Sema6A (Suto et al., 2007, Barallobre et al., 2000). Repulsive targeting roles of semaphorins have also been reported in establishing correct projections of olfactory receptor neurons to appropriate glomeruli in both mice and *Drosophila* (Cloutier et al., 2004; Komiyama et al., 2007; Latterman et al., 2007; Sweeney et al., 2007). Taken together, these examples demonstrate that secreted or membrane-bound guidance cues can act as short-range signals for restricting axonal targeting to defined areas. Thus, it is likely that coordination between attractive and repulsive gradients and more intimate cell adhesion contacts refines the precision of synaptic targeting from general areas to individual target cells.

1.4 Regulation of genetically encoded wiring instructions

In order to achieve complex wiring specificity using limited genetic material the expression of targeting molecules has to be tightly regulated at multiple levels. Here I outline three regulatory mechanisms: transcriptional regulation, context-dependent differences in downstream signaling of cell surface receptors, and combinatorial use of isoform diversity. Together these mechanisms could allow for sufficient molecular and temporal differences between sub-populations of neurons and individual cells in order to achieve precision in neural circuit formation.

Cell-specific expression of guidance and targeting molecules is determined by the cell's transcriptional program. Several studies have established the involvement of specific transcription factors that regulate synaptic specificity at the level of transcription. In *Drosophila*, the transcription factor Acj6 controls the correct targeting of neurons in the central optic lobe and in the olfactory system (Certel et al., 2000; Komiyama et al., 2003; Komiyama et al., 2004). It is not clear whether Acj6 regulates the transcription of the same genes involved in targeting of neurons belonging to these two different sensory systems. A more detailed mechanism has been described for another transcription factor, Sequoia, which is expressed at different times in R7 and R8 photoreceptor neurons (Petrovic and Hummel, 2008). This study showed that N-cadherin is involved in targeting of R7/R8 photoreceptor neurons under the transcriptional control of Sequoia. Therefore a temporal pattern of transcription factor expression allows the two neuronal populations to use N-cadherin for targeting into separate areas (Petrovic and Hummel, 2008). In other studies, the transcription factor Pea3 was shown to regulate the connectivity of motor neuron dendrites in the mouse spinal cord (Vrieseling and Arber, 2006) and their axonal arborization in target muscles through regulation of Cadherin-8 and Sema3E transcription (Livet

et al., 2002). Interestingly, the expression of Pea3 coincides with the arrival of the motor axon to the muscle target area (Livet et al., 2002), and this regulation of transcriptional program initiation is achieved through extrinsic, target-derived signals received by the neuron locally at the target site (Lin et al., 1998; Haase et al., 2002). From these studies it is evident that both temporal and spatial regulation of a neuron's transcriptional program fine-tunes the expression of targeting molecules.

Cell surface receptors can have multiple ligands and downstream effects depending on the context. For example, mammalian and *Drosophila* Dscam can bind homophilically with other Dscam molecules, or heterophilically with other ligands such as Netrin (Wojtowicz et al., 2004; Agarwala et al., 2000; Andrews et al., 2008; Ly et al., 2008; Liu et al., 2009). Intracellularly, Dscam activates the Pak1 kinase, either directly or through interaction with the adaptor protein Dock (Schmucker et al., 2000; Li and Guan, 2004), but Pak1 activity is not required for Dscam-mediated dendritic repulsion and self-avoidance (Hughes et al., 2007), indicating that other signaling molecules are involved in this function. In another study activation of Pak1 by Dscam was shown to be mediated by Netrin (Liu et al., 2009) and Netrin has also been suggested to be an attractive cue for Dscam in axon guidance, turning and midline crossing (Liu et al., 2009; Ly et al., 2008; Andrews et al., 2008). In some contexts homophilic binding between Dscam proteins can also be attractive (Yamagata and Sanes, 2008; Zhan et al., 2004). Zhan et al. proposed a model in which low levels of signaling may be permissive of an attractive homophilic interaction between Dscam proteins on different cells, in contrast high levels of Dscam signaling results in sister branch repulsion in the same cell (Zhan et al., 2004).

The precision of synaptic specificity may be regulated by generating molecular diversity through alternative splicing. Neurons can be classified based on several factors, notably their

morphology, function, electrophysiological and neurochemical properties. However, even neurons that are seemingly identical can have different expression profiles through alternatively-spliced molecular isoforms. This has been proposed to serve as a molecular "barcode", allowing each neuron to have a unique identity (Schmucker and Flanagan, 2004). In invertebrates the indisputable candidate for such a function is Dscam. With mutually exclusive alternative splicing of three exon clusters Dscam proteins can have more than 19,000 different extracellular domains (Schmucker et al., 2000). Single photoreceptor neurons have been shown to express a repertoire of up to 50 different isoforms (Neves et al., 2004), thereby allowing neighboring neurons to express non-overlapping sets of isoforms.

Vertebrate Dscam has not conserved this form of alternative splicing, despite having conserved functions such as axon guidance and synaptic specificity (Schmucker and Chen, 2009). This raises the question whether molecular diversity is functionally important for neural circuit wiring or if there are other families of synaptic targeting molecules in vertebrates that show similar levels of diversity. Alternative splicing of the three protocadherin gene clusters (*α-* , *β-* , and *γ-protocadherin*) can create 58 possible protocadherin proteins that have different extracellular domains (Kohmura et al., 1998; Wu et al., 1999). Similar to *Drosophila* Dscam, protocadherins also function through isoform-specific homophilic interactions (Schreiner and Weiner, 2010). Single cell analysis of Purkinje cells has shown that single cells express distinct isoforms implying that this diversity is relevant in a cell-specific manner (Esumi et al., 2005; Kaneko et al., 2006). Similar to the role of *Drosophila* Dscam in sensory neuron dendrites (Soba et al., 2007; Matthews et al., 2007), homophilic binding of protocadherin isoforms has been shown to be involved in dendritic self-avoidance in the mouse (Lefebvre et al., 2012). However, the importance of protocadherin diversity for synaptic specificity has yet to be determined.

Other vertebrate protein families that generate a high degree of diversity through alternative splicing are the neurexins and neuroligins. Neurexins are encoded by three genes, *Neurexin1-3*, that can generate long *α-Neurexin* and short *β-Neurexin* transcripts from two distinct promoters (Ushkaryov et al., 1992). Alternative splicing of five splice sites, named 1 through 5, in the extracellular domains can create more than 2,000 protein isoforms (Missler and Sudhof, 1998; Tabuchi and Sudhof, 2002., Rowen et al., 2002) , and recent studies have suggested that this number could be even higher due to newly-characterized splice sites (Treutlein et al., 2014). The neurexin binding partners, neuroligins are encoded by five genes, *Neuroligin1-4* and *4Y*, and although not as extensive as neurexins, also exhibit alternative splicing at two sites, A and B (Ichtchenko et al., 1996; Jamain 2002). Different neuroligins are preferentially found at different synapses, notably neuroligin-2 which is exclusively found at inhibitory synapses (Varoqueaux et al., 2004), and alternative splice variants dictate binding selectivity to different neurexins. For example, all α-neurexin isoforms and splice site 4 positive β-neurexins cannot associate with splice site B positive neuroligin-1 (Boucard et al., 2005) and in addition presence of these neuroligin-1 isoforms shifts the postsynaptic specialization from inhibitory to excitatory (Chih et al., 2006). Therefore there is strong evidence that the diversity of neurexins and neuroligins is relevant for specification of the type of synapse formed, however how, and if, this influences initial target selection is not clear.

1.5 Hard-wired circuits self-assemble using genetically encoded wiring instructions

All behaviors have a neural basis that can be attributed to specific circuits, whether it is learning a task, focusing attention to salient stimuli, avoiding predators, locomotion, or feeding.

Innate behaviors and instincts assure the survival of a species and it is therefore assumed there must be a species-specific blueprint of the neural circuits that underlie them (Manoli et al., 2006; Baker et al., 2001). The general principle of any innate behavior is that upon detection of relevant information a behavioral program is executed in a stereotyped manner (Wine, 1984; Manoli et al., 2006). The stereotypy of behavior between individuals implies that the circuit has to be hard-wired; in other words extremely precise, invariable between animals, and therefore assembled without sensory-driven experience. Thus to achieve invariable wiring the instructions for assembling a hard-wired circuit must be genetically encoded.

This makes hard-wired circuits very useful for studying neural circuit formation, especially in genetically tractable model organisms such as the fruit fly *Drosophila melanogaster*. Although flies are capable of complex behaviors and learning, much of their neural connectivity is hard-wired (Jefferis et al., 2001; Hiesenger et al., 2006). Insect behavior is dependent on evaluating sensory information from the environment in which they are most likely to find food, mates and avoid predation. Therefore responses to certain stimuli should be present from birth and suited for the environment that the insect inhabits. One example is found in different subspecies of butterflies that show innate color preference based on the flowers that their subspecies commonly feeds on (Weiss et al., 1997; Goyret et al., 2008). *Drosophila* also show an innate attraction for shorter wavelength light that is mediated by a hard-wired circuit that relays photoreceptor neuron inputs to the optic lobe (Yamaguchi et al., 2010; Karuppudrai et al, 2014). Another innate preference arises from the olfactory system, where flies strongly avoid CO_2 due to activation of a specific olfactory glomerulus that is dedicated to CO_2 odor processing (Suh et al.,2007; Semmelhack et al, 2009). A more complex behavior than choice preference that has been extensively studied with great success is male courtship behavior. Courtship in flies

involves an integration of sensory cues that lead to stereotyped motor behaviors, and all of these have been linked to the expression of a single gene, *fruitless*, in identifiable neurons in the male *Drosophila* brain (Ryner et al., 1996; Lee et al., 2000; Manoli et al., 2005; Stockinger et al., 2005). These examples of innate circuitry point out that *Drosophila* offers a variety of systems to study different aspects of neural circuit formation and function. In the next section I will describe the *Drosophila* mechanosensory system and the advantages that it offers for investigating precise synaptic targeting.

1.6 The *Drosophila* mechanosensory system

Mechanosensation in adult *Drosophila* is important for multiple aspects of sensing the environment, such as proprioception, detecting tactile stimuli during locomotion, and cleaning (Kernan and Zuker, 1995). The external mechanosensory organs are located at the exoskeleton and each mechanosensory organ arises from several rounds of asymmetrical division of a single sensory organ precursor cell giving rise to five cells: a hair-like bristle that is innervated by a single neuron surrounded by a support cell, a sheath cell, and a glial cell (Roegiers et al., 2001). Twelve symmetrical pairs of large mechanosensory bristles line the back of the fly in stereotyped positions, which makes specific mechanosensory neurons uniquely identifiable from one animal to another based on the location of its corresponding bristle (Ghysen, 1980). Each mechanosensory neuron is named after the bristle that it innervates, for example, on the posterior scutellum there are only two bristles, the left and right posterior scutellars (pSc), each innervated by a posterior scutellar (pSc) neuron (**Fig. 1.2a, b**).

Touching a mechanosensitive bristle activates the neuron that innervates it. Deflection of the bristle exerts mechanical stress on the dendritic tip of the neuron (Thurm, 1965) leading to neuronal depolarization through opening of mechanosensitive channels (Walker et al., 2000). The action potential is propagated through the axonal projection that travels several millimeters from the periphery into the thoracic ganglion of the CNS. Although it is not known how many cells each mechanosensory neuron synapses onto, or how the signal is integrated and relayed, the motor output of the circuit has been well characterized (Vandervorst and Ghysen, 1980; Corfas and Dudai, 1989; 1990; Canal et al., 1998; Philis et al., 1993). Upon touch activation, the fly uses either the first (anterior) or the third (posterior) pair of legs to brush the stimulated area. This response appears to be protective against potential parasites crawling on the back of the fly. The leg that is activated depends on the position of the stimulated bristle, such that when the anterior lateral bristles are stimulated the fly responds with the ipsilateral first leg, while the posterior dorsal bristles are brushed with the ipsilateral third leg (Vandervorst and Ghysen, 1980; Corfas and Dudai, 1989). The *Drosophila* grooming reflex has been used in several studies to isolate mechanosensitive-deficient mutants and demonstrate sensory habituation in flies (Corfas and Dudai,1989; Canal et al., 1998; Philis et al., 1993). Importantly, using this behavior it was demonstrated that even when axons were misguided to enter the CNS in inappropriate positions the correct behavioral response was retained, implying that distinct molecular mechanisms regulate mechanosensory axon guidance and axon targeting (Vandervorst and Ghysen, 1980).

Inside the CNS mechanosensory neurons elaborate very complex yet highly stereotyped axonal arbors that increase in complexity from anteriorly to posteriorly-positioned mechanosensory neurons (**Figure 1.3)** (Ghysen, 1980). The high degree of stereotypy between animals indicates a tight genetic regulation on the synaptic connectivity for each neuron, and the

axonal branching pattern can thus be used as a readout for differences in connectivity. Mechanosensory axonal branch lengths and positions can be quantitatively analyzed to measure the differences in axonal branch targeting between individuals (**Fig. 1.2c, d**) (Chen et al., 2006; Neufeld et al., 2011; Cvetkovska et al., 2013; Kays et al., 2014). For example, the pSc and pDc mechanosensory neurons have a set of "core" branches that are present in almost all flies (**Fig. 1.2c, d**). Thus, within a complex axonal arbor we can identify with certainty even the same axonal branch among different individuals. Several parameters of the axonal branching pattern can be quantitatively analyzed such as their frequency of occurrence, positions, and lengths, and this can be used to examine the mechanisms underlying different aspects of synaptic targeting of these neurons (Chen et al., 2006; Cvetkovska et al., 2013). For example, the stereotyped targeting of the pSc neuron has been previously used to identify roles for the PlexinA receptor in suppressing axonal branch growth and axonal varicosity formation, and for the PlexinB receptor in promoting axonal branch growth (Neufeld et al., 2011).

1.7 Thesis introduction

Revealing the mechanisms that instruct assembly of hard-wired circuits could allow us to apply them to more complex systems. The aim of this dissertation is to explore the molecular mechanisms of synaptic target selection in a single identifiable neuron in a hard-wired circuit. The general objectives are to assess synaptic specificity at a molecular, morphological and functional level. **Chapter 2** describes a novel method for combined structural and functional analysis of axonal targeting of single mechanosensory neurons performed within the same animal. **Chapter 3** explores how regulated expression of Dscam protein levels is important for correct wiring. **Chapter 4** exploits the utility of the mechanosensory system to identify genes that are used by a specific neuron to establish its wiring diagram, and suggests a possible dual role of Teneurin-m in synaptic targeting. **Chapter 5** discusses general concepts arising from these studies and their future directions. The results of this work contribute to our general knowledge by characterizing the role of specific genes in synaptic target selection at the level of identifiable axonal branches and their effect on circuit function, an approach which has not been done before. This work also contributes to human health as we implicate the dysregulated expression of the Dscam protein as a shared molecular mechanism between two prevalent forms of intellectual disability.

1.8 Figures

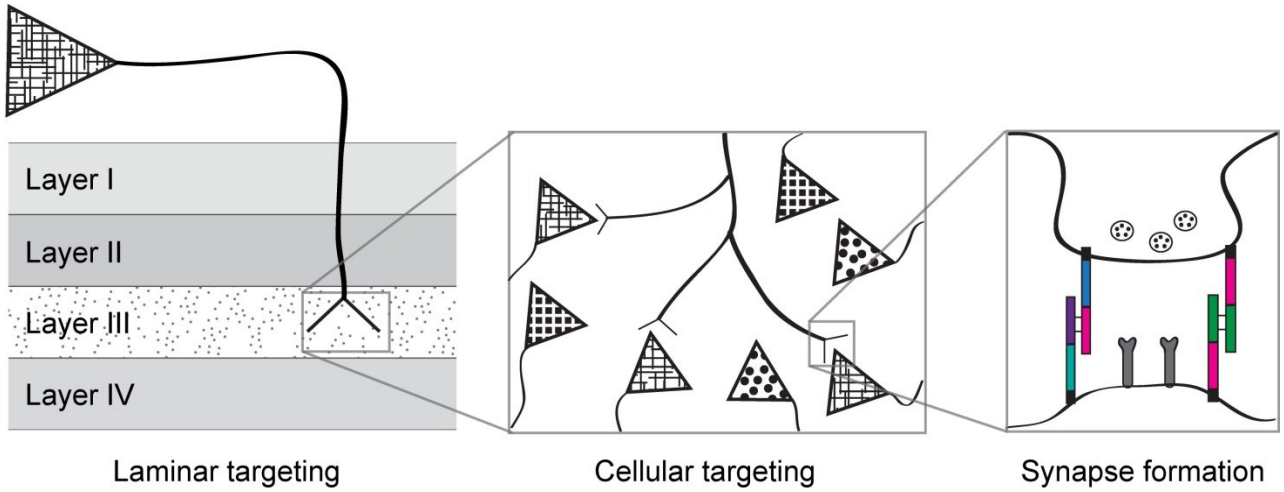

Figure 1.1 Synaptic targeting includes several levels of decision making by an axon.

First, in order to form specific connections, neurons terminate their axons into defined target areas. Laminar targeting is an example where an axon targets to a specific layer, in the left panel shown as layer III, while it bypasses layers I and II and never extends into layer IV. Once within the target area, the axon branches out to contact other cells that are its appropriate partners (lined pattern cells, middle panel). The final stage of the targeting process is the formation of a functional synapse (right panel).

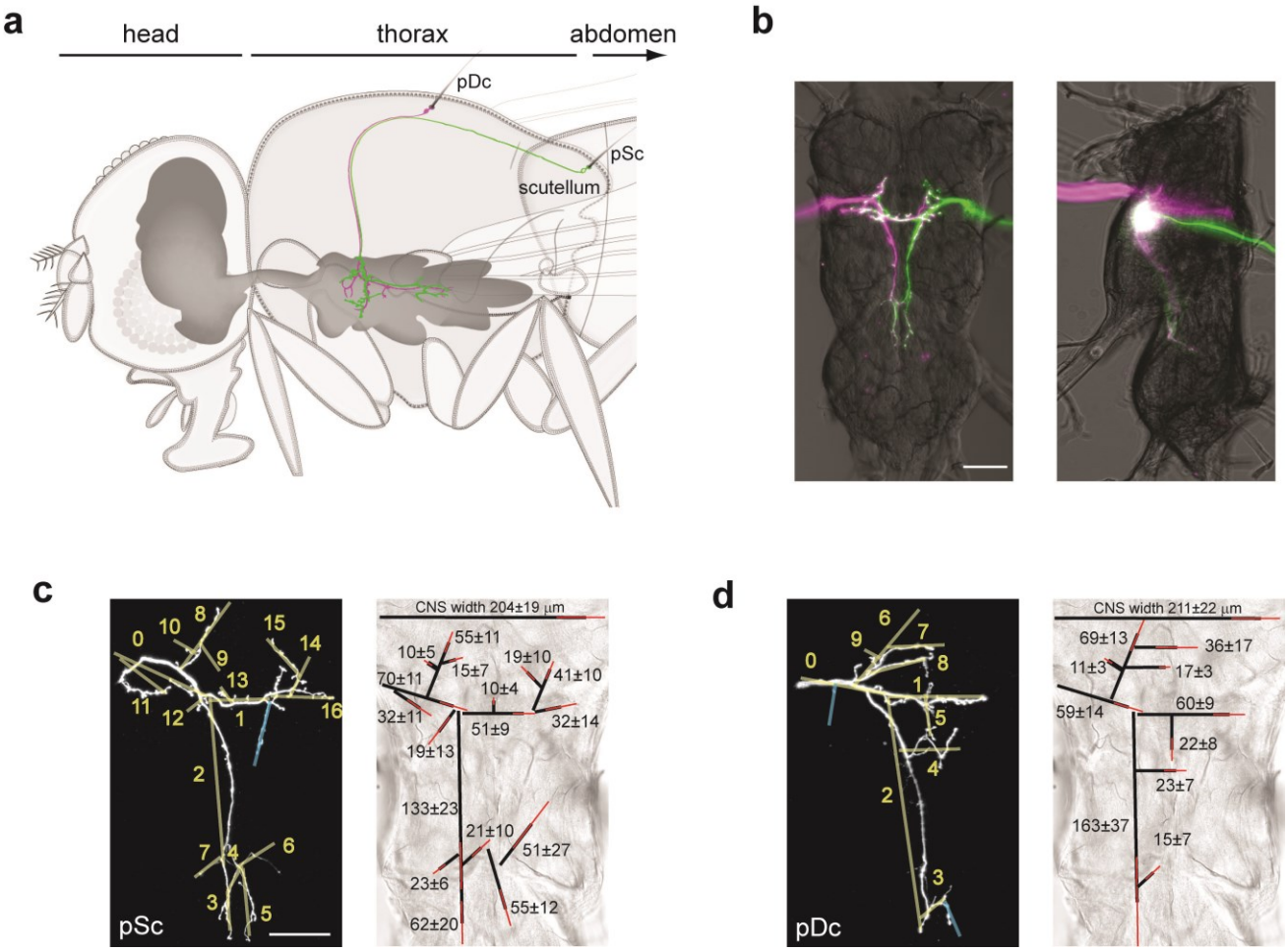

Figure 1.2 A single mechanosensory neuron innervates a single bristle and elaborates a stereotypical axonal branching pattern within the central nervous system.

a, Mechanosensory neurons innervating the major bristles (macrochaetae) along the thorax of the fly project their axons into the thoracic ganglion of the central nervous system. Each macrochaeta is identifiable and named, and since one neuron innervates one bristle, the same neuron can be identified between animals based on the location of its corresponding bristle. The axonal projections of the left posterior dorsocentral (pDc) and the left posterior scutellar (pSc) neurons are shown in magenta and green, respectively. These two neurons elaborate complex and distinct stereotypical axonal arbors.

b, Ventral (left panel) and side view (right panel) of a dissected thoracic ganglion with fluorescently labeled left and right pSc axons shown in magenta and green, respectively. Scale bar is 50 μm.

c, The wildtype branching pattern of the pSc neuron consists of 16 identifiable and invariant core branches (yellow). One variable branch occurring in 50% of animals is shown in blue. Branch lengths of the pSc core branches can be measured, and the average lengths (black) and standard deviations (red) are shown. Branch lengths and frequency of occurrence of these invariant branches can be used as a readout of synaptic connectivity of the pSc neuron.

d, The wildtype branching pattern of the pDc neuron consists of 10 identifiable core branches (yellow), and on average 3 variable branches, the most variable (blue) occurring at 50%.

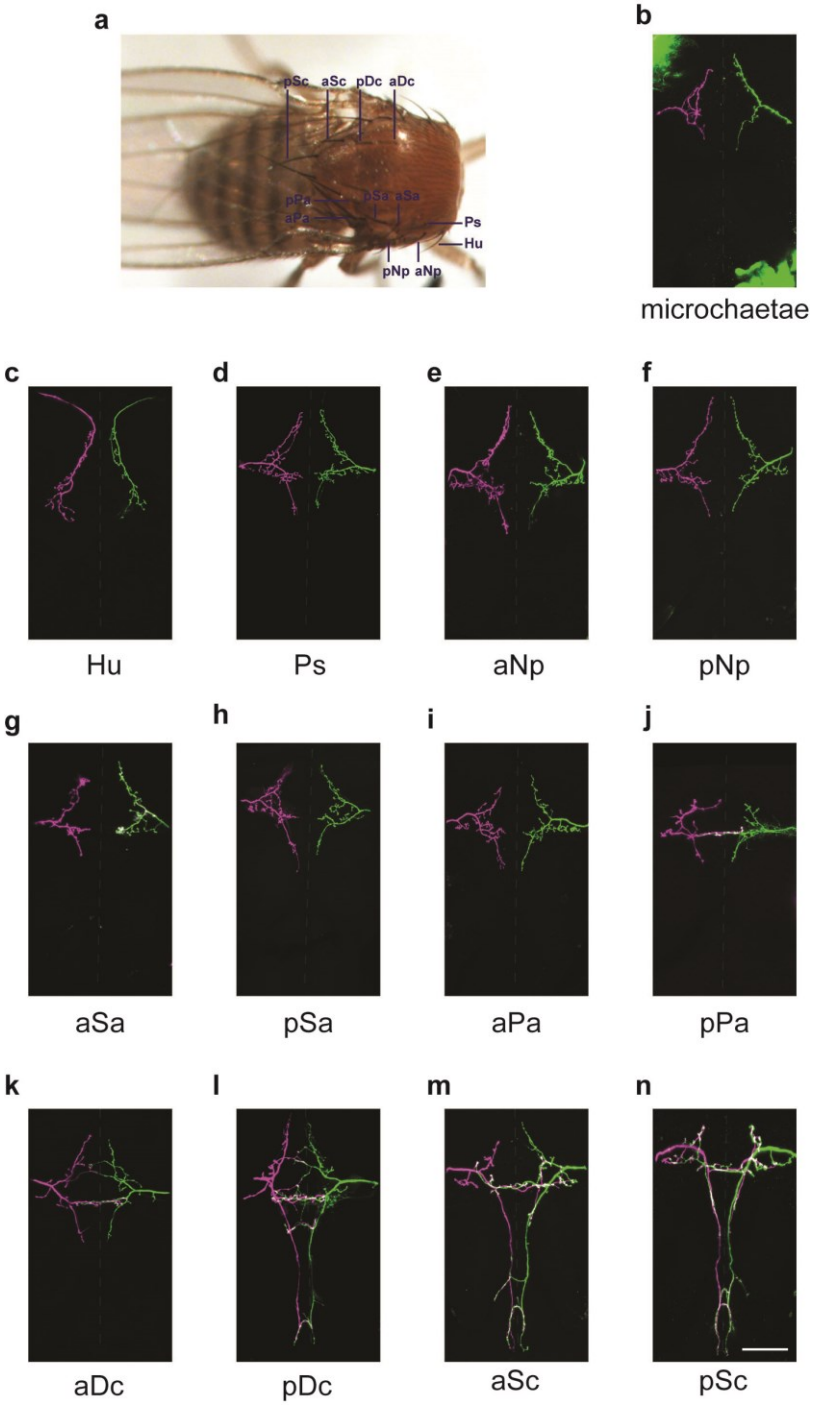

Figure 1.3 Each of the 12 pairs of macrochaetae mechanosensory neurons has a characteristic axonal arbor that increases in complexity from anterior to posterior macrochaeta location.

a, The exterior of the back of the fly is shown with the names and positions of the macrochaetae labeled. The humoral bristles (Hu) are the most anterior, and located on the postpronotum. The presutural bristles (Ps) are located dorsally on the presutural area. The anterior and posterior notopleural bristles (aNp and pNp) are located laterally on the notopleuron. The anterior and posterior supraalar (aSa and pSa) and anterior and posterior postalar (aPa and pPa) bristles are located laterally on the prealar and postalar calluses, respectively. The anterior and posterior dorsocentral bristles (aDc and pDc) are located dorsally on the scutum. The anterior and posterior scutellar bristles (aSc and pSc) are the most posterior, and located on the scutellum. Microchaetae line the dorsal thorax, except on the scutellum.

b, The simple axonal arbors of left and right microchaetae from two different regions of the thorax are shown. Depending on the location, microchaetae mechanosensory neurons have slightly different arbors.

c – n, Each pair of macrochaeta was labeled with DiI on the left (magenta) and DiD on the right (green) in the same animal. The symmetrical axonal arbors are shown for each pair. Dotted lines mark the midline of the CNS. Scale bar is 50 μm.

Chapter 2

Assessing neuronal connectivity through structural and functional analysis of single neurons

2.1 Relation to overall project

Single identifiable mechanosensory neurons in *Drosophila* have highly stereotyped axonal arbors that provide a quantitative readout for synaptic targeting (Chen et al., 2006; Neufeld et al., 2011; Cvetkovska et al., 2013). However, examining the effects of genetic manipulation on synaptic targeting decisions made by single neurons and the effect on the overall function of the circuit has not been possible in the same animal. To address this problem we developed a combined functional and structural assay to analyze the function of the *Drosophila* mechanosensory circuit through behavior and visualize the primary sensory neuron in the same animal. This chapter describes the protocol and validates the method through several experiments.

2.2 Abstract

We describe a method to image the complex axonal branching structure of identified mechanosensory neurons in *Drosophila*, combined with a behavioral assay to evaluate the functional output of the neuron. Stimulation of identified mechanosensory neurons in live animals produces a stereotyped grooming reflex. The mechanosensory axonal arbor within the central nervous system is subsequently labeled with a lipophilic fluorescent dye and imaged using fluorescence microscopy. The behavioral output can therefore be correlated to the axonal morphology of the stimulated neuron in the same animal. Combining this protocol with genetic analysis provides a powerful tool to identify the roles of genes involved in different aspects of hard-wired neural circuit formation underlying an innate behavior. From behavioral analysis to axonal imaging, the protocol takes four days.

2.3 Introduction

The investigation of how neurons form precise connections with their partners during circuit development is crucial for our understanding of brain function and behavior. For hard-wired neural circuits underlying innate behaviors, it is generally thought that neurons distinguish between correct versus incorrect synaptic targets using instructions encoded in the genome. To better understand how molecules can encode pre-specified synaptic targeting patterns, the hard-wired and stereotyped neural circuitry of invertebrates have been used in conjunction with genetic analyses to identify these molecules (Shen, 2004; Chen et al., 2006).

Labelling single neurons

The importance of visualizing single neurons within the complexity of brain tissue has been evident since the development of the Golgi staining method and the characterization studies of Ramon y Cajal in the 19th century (Cajal, 1888; Cajal, 1896). Due to a neuron's intrinsically polar structure and the ability to project processes over long distances, neuronal labelling relies on retrograde or anterograde transport of tracers. The use of horseradish peroxidase as a retrograde tracer was widespread during the 1970s, however it had many limitations such as having to sever axons for efficient uptake, providing substrates for visualization, and the manipulation of toxic substances (Adams, 1977). Labelling of neurons with fluorescent carbocyanine dyes was first introduced in the 1980s (Honig and Hume, 1986) and since then use of these lipophilic compounds as neuronal tracers has become a standard in both vertebrate and invertebrate neuroscience.

Carbocyanine dyes are structurally composed of a bridged double ring chromophore that specifies their fluorescent properties, and long hydrocarbon chains that allow them to insert into

the lipid bilayer. They diffuse laterally through the membrane, are retained in the cell for a long time and are not cytotoxic (Honig and Hume, 1986). Several spectrally-separated high quantum yield variants exist that in theory can allow for simultaneous four-color imaging (Godement et al., 1987; Ragnarson et al., 1992; Briehner and Gumbiner, 1994, Agmon et al., 1995). Anterograde labeling with carbocyanine dyes has been especially useful in examining the morphology and fine branching of single axons within insect nervous systems (Chen et al., 2006; Cvetkovska et al., 2013; Williams and Shepherd, 2002).

Several other techniques exist to label neurons in flies. Most commonly, transgenic lines that express Gal4 in restricted populations of cells are used to drive UAS-based expression of fluorescent proteins. This strategy is limited however, because no Gal4 line has been found to be specific for a single neuron, and this inevitably results in multiple axons being labeled. Highly specific Gal4 promoters that can identify a small number of neurons may not express Gal4 for long enough time for fluorescent proteins to label the entire axon until adulthood, such as the two lines used in this protocol (455-Gal4, DC-Gal4). Complex genetic methods can be used to circumvent these limitations, for example by using combinations of spectrally distinct genetically-encoded fluorophores to resolve single axons (Livet et al, 2007). However, our protocol using spectrally-distinct dyes provides the simplest method to resolve single axons. This protocol also has broad applicability to other sensory axonal projections within *Drosophila* such as chemosensory neurons (Tissot et al., 1997), as well as other insect model systems that do not have Gal4 lines, such as the grasshopper and the cockroach (Myers and Bastiani, 1993; Zill et al., 1993). Dye labeling of axonal projections has also been used in vertebrate systems, where Cre-based expression shares similar limitations of the Gal4 system in invertebrates (Bishop et al., 2000; Rolf et al., 2002; Inatani et al., 2003).

The *Drosophila* cleaning reflex as indication of circuit function

Mechanosensitive neurons in the fly detect mechanical stimuli from the environment through deflection of hair-like bristles that activate the single neuron that innervates them. In the fly, touching mechanosensitive bristles can activate a grooming reflex from the legs to repeatedly brush the stimulated bristles (Cvetkovska et al., 2013; Canal et al., 1998; Vandervorst and Ghysen, 1980; Corfas and Dudai, 1989; 1990; Phillis et al., 1993). For example, stimulation of the notopleural bristle located on the lateral notum and hence, activation of the notopleural neuron, always results in the fly sweeping its front leg over the stimulated area, whereas stimulation of the posterior scutellar bristles evokes a stereotyped response from the third (rear) pair of legs. This specificity of stimulating single mechanosensory neurons to activate specific legs was first used in 1980 to demonstrate an independence between synaptic targeting of an axon versus its axon guidance into the central nervous system, where axons can be misrouted into different nerve roots but still activate the correct cleaning reflex leg (Vandervorst and Ghysen, 1980). While the exact postsynaptic targets of mechanosensory neurons are not known, their distinct characteristic branching patterns indicate that they must synapse onto different subpopulations of interneurons, which then relay the information to activate the appropriate leg response.

The behavioral assay that we developed, which I describe in this protocol, allows for functional analysis of an identified mechanosensory neuron using the cleaning reflex, along with morphological analysis of its axonal branching pattern all within the same animal. Combining this approach with genetic analysis opens possibilities of investigating the relationship between fine-scale axonal targeting and circuit function, as well as to identify new genes that are involved in neural circuit formation.

2.4 Detailed protocol

2.4.1 Experimental design

In this protocol we describe how to measure mechanosensory circuit function through a behavioral response with subsequent imaging of the axonal morphology of the primary mechanosensory neuron involved in the behavior. The behavioral assay involves the mechanical stimulation of only a left and right pair of bristles by applying a controlled amount of fluorescent dye onto the bristles to elicit a cleaning reflex. To visualize the axonal branching patterns of single mechanosensory neurons, lipophilic carbocyanine fluorescent dyes are applied peripherally and are allowed to anterogradely diffuse along the axonal branches to label all of its fine projections in the CNS. Standard fluorescence microscopy can be used to image the axonal arbors in the CNS, and the axonal branching pattern can be quantitatively analyzed by measuring the lengths and positions of each identifiable branch. This protocol is inexpensive, reliable, can be performed in four days (**Figure 2.1**), and uses an established system for the study of synaptic connectivity and circuit function.

Simple controls can be performed at different steps to verify the fidelity of the technique. To ensure that the neural circuitry underlying the grooming response is intact, *Drosophila* are pre-selected using stimulation of the notopleural bristles which produces a cleaning response at close to 100% reliability in healthy flies. To ensure that the fluorescent dye can label entire axonal arbors with strong fluorescent signal, multiple bristles along the notum can be plucked to label several mechanosensory neurons at once with a large volume of dye covering the thorax, and this ensures overlabelling of many axons within the CNS. To control for variability between experiments, animals of the same age and sex should be used, and experiments should be

performed at the same time of day to control for circadian cycle effects, and within the same season to control for differences in food consistency that can occur with changes in relative humidity.

Depending on the nature of the experiment, the combined structural and functional analysis can be performed, or this protocol can be separated into only the behavioral assay or the morphological analysis.

2.4.2 Materials

Reagents

Drosophila stocks

w $^{-}$

455-Gal4/CyO

DC-Gal4

UAS-dsRNA Dscam

UAS-dsRNA PlexinA$^{VDRC\ 107004}$*/CyO*

Carbocyanine dye solutions

20 µg/µL DiI dye in ethanol:

100 mg DiI (Life Technologies, D282) in 2 mL of 100% ethanol for stock solution of 50 µg/µL. Can be stored at 4 °C protected from light for up to six months.

20 µL of stock DiI (50 µg/µL) in 30 µL of 100% ethanol for working solution of 20 µg/µL DiI. Heat to 40°C with shaking before use. Can be stored at room temperature (23 – 25 °C) protected from light for up to one month.

32 µg/µL DiD dye in ethanol:

10 mg DiD (Life Technologies, D7757) in 250 µL of 100% ethanol for stock solution of 40 µg/µL. Store at 4 °C protected from light for up to six months.

20 µL of stock DiD (40 µg/µL) in 5 µL of 100% ethanol for working solution of 32 µg/µL DiD. Heat to 40°C with shaking before use. Store at room temperature (23 – 25 °C) protected from light for up to one month.

10 µg/µL DiO dye in ethanol:

100 mg DiO (Life Technologies, D275) in 2 mL of 100% ethanol for stock solution of 50 µg/µL. Store at 4 °C protected from light for up to six months.

10 µL stock DiO (50 µg/µL) in 40µL of 100% ethanol for working solution of 10 µg/µL. Heat to 40°C with shaking before use. Store at room temperature (23 – 25 °C) protected from light for up to one month.

2.5 µg/µL DiO dye in DMF:

100 mg DiO (Life Technologies, D275) in 2 mL of DMF for stock solution of 50 µg/µL. Store at 4 °C protected from light for up to six months.

2.5 µL stock DiO (50 µg/µL) in 40µL of DMF for working solution of 2.5 µg/µL. Store at room temperature (23 – 25 °C) protected from light for up to one month.

0.2 M Carbonate-Bicarbonate buffer at pH 9.5:

13 mL of 0.4M Carbonate buffer (21.2 g of anhydrous sodium carbonate in 500 mL of ddH_2O)

37 mL of 0.4M Bicarbonate buffer (16.8 g of sodium bicarbonate in 500 mL of ddH_2O)

50 mL of ddH_2O

3.7% paraformaldehyde in 0.2 M Carbonate-Bicarbonate buffer at pH 9.5:

13 mL of 0.4M Carbonate buffer

37 mL of 0.4M Bicarbonate buffer

40 mL of ddH_2O

10 mL of 37% paraformaldehyde (5.87g paraformaldehyde in 10 mL ddH_2O)

Equipment

Borosilicate capillary glass OD/ID:1.00mm/0.78mm (Harvard Apparatus, W4 64-0778)

Glass slides 75x25 mm (Fisher, 12-550-A3)

Glass coverslips 18x18 mm (Fisher, 12542A)

Double sided tape

Cyanoacrylate glue

Insect pins (Fine Science Tools, 26000-25)

Micromanipulator (Harvard Apparatus, 60-0569)

Micropipette holder for behavior experiments (Harvard Apparatus, W4 64-1228)

Micropipette holder for dye-filling (Harvard Apparatus, W4 60-0604)

Dumostar no. 5 and no. 55 Forceps (Fine Science Tools, 11295-00 and 11295-51)

Vannas spring scissors (Fine Science Tools, RS 5618)

Eppendorf 2 mL tubes (Fisher, 22363344)

Gel loading tips (Fisher, 213802M)

Sylgard coated 35 mm dish

10 cm Petri dishes

15 cm Petri dishes

Beakers

Shaking heatblock

Whatman no. 1 filter paper

30 mL syringe

Tygon R-3603 tubing, 3.2 mm ID x 4.8 mm OD x 0.8 mm Wall

Micropipette puller (P-97 Flaming/Brown micropipette puller, Sutter instruments)

Dissecting microscope with epifluorescent lamp (Zeiss Stereo Discovery V12)

Imaging microscope (Zeiss Axio Scope A1 epifluorescent or Olympus FluoView FV1000 laser scanning confocal)

2.4.3 Behavioral Assay

To control for behavioral variability between experiments, we use two day old female animals, and all experiments are performed in the afternoon to control for circadian cycle effects, and within the same season to control for differences in food consistency that can occur with changes in relative humidity.

Flies are anaesthetized using CO_2 and decapitated using spring scissors. Flies are allowed to recover in a humidity chamber consisting of a 150 mm dish with wet Whatman filter paper. After a 1 hour recovery period the flies should be standing on all six legs and generally responsive (**Figure 2.2a)**.To ensure that the neural circuitry underlying the grooming response within the thoracic ganglion is intact, flies are pre-selected using stimulation of the notopleural bristles. Gentle deflection of the anterior notopleural bristle with forceps (**Figure 2.2b**) produces a cleaning response movement of the ipsilateral first (anteriormost) leg at close to 100% reliability in healthy flies.

The micromanipulator is assembled by attaching a 30 mL syringe to the electrode holder's pressure port. The DiO or DiD dye solution is reconstituted by shaking at 1200 rpm in a 40 °C heat block for 5 minutes. A micropipette is backfilled with 1–2 µL of dye solution using gel loading tips. A micropipette tip diameter of 20 µm allows using only slight pressure to eject a small volume (~20 nL) onto the fly.

Using the micromanipulator a small amount of dye solution is pressure ejected on the posterior scutellum to cover only the two pSc bristles (**Figure 2.2c**). Care must be taken to always approach the scutellum from the posterior, parallel to the scutellar bristle, in order to avoid accidentally touching the dorsocentral bristles. If dye spills on the side of the scutellum, the thorax, or the wings, the flies are discarded as this may result in a false positive behavioral response.

A positive cleaning response from stimulation of the pSc bristle is defined as the third (rear) pair of legs reaching dorsally and brushing the thorax (**Figure 2.2d**), and can be verified

by the transfer of the fluorescent dye onto the legs (**Figure 2.2e**). Individual animals that respond or do not respond are identified, counted and separated.

2.4.4 Bristle plucking and fixation

Flies from responder or non-responder groups are anaesthetized using CO_2 and glued onto insect pin heads at a region between the posterior thorax and anterior abdomen, slightly ventrally. This orientation is best for accessing the dorsal bristles. For accessing laterally-located bristles, the ventral abdomen of the fly is glued parallel to the pin head (**Figure 2.2f**). After the glue dries (~ 5 minutes) the flies should be alive and active.

The bristles are plucked using a pair of fine forceps (e.g. Dumont no. 55), by grabbing the bristle close to the base and *quickly* pulling against the direction of growth of the bristle (**Figure 2.2g, h**). It is critical to avoid breaking the bristle near or at the base, as this will prevent dye from entering the bristle socket. ~50% of the abdomen is removed (**Figure 2.2i**) using spring scissors and the flies are immediately immersed in a 2 mL tube containing 250 µL solution of 3.7% paraformaldehyde in 0.2 M carbonate-bicarbonate buffer pH 9.4. Flies are completely fixed at 4 °C overnight.

2.4.5 Carbocyanine Dye Labeling

The fluorescent carbocyanine tracers DiI and DiD are reconstituted by shaking at 1200 rpm in a 40 °C heat block for 5 minutes. The micropipettes are backfilled with 1–2 µL of dye solution using gel loading tips and attached to a dual electrode holder on a micromanipulator. For

efficient dye filling the tip of the micropipettes should be about half the diameter of the bristle socket (~10μm).

Fixed flies are washed from fixative in 0.2 M carbonate-bicarbonate buffer for a few seconds, and then in ddH_2O for a few seconds, and then completely dried.

Using a micromanipulator the fluorescent dyes are applied at the empty bristle socket by gently touching the tip of the micropipette on the socket (**Figure 2.2i**). The labeled flies are placed in a 10 cm Petri dish filled with 0.2 M carbonate-bicarbonate buffer (**Figure 2.2j**), such that the fly's remaining abdomen is immersed but the dye-filled bristle socket is above the buffer (**Figure 2.2k**). The flies are left undisturbed in a dark area at room temperature for two days.

2.4.6 Dissection and Imaging

After allowing two days for the dye to completely label the entire axonal arbor the thoracic ganglion of the fly is dissected. The ganglion is located on the ventral side of the thorax, and extends from anterior to posterior throughout the ventral thorax (see **Chapter 1**, **Figure 1.2**). It is translucent and ~500 x 300 μm in size with the thinnest part 40 μm wide.

The dissected ganglion is slide-mounted with #1 thickness coverslips so that the ventral side of the ganglion is facing up (see **Chapter 1**, **Figure 2.1b–d**). The labeled axon is imaged immediately using a Zeiss AxioScope A1, or an Olympus FluoView FV1000 laser scanning confocal microscope. Images are acquired using a 40× objective, N.A. 1.0, so that the entire axonal arbor (~135 μm x 245 μm for the pSc) fits within one field of view.

2.4.7 Image Analysis

Images are selected for analysis based on low background fluorescence and homogenous and strong labeling of fluorescent dye throughout a single axon. Image analysis is performed on maximal intensity projections. Transmitted light images are acquired to measure the CNS width and to verify there was no damage to the CNS or occlusions at the surface. Images are adjusted for contrast and brightness only, applied to the whole image. Axonal branch lengths and numbers are measured using a custom written program in MatLab (MathWorks).

For analysis of pSc and pDc axon phenotypes, a prototypical skeleton of the wildtype axonal arbor was designated by identifying axonal branches that were invariant among w^- flies. Primary and secondary axonal branches were identified that occurred at greater than 80% frequency and tertiary branches that occurred at greater than 60% frequency. The midline is defined as a 10μm-wide region running along the anterior-posterior axis of the CNS. Any branch entering or crossing this region is considered a midline-crossing branch. The length of the primary axon entry point into the CNS (**Figure 1.2c**, "branch 0") is dependent on the number of images collected above the entry point as the axon travels within its fascicle, and so was not included in the branch length measurement calculations.

2.4.8 Statistical Analysis

To compare branch lengths among genotypes first they should be verified that they are normally distributed from their means. For single comparisons a two tailed t-test is used set at $p < 0.05$. For comparing branch lengths of multiple mutant genotypes to a wildtype, one way ANOVA followed by Dunnett's post-hoc pairwise comparison is used to determine statistical significance.

For statistical testing of discrete measurements, non-parametric Mann-Whitney U test is used to determine statistical significance in branch numbers between wildtype and mutant genotypes. For statistical testing in frequency distributions of phenotype occurrence, the statistical significance for each category between genotypes is determined by performing multiple comparisons using a two tailed *t*-test for proportions set at $p < 0.05$. In behavioral experiments statistical significance in response rate between each genotype is determined using a two tailed *t*-test for proportions set at $p < 0.05$.

2.5 Validation of method

2.5.1 Combining structural and functional analysis with genetic manipulations

To examine how different molecules affect the mechanosensory neuron's targeting decisions, Gal4 lines can be used to drive expression of UAS lines solely within mechanosensory neurons. Different genes can be either overexpressed using the UAS promoter, or knocked down using UAS-dsRNA constructs for RNA interference. This method also allows for mosaic analysis of a molecule's cell-autonomous effects by using cell-type specific Gal4 drivers. As an example, we used the 455-Gal4 driver to express dsRNA against *Dscam* and *PlexA* solely within scutellar neurons (Hinz et al.,1994), and the DC-Gal4 driver to knock down *Dscam* solely within dorsocentral neurons (Garcia-Garcia et al., 1999) (**Figure 2.3**). Dscam has been previously shown to have an essential function within mechanosensory neurons for axonal branch targeting. Loss of Dscam causes a severe collapsed axonal arbor phenotype (Chen et al., 2006), whereas loss of PlexA causes supernumerary axonal branches to form throughout the arbor (Neufeld et al., 2011). The 100% penetrant phenotype of Dscam loss of function can be used as a benchmark to assess the strength of a Gal4 driver and screen through different mechanosensory

Gal4 lines by expressing *Dscam* dsRNA against and by comparing the extent of phenocopy. This obvious phenotype can also be used to determine the specificity of different Gal4 lines using dye labeling of different mechanosensory neurons to determine which neurons express Gal4 and produce the Dscam loss of function phenotype (**Figure 2.4**).

The most useful Gal4 drivers are those expressed in small subsets of cells. Confirming how restricted the expression of each Gal4 line is allows for manipulation of a few identifiable neurons within the context of a mosaic animal that is otherwise wildtype. Using multi-color dye labeling of the pSc and pDc neurons, we confirmed that the 455-Gal4 driver solely affected the scutellar neurons and produced wildtype phenotypes in dorsocentral neurons, and vice versa for the DC-Gal4 driver (**Figure 2.3**). Thus, multi-color imaging can serve as a control within the same animal to verify cell-autonomous phenotypes (**Figure 2.3**).

Furthermore, using specific Gal4 drivers to manipulate only mechanosensory neurons ensures that neurons and effector cells within the cleaning reflex circuitry that are downstream of the mechanosensory neuron remain unaffected, and any changes in behavioral response are due to changes within the mechanosensory neuron itself.

2.5.2 Correlating synaptic connectivity with grooming behavior in the same animal

We performed the combined structural/functional protocol using the 455-Gal4 line to express *Dscam* dsRNA within scutellar neurons, and confirmed that the loss of Dscam structural phenotype was always obvious qualitatively and quantitatively. For example, *Dscam* RNAi pSc "yes response" neurons ($n = 9$) had on average 5.2 ± 2.4 total axonal branches with a total arbor size of 260.6 ± 146.9 µm, and the *Dscam* RNAi pSc "no response" neurons ($n = 20$) had an

average of 4.7 ± 1.8 total branches and an arbor size of 279.1 ± 112.3 μm. In comparison, control 455-Gal4 "yes response" neurons (*n* = 14) had an average of 25.2 ± 3.2 axonal branches and an arbor size of 926.7 ± 92.9 μm and the 455-Gal4 "no response" neurons (*n* = 13) had 22.2 ± 5.2 average total branches and an arbor size of 870.5 ± 150.5 μm (**Figure 2.5**). As the pSc is the primary sensory neuron in the reflex circuit, the response rate of the *Dscam* RNAi animals was significantly reduced to only 7% that were able to detect pSc bristle stimulation (**Figure 2.5a**), and the few *Dscam* RNAi animals that could respond were likely due to the variability in dsRNA expression in the pSc neuron (**Figure 2.5b, c**). Dscam loss of function emphasizes the relationship between structural connectivity and neural function. Further negative controls can be used to verify Gal4 drivers to produce a complete loss of response, such as knockdown of genes involved in synaptic transmission.

2.5.3 Caveats and perspectives

By separating animals that succeed and fail to respond to mechanical stimulation and labeling the primary sensory neurons, we aim to correlate axonal structure to the ability of the animal to elicit a grooming reflex. The goal of such analysis is to determine the minimal identifiable branch requirements to successfully activate the downstream circuit. Our results show that even the very simple arbors in Dscam loss of function animals were sometimes able to elicit a response (**Figure 2.5**). There are several caveats that should be pointed out. In our protocol we are stimulating both left and right pSc neurons, therefore it is important that we have high quality labeling of both left and right axons. In addition, possibly due to neuron-to-neuron variability in dsRNA expression, we do observe differences in phenotype severity even within

the same animal, so that one side would be more severely affected than the other. In this situation, an animal may respond behaviorally if one of the neurons can compensate for loss of synaptic contacts of the other, or if the combination of left and right arbor is sufficient to activate the circuit.

It is important to note that in this protocol, we define a cleaning response simply as the rear pair of legs brushing the notum and the consequent transfer of the fluorescent dye onto the legs (**Figure 2.2d, e**). Thus, the data is grouped into a binary set of "yes response" and "no response." Analyzing only total branch numbers and lengths in 455-Gal4 control and *Dscam* RNAi genotypes, we found no significant difference between the "yes response" and "no response" neurons ($p > 0.05$) (**Figure 2.5b, c**). Our representative grooming behavior results illustrate that very large data sets are required to correlate specific synaptic connectivity patterns with behavioral outputs even when comparing only within control animals. In addition, several factors contribute to the cleaning response rate, such as the genetic background of the animal and the type of stimulus presented. For example, the response rate for pSc neurons in w^- wildtype flies at 34% ($n = 68$) is significantly higher than for *455-Gal4/+* controls at 19% ($n = 118$, $p < 0.01$) (**Figure 2.5a**). Previous studies examining response rates from stimulation of single macrochaeta have reported widely varying rates from 10% to 80% for the pSc neuron, possibly because of inconsistencies in the stimulation protocols using mechanical stimuli such as an eyelash or hair (Canal et al., 1998; Vandervorst and Ghysen, 1980; Corfas and Dudai,1989; Philis et al., 1993)

Response rates increase with viscosity of the solvent used to dissolve the fluorescent dye, so that when DiO was dissolved in DMF, a more viscous solvent than ethanol, pSc neurons produced greater response rates proportionally across all genotypes being examined (Cvetkovska

et al., 2013). Thus, the behavioral assay can be further enhanced by optimizing the viscosity of the solvent used for the fluorescent dye which may allow for increased differentiation between "yes response" and "no response" synaptic connectivity patterns. For the "yes response" group, the assay could also be further developed to potentially quantify the level of cleaning efficiency, for example in the amount of fluorescent dye removed (Melzig et al.,1996), to further correlate specific synaptic connectivity with a quantitative behavioral output. Finally, future experiments combining functional imaging (i.e., optical physiology) (Jin et al., 2012) with single neuron sequencing (Xu et al., 2012; Evrony et al., 2012) of physically isolated mechanosensory neurons will further bridge the relationships between genes, neuronal structure, synaptic targeting and function, and animal behavior.

2.6 Figures

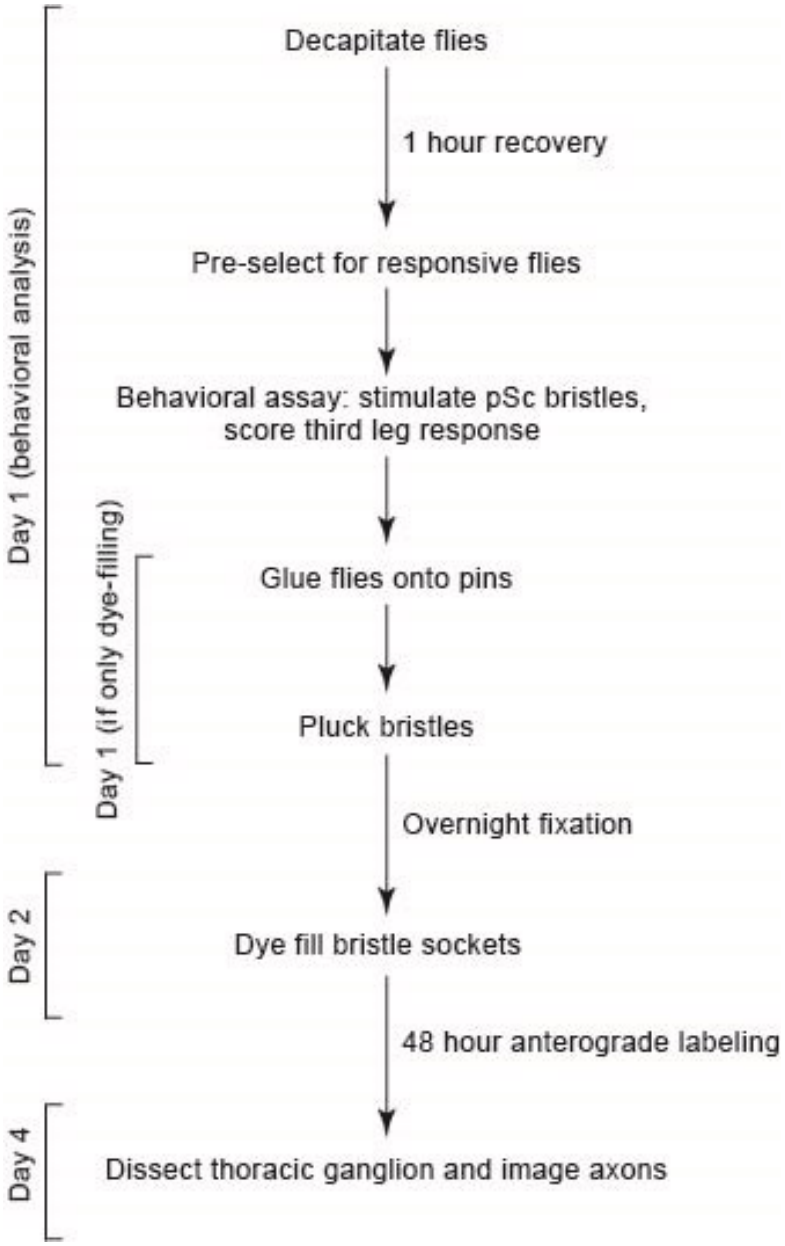

Figure 2.1 Flowchart of the experimental procedure.

From behavioral assay to imaging axonal morphology, the experimental procedure is performed in 4 days.

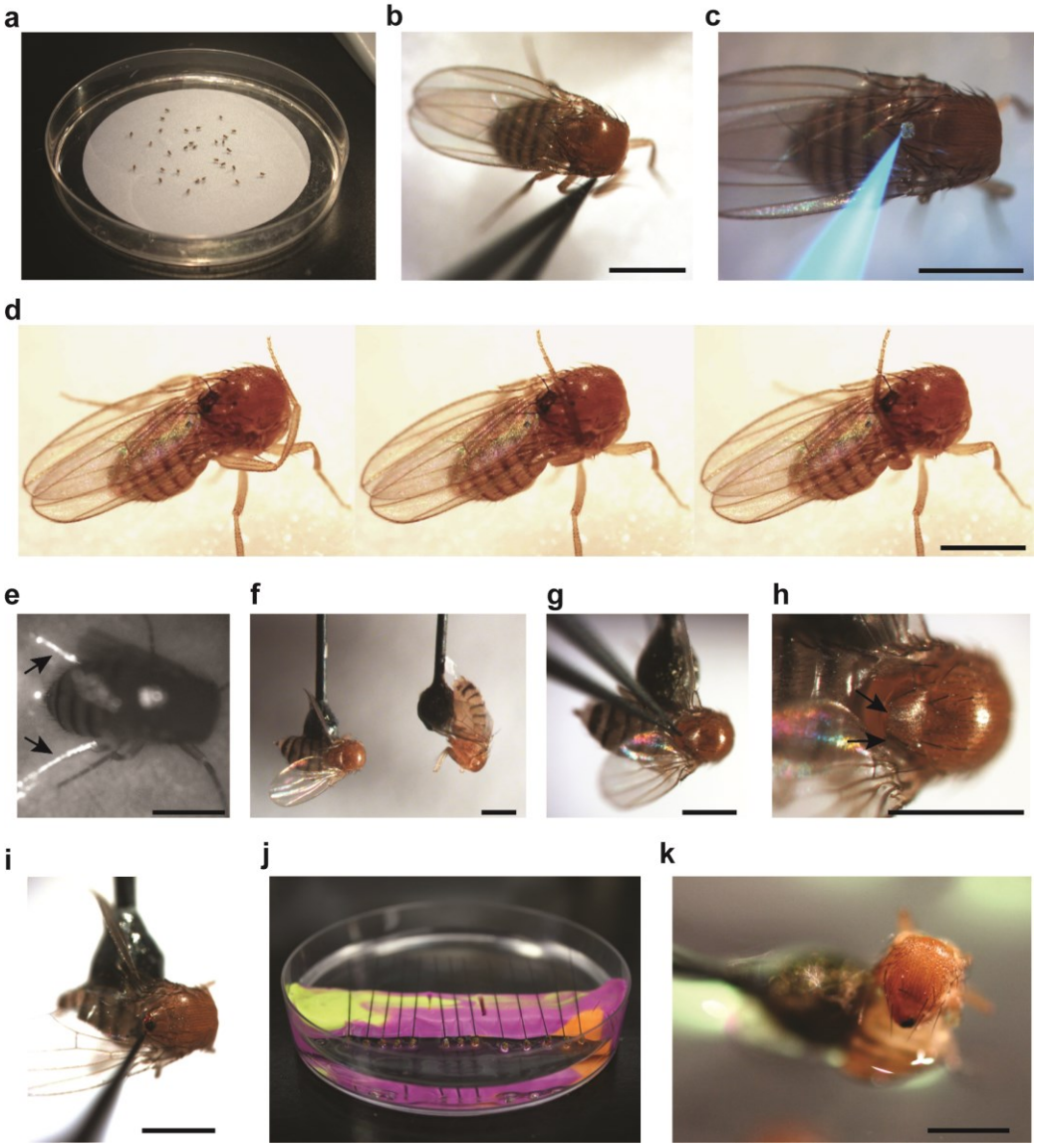

Figure 2.2 The behavioral output and structure of a single mechanosensory neuron can be measured in single animals.

a, After decapitation, flies are left to recover for 1 hour in a humidified chamber made from a 15 cm petri dish with PBS soaked filter paper. The decapitated flies should be standing on the filter paper after recovery from CO_2 anesthesia.

b, Behaviorally responsive flies are preselected for by stimulating the anterior notopleural bristle using fine forceps. The fly will react using its first leg to brush the stimulated area.

c, Stimulation of the pSc bristle is performed by applying DiO fluorescent dye only at the tip of the scutellum, and the dye should only deflect the two pSc bristles.

d, Upon pSc stimulation, the third leg of the fly will brush the entire notum, starting at the anterior dorsocentral region and progressing to the posterior tip of the scutellum. Blue DiD dye is shown for clarity.

e, The fluorescent dye will be transferred to the rear legs upon a positive cleaning response (arrows).

f, Flies are glued onto insect pin heads for bristle plucking. The lateral side of the flies can be either glued perpendicular to the pin head for access to the dorsally located bristles, or along the abdomen, parallel to the pin head for access to the laterally-located bristles.

g, Bristles are plucked using fine forceps by pulling against the direction of growth and close to the base. Plucking of a pSc bristle is shown.

h, Bristle sockets should be completely exposed (arrows) to allow access of the dye to the neuron underneath.

i, Bristle sockets are dye-filled with DiI (red, left pSc), and DiD (blue, right pSc).

j, Dye-filled flies are placed on clay and left undisturbed and protected from light in a 10 cm petri dish with 0.2 M carbonate-bicarbonate buffer.

k, A close-up view of a half-submerged fly is shown. The abdomen should be submerged in buffer and the upper thorax with the dye-filled sockets kept above the surface of the buffer. Scale bars are 1 mm.

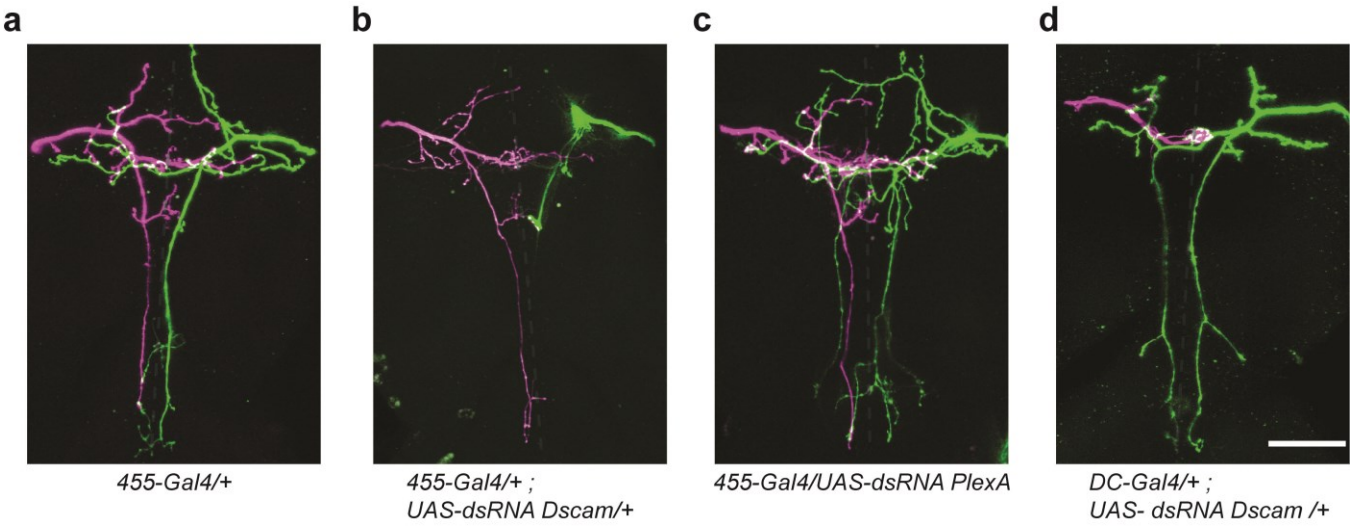

Figure 2.3 Different Gal4 drivers can be used to express dsRNA solely within specific mechanosensory neurons.

a, The 455-Gal4 driver is scutellar-specific and expresses only in the four scutellar mechanosensory neurons, the left and right aSc and pSc neurons. A representative example of the pDc (magenta) and pSc (green) neurons' axonal arbors in a control *455-Gal4/+* animal is shown.

b, RNAi-mediated knockdown of *Dscam* only in the scutellar mechanosensory neurons in a *455-Gal4/+ ; UAS- dsRNA Dscam /+* animal results in a characteristic *Dscam* null phenotype in the pSc axon (green) with clumped axonal branches, while the pDc axon (magenta) remains unaffected.

c, Gal4 driving UAS expression of double stranded RNA against *PlexA* in a *455-Gal4/UAS-dsRNA PlexA* animal results in a characteristic PlexA knockdown phenotype in the pSc neuron (green) with excessive, supernumerary branches, while the pDc (magenta) remains unaffected.

d, The DC-Gal4 driver expresses UAS constructs only in the four dorsocentral neurons. Specificity of the driver is shown in a *DC-Gal4/+ ; UAS- dsRNA Dscam /+* animal, where the pSc neuron is unaffected (green) and the pDc neuron (magenta) exhibits a *Dscam* null phenotype. Dotted lines mark the midline of the CNS. Scale bar is 50 μm.

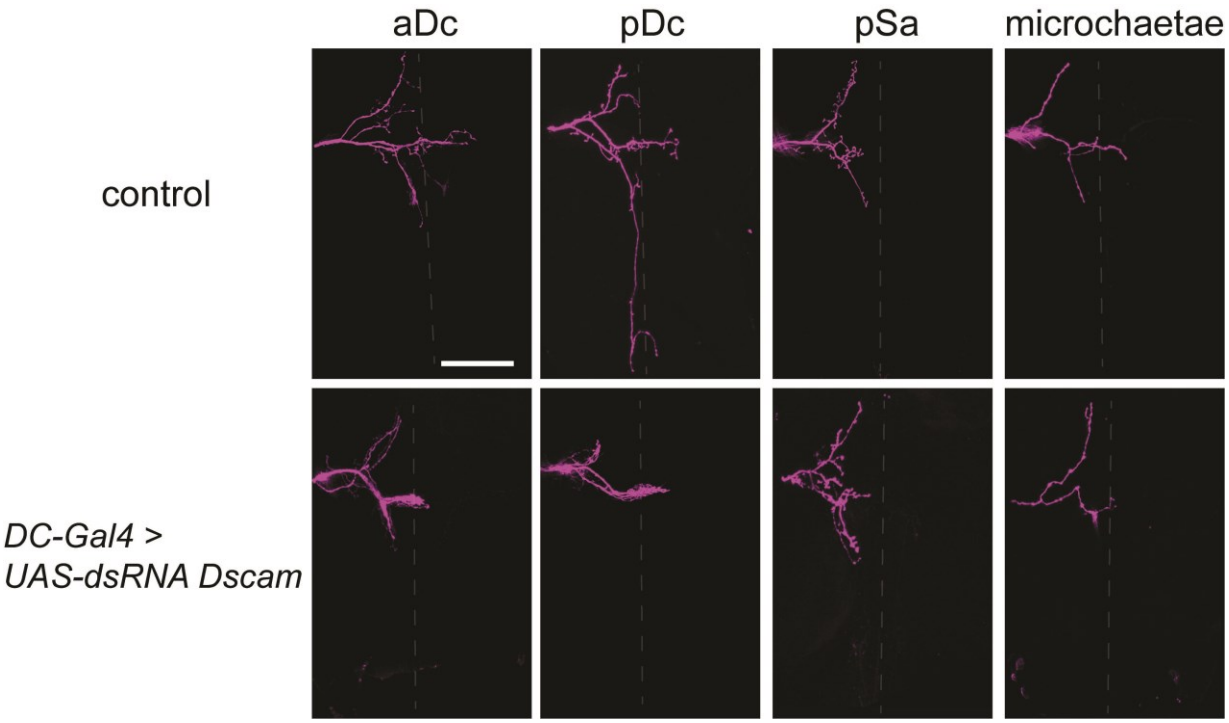

Figure 2.4 The Dscam loss of function phenotype can be used to test the specificity of Gal4 drivers in different mechanosensory neurons

The specificity of the DC-Gal4 driver for only the dorsocentral mechanosensory neurons was confirmed by RNAi-mediated knockdown of *Dscam*. The collapsed axonal arbor characteristic of Dscam loss-of-function was observed solely in the aDc and pDc neurons. The closely located pSa neuron and microchaetae had unaffected axonal arbors in *DC-Gal4/+ ; UAS- dsRNA Dscam /+* animals.

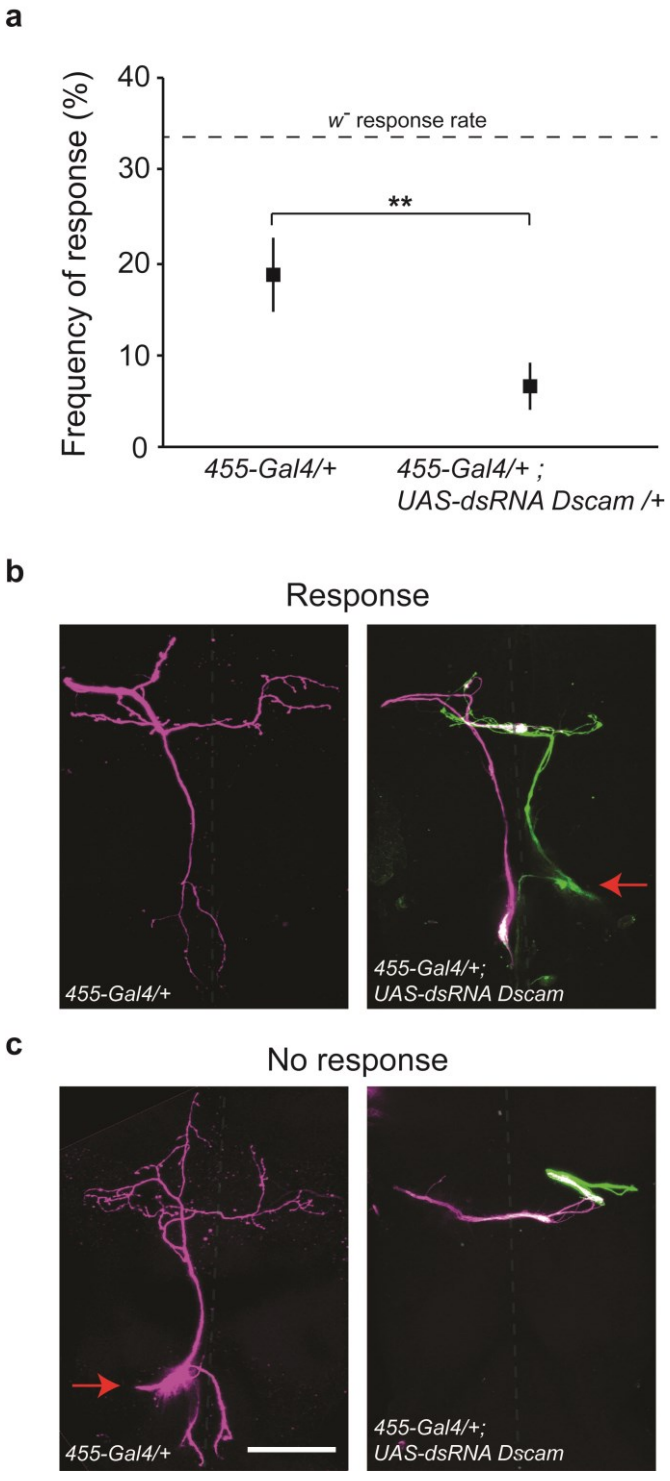

Figure 2.5 Specific Gal4 drivers for the presynaptic mechanosensory neuron can be combined with a behavioral assay to examine the functional output of the neuron after experimental manipulations.

a, Knockdown of Dscam specifically in the scutellar neurons severely impairs behavioral output and synaptic targeting. Stimulation of the pSc neurons in *455-Gal4/+ ; UAS- dsRNA Dscam /+* animals resulted in severely impaired behavioral output, compared to *455-Gal4/+* controls (*t*-test for proportions, $p < 0.01$). Only 7% of RNAi animals ($n = 114$) responded to pSc stimulation, while 19% of *455-Gal4/+* controls ($n = 118$) elicited a cleaning reflex. For comparison, the response rate of wildtype w^- flies are shown as a reference (dotted line).

b, c, Representative images of dye filled pSc axons in *455-Gal4/ +* controls and *455-Gal4/+ ; UAS- dsRNA Dscam/+* animals that succeeded or failed to respond to pSc stimulation. *455-Gal4/+ ; UAS- dsRNA Dscam/+* animals have severely reduced axonal arbors. Correlating axonal morphology with behavioral output can provide a link between specific synaptic connectivity and neural function, such as the extending branches in *455-Gal4/+ ; UAS- dsRNA Dscam/+* positive responding neurons, shown in the representative image. Red arrows indicate axon guidance errors. Dotted lines mark the midline of the CNS. Scale bar is 50 µm.

Chapter 3

Overexpression of Down Syndrome Cell Adhesion Molecule impairs precise synaptic targeting

3.1 Relation to overall project

In previous studies (Chen et al., 2006) and in the experiments outlined in **Chapter 2** it was shown that Dscam has a critical role in the targeting of mechanosensory axons. The human *Dscam* gene is located within the Down Syndrome Critical Region, a chromosomal region that when triplicated is sufficient to cause Down syndrome phenotypes. Given its important role in synaptic targeting and its possible link to Down syndrome, we hypothesized that Dscam overexpression may impair synaptic targeting and consequently lead to circuit dysfunction. In the following study we examined how excessive expression of Dscam protein by two mechanisms, either through gene triplication or through dysregulation of protein synthesis, contributes to miswiring of neuronal circuits.

3.2 Abstract

Fragile X syndrome is caused by loss of Fragile X Mental Retardation Protein (FMRP), an RNA binding protein that suppresses protein translation. We identified *Down Syndrome Cell Adhesion Molecule* (*Dscam*) RNA, a molecule involved in neural development and implicated in Down syndrome, bound to FMRP. Elevated Dscam protein levels in *Drosophila* FMRP null animals and in animals with three copies of the *Dscam* gene both produced specific and similar synaptic targeting errors in a hard-wired neural circuit which impaired the animal's sensory perception. Reducing Dscam levels in FMRP null animals reduced synaptic targeting errors and rescued behavioral responses. These results demonstrate that excess Dscam protein may be a common molecular mechanism underlying altered neural wiring in major causes of intellectual disability.

3.3 Introduction

The formation of inappropriate neuronal connections is thought to underlie the behavioral and cognitive deficits in human disorders such as intellectual disability syndromes, Autism Spectrum Disorders, and schizophrenia (Mitchell, 2011). While the precise etiology and the genetic factors that cause complex disorders such as autism are still largely unclear, the causes of the two most common intellectual disabilities, Down syndrome and Fragile X syndrome, have been known since the second half of the last century (Lejeune et al., 1959; Pieretti et al., 1991; Fu et al., 1991). Yet, the mechanisms that lead to improper neuronal wiring in these disorders are not known. It is also not known whether the overlapping neural phenotypes of neurodevelopmental disorders arise due to shared mechanisms.

It is an interesting observation that both Fragile X and Down syndrome are characterized by elevated protein levels. In the case of Down syndrome this is due to triplication of chromosome 21 and increased expression of all the genes located there. In Fragile X syndrome, transcriptional silencing of the *Fragile X Mental Retardation 1* (*Fmr1*) gene through expansion of a trinucleotide CGG repeat in the gene locus (Verkerk et al., 1991, Verheij et al., 1993) leads to loss of its protein product, Fragile X Mental Retardation Protein (FMRP). FMRP is an RNA binding protein that binds approximately 4% of brain mRNAs (Ashley et al., 1993; Brown et al., 2001; Darnell et al., 2001; Miyashiro et al., 2003). FMRP can form complexes with ribonucleoprotein particles to interfere with the initiation and elongation step of translation, and so is generally thought to negatively regulate protein synthesis (Laggerbauer et al., 2001; Li et al., 2001). Thus in Fragile X syndrome, loss of FMRP results in excessive protein synthesis of the RNAs that FMRP would normally suppress (Bassel and Warren, 2008).

Thousands of RNA targets of FMRP have been discovered using high-throughput RNA sequencing or microarray screens in an effort to identify key molecules involved in Fragile X syndrome and Autism Spectrum Disorders (Ascano et al., 2012; Brown et al., 2001; Darnell et al., 2011). One RNA target identified in these screens is *Down Syndrome Cell Adhesion Molecule* (*Dscam*) (Brown et al., 2001; Darnell et al., 2011). In humans, *Dscam* is a large gene (~800 kilobases) located in the Down Syndrome Critical Region, a 4 megabase region in Chromosome 21 implicated in many Down syndrome phenotypes (Takashima et al., 1981; Antonarakis et al., 1998; Yanakawa et al., 1998; Korenberg et al., 1994; Barlow et al., 2001; Hildmann et al., 1999; Alves-Sampaio et al., 2010). Dscam is a member of the immunoglobulin superfamily of cell surface receptors with conserved functions in neural development across invertebrates and vertebrates such as axon guidance, axonal and dendritic branching and targeting, and synapse maturation (Schmucker and Chen, 2009). *Drosophila Dscam* is identical in protein domain structure to its vertebrate homolog (Schmucker and Chen, 2009) however it has a unique feature: through alternative splicing, the gene can produce more than 100,000 different protein isoforms (Schmucker et al., 2000; Yu et al., 2009). This extensive isoform diversity has been proposed as a synapse-specific molecular label through homophilic binding of Dscam isoforms on two cells (Schmucker and Flanagan, 2004). However, it remains unclear exactly how Dscam is used in axons to specify correct targets. It is also not known how overexpression of Dscam could result in miswiring of neural connections, as might occur in Down syndrome.

We examined how excessive levels of Dscam protein affect the fine-scale targeting of single mechanosensory axons in *Drosophila*. We found that Dscam is a target of translational regulation by FMRP, and that correct levels of Dscam protein are required for proper axonal

targeting and circuit function. This study provides evidence that overexpression of Dscam may contribute significantly to the miswiring phenotypes in Fragile X syndrome and Down syndrome.

3.4 Materials and Methods

3.4.1 *Drosophila* Strains

The following $dFmr^{null}$ fly stocks were used: $dFmr^{3}$ (F. Bolduc, University of Alberta), $dFmr^{\Delta 113}$, $dFmr^{\Delta 50M}$, and *Df(3R)Exel6265* (A.P. Haghighi, McGill University) , and have been verified to lack FMRP (Figure 1) (Dockendorff et al.,2002; Bolduc et al., 2008; Zhang et al., 2001). Trans-heterozygous mutant flies were generated by mating $dFmr^{\Delta 50}$/*TM6b* or $dFmr^{\Delta 113}$/*TM6b* with $dFmr^{3}$/*TM6, Sb, Tb* or *Df(3R)Exel6265*/*TM6b*. To overexpress FMRP, flies homozygous for an extra copy of the entire *dFmr* transcriptional unit were used, thus expressing four copies of *dFmr* (Dockendorf et al., 2002).

Flies with site-specific insertions of a bacterial artificial chromosome (BAC) containing the entire genomic locus of *Dscam* were used to express an extra copy of the *Dscam* gene (H. Bellen, Howard Hughes Medical Institute, Baylor College of Medicine) (Venken et al., 2006). Lines *5-*, *7-*, *13-*, *19-*, *20-* and *33-*$Dscam^{BAC}$ were used for experiments. Flies with three copies of *Dscam* were obtained by crossing $Dscam^{BAC}$ homozygotes with w^{-} flies. *5-*$Dscam^{BAC}$/+ and *20-*$Dscam^{BAC}$/+ are shown in **Figure 3.5e.**

$Dscam^{21}$/*CyO* and $Dscam^{23}$/*CyO* (W. Grueber, Columbia University) were used as $Dscam^{null}$ mutants (Schmucker et al., 2000). $Dscam^{null}$ mutants are embryonic lethal, so

Dscam^{null} early embryos were collected for negative controls in the immunoblotting experiments (Chen et al., 2006). Double mutant flies heterozygous for *Dscam* and homozygous null for *dFmr* were created by mating *Dscam*^{23}*/CyO; dFmr*^{3}*/TM6b* to *dFmr*$^{\Delta 113}$*/TM6b* flies. *Dscam*^{23}/+; *dFmr*$^{\Delta 50M}$*/dFmr*^{3} and *Dscam*^{23}/+; *dFmr*$^{\Delta 113}$*/dFmr*^{3} are shown in **Figure 3.5f**.

For RNAi experiments, we used the following *UAS-dsRNA-dFmr* lines: RNAi lines (*2-1*), (*1-7*) and (*1-10*) (F. Bolduc, University of Alberta) (Bolduc et al., 2008), and line 8933 from the Vienna *Drosophila* RNAi Center (Vienna, Austria). Fragile X mutants *dFMR*$^{\Delta 113}$*/dFmr*^{3}and *dFmrRNAi*^{8933}are shown in **Figure 3.5d**. Gal4 expression within only the scutellar neurons was achieved using the *455-Gal4* line (Hinz et al., 1994). To reduce Dscam levels in *dFmr* RNAi knockdowns, *455-Gal4/CyO; UAS-dsRNA-dFmr* animals were crossed to *Dscam*^{23}*/CyO; UAS-dsRNA-dFmr*. To overexpress FMRP only within the scutellar neurons, *455-Gal4/CyO* animals were crossed to *UAS-dFmr* (F. Bolduc, University of Alberta).

3.4.2 Immunoprecipitation and RT-PCR

Immunoprecipitation experiments were performed in quintuplicate using adult fly brains and verified in sextuplicate from third instar wandering larval brains. FMRP-mRNA complexes were immunoprecipitated from wildtype or *dFmr*^{null} samples using mouse monoclonal anti-FMRP antibody 6A15 (Abcam, Cambridge, MA) coupled to protein G Dynabeads (Life Technologies, Carlsbad, CA). Eluted mRNAs were used as template for RT-PCR using the following gene-specific reverse transcription primers: *dFmr* CTCTCTCCACGCTGCTCATT, *Dscam(Exon 11)* TGATCATAATCACAGCCGAGAGG, and *Futsch* CTCGCTGGAAGTCTTTGTCC. PCR amplification was performed using the following forward and reverse primers (respectively for each gene): *dFmr*

CGTGCCCGAGAGTATGAAAT, GTCTCAAAACCGATGTACGC; *Dscam* CAACGGAGATGTGGTTTCCT, GGTTATCTCGCTCCCAGACA; *Futsch* ATCACCGCAAGTTTTGAAGG, GCGAAGTCTTTTGGTGCTTC. All other mouse monoclonal antibodies used for immunoprecipitation were obtained from the Developmental Studies Hybridoma Bank. Immunoprecipitation of FMRP-mRNA complexes was also confirmed using another mouse monoclonal antibody 5B6 (developed by K.S. Broadie). Immunoprecipitation of ELAV-mRNA complexes was performed using the mouse monoclonal antibody 9F8A9 (developed by G.M. Rubin) and actin complexes were immunoprecipitated using the mouse monoclonal antibody JLA20 (developed by J.J-C. Lin).

3.4.3 Pyrosequencing

Immunoprecipitation was performed on adult fly brains using both the 5B6 and 6A15 monoclonal antibodies. Reverse transcription of mRNA extracted from input and immunoprecipitated samples was performed using *Dscam*-specific reverse primers for Exon 11 and Exon 7, CCGCCGATTCCTGGTCGTTTCTTAC. The cDNA was PCR amplified using 454 Lib-L unidirectional sequencing fusion primers containing the 454 adaptor sequence (Primer A/forward CCATCTCATCCCTGCGTGTCTCCGACTCAG; Primer B/reverse CCTATCCCCTGTGTGCCTTGGCAGTCTCAG) and target-specific sequences for Exon 4 forward AAGCTGGTCTTCCCTCCATT and reverse CTCTCCAGAGGGCAATACCA, Exon 6 forward AGTGCCACAAAAGGACGATT and reverse GCTTGTTTACGGGTTGTTCC and Exon 9 forward CTACACTTGCGTTGCCAAGA and reverse TCAGCCTTGCATTCAACCTT. The PCR products were sequenced using the Roche GS-FLX Titanium sequencer. Samples were prepared in experimental triplicates and pyrosequencing experiments were verified in two

sequencing runs. Sequences were analyzed using a custom written program in MatLab (MathWorks, Natick, MA) to identify isoforms, and positive identification of isoforms was established for ~70% of sequences. A frequency distribution of isoforms was generated for each exon, experimental replicate, and sample. A goodness-of-fit test based on the chi-square distribution was used to calculate statistical significance between frequency distributions of samples. For visual display of isoform frequency distributions, heatmaps were generated using MatLab (MathWorks).

3.4.4 Quantitative Real-Time PCR

Total RNA was extracted from adult fly heads using Trizol reagent (Life Technologies). Reverse transcription was performed using a *Dscam*-specific reverse primer and a *Ribosomal Protein 49* (*Rp49)*-specific reverse primer CATCAGATACTGTCCCTTGAAGC. Taqman Fast-Advanced Master Mix (Life Technologies) was used with the following primers and double quenched 5'-FAM/ZEN/IowaBlackFQ-3' probes (Integrated DNA Technologies, Coralville, IA): *Rp49* forward GCGCACCAAGCACTTCATC, *Rp49* probe 5'-FAM-ATATGCTAAGCTGTCGCACAAATGGC-IBFQ-3', *Rp49* reverse GACGCACTCTGTTGTCGATACC, *Dscam* forward ACGATGTAGTTTACAATCAGACAA, *Dscam* probe 5'-FAM-ACCTGCGGGATGAGCTCGGATACA-IBFQ-3', *Dscam* reverse GCCTCGCTTAATCCGGTCA. PCR amplification was detected using the Applied Biosystems StepOne Plus Real Time PCR System (Life Technologies) and cycle threshold (CT) values calculated using the StepOne software. Experiments were performed in six experimental replicates with three to six technical replicates. CT values were normalized to *Rp49* control levels and technical replicates were averaged within each experimental replicate. *Dscam* mRNA

levels from experimental genotypes were compared to wildtype levels from within the same experiment and reported as fold changes from wildtype.

3.4.5 Immunoblotting and Protein Quantification

Immunoblot protein quantification experiments were performed nine times using third instar wandering larval brains and replicated in duplicate in adult brains. Proteins were separated by electrophoresis on a NuPAGE Novex 12% Bis-Tris Gel (Life Technologies) and transferred to a polyvinylidene fluoride membrane. The membrane was incubated with the following antibody dilutions: 1:1000 anti-Dscam rabbit polyclonal (J. Clemens, Purdue University), 1:250 anti-dFmr 6A15 mouse monoclonal (Abcam), and anti-actin C4 mouse monoclonal (CedarLane, Burlington, ON). Secondary antibodies used were fluorescent anti-rabbit IRDye CW800 and anti-mouse IRDye CW800 (LI-COR, Lincoln, NE). Proteins were visualized using the Odyssey infrared imaging system (LI-COR). Protein bands were quantified by averaging the intensities of five randomly chosen 3x3 pixel regions, and Dscam and FMRP levels were normalized to actin.

3.4.6 Immunohistochemistry and Fluorescence *In Situ* Hybridization

Immunohistochemistry experiments on identified mechanosensory neurons were performed 15 times in wildtype, 12 times in $dFmr^{null}$, and 3 times for *dFmr* RNAi animals. Co-labeling of fluorescence *in situ* hybridization for *Dscam* mRNA with fluorescence immunohistochemistry for FMRP within identified pSc neurons was reproduced 8 times. Cryosections of the thorax along the rostral-caudal, dorsal-ventral axis were cut at 10 µm thickness from adult female flies. Custom fluorescent RNA probes against *Dscam* were designed to bind all isoforms within the constant mRNA sequences, and were conjugated to the

Quasar670 dye (Biosearch Technologies, Novato, CA). Fluorescence immunohistochemistry with fluorescence *in situ* hybridization was performed as described (Raj et al., 2008). Mouse monoclonal antibody 5A11 for FMRP (developed by H. Siomi) at 1:100, or mouse monoclonal antibody 5B6 for FMRP at 1:100 was added for overnight incubation. Secondary antibody goat anti-mouse AlexaFluor488 (Life Technologies) was applied during the wash steps, and a Hoechst dye was applied on the final wash to label nuclei.

Fluorescence microscopy was performed using an Olympus laser scanning confocal microscope FV1000. Fluorescence *in situ* hybridization images were acquired using a 60× oil objective, N.A. 1.4. Quantitative analysis of FMRP intensities was performed by measuring the average pixel intensity in the FMRP channel in a region of interest centered around the nucleus of the mechanosensory neuron. Knockdown efficiency of the *UAS-dsRNA-dFmr* was thus quantified from three experiments and compared to FMRP intensities from wildtype neurons in three experiments.

3.4.7 Carbocyanine dye labeling and imaging

Lipophilic dye labeling of single mechanosensory axons was performed as described in the detailed protocol in **Chapter 2**.

3.4.8 Image Analysis

Image analysis, branch measurements and statistical analysis were performed as described in **Chapter 2**. A total of 74 wildtype, 100 $dFmr^{null}$, 74 Dscam X3, 84 $Dscam^{null}$/+; $dFmr^{null}$ double mutant animals were analyzed. Sample sizes were chosen based on previous studies (Chen et al., 2006; Neufeld et al., 2011). Qualitative analysis of axonal targeting

variability was performed blind to genotype by shuffling the axonal arbor data among all genotypes and 28 different targeting variability types were identified. Wildtype variability was identified (12 types), and 16 error types were found with a frequency of less than 10% in wildtype. Errors in all 16 categories were found in *dFmr*^{null} animals. Dscam X3 animals had errors in 15 categories, but five of these 15 error types were not significantly different from wildtype, thus the ten error types significantly higher in both *dFmr*^{null} and Dscam X3 mutants compared to wildtype were defined as the targeting error phenocopy. Fragile X mutant targeting errors were considered rescued in the double mutant animals if the error frequency was significantly lower in the double mutant than in the *dFmr*^{null}.

3.4.9 Behavioral Analysis

The behavioral assay was performed as described in the detailed protocol in **Chapter 2**. The scutellum specific 455-Gal4 driver was used to drive *UAS-dsRNA-dFmr* only in the four scutellar mechanosensory neurons to ensure that the postsynaptic neural circuitry was left unperturbed by the gene manipulations. Experiments were performed on two day old female flies with the experimenter blind to genotype. A total of 121 w^- controls, 121 *455-Gal4*/+ controls, 125 *UAS-dsRNA-dFmr* controls, 77 *Dscam*^{23}/+ controls, 120 Dscam X3, 139 *455-Gal4*/+; UAS-*dsRNA-dFmr* mutants, and 120 double mutant (*Dscam*^{23}/*455-Gal4*; *UAS-dsRNA-dFmr*) animals were analyzed using DiD stimulation (40 mg/ml in ethanol). Sample sizes were chosen based on previous studies (Canal et al., 1998; Corfas and Dudai, 1989; Phillis et al., 1993). All behavioral results were verified using DiO dissolved in DMF, a more viscous solvent, to stimulate the pSc bristles which produced greater response rates in all genotypes, and produced identical results among genotypes.

3.5 Results

3.5.1 FMRP binds *Dscam* mRNA to suppress its translation

We identified *Dscam* RNA as a target of FMRP by immunoprecipitation of FMRP from *Drosophila* brains (**Figure 3.1a**). Several controls were done to confirm the specificity of this RNA-protein interaction. *Dscam* RNA did not immunoprecipitate with a different neuronal RNA binding protein, ELAV, nor in FMRP null mutant brains (**Figure 3.1a**). ELAV has been shown to associate to the 3′ untranslated region of *brat* mRNA (Hilgers et al., 2012), and this was used as a positive control of ELAV-mRNA complex precipitation (**Figure 3.2a**). Immunoprecipitation of other proteins, such as actin, did not co-precipitate any mRNAs (**Figure 3.2b**)

The physical interaction between *Dscam* mRNA and FMRP is required for the suppression of Dscam protein translation, as Dscam protein levels were elevated in FMRP null mutants at amounts similar to animals with 3 copies of the *Dscam* gene (**Figure 3.1b**). Conversely, animals with multiple copies of the *Drosophila Fragile X Mental Retardation* (*dFmr*) gene had a lower Dscam protein expression compared to wildtype, and even a modest increase in FMRP levels decreased Dscam protein by approximately 60% (**Figure 3.1b**). The sensitivity of this bi-directional change in protein levels demonstrated a tight regulation of Dscam protein translation by FMRP. These results demonstrate that FMRP suppresses Dscam protein expression at the level of translation and not by affecting mRNA stability or turnover, as *Dscam* mRNA levels remained unchanged in FMRP null animals (**Figure 3.1c**).

3.5.2 Dscam and FMRP are expressed in identifiable mechanosensory neurons

To understand how this regulation of Dscam expression by FMRP is involved in neural wiring, we used the hard-wired mechanosensory neural circuit to quantitatively analyze axonal targeting decisions (Ghysen, 1980; Chen et al., 2006; Neufeld et al., 2011) (**Figure 3.3**). As discussed in **Chapters 1** and **2**, a single mechanosensory neuron innervates a single bristle on the back of the fly, and because each bristle is uniquely identifiable, the same neuron among different animals can be identified based on the location of its corresponding bristle. In this study, we focused our analysis on the left and right posterior scutellar (pSc) neurons, and we verified FMRP expression within identified pSc neurons using immunohistochemistry in combination with fluorescent *in situ* hybridization for *Dscam* mRNA (**Figure 3.3a-d**). The pSc neuron extends its axon into the central nervous system and synapses with specific interneurons, giving it a stereotyped and unique axonal arbor (**Figure 3.3e**) (Ghysen, 1980). To quantitate the variability of this synaptic targeting in wildtype animals, we measured the branch lengths and positions of the pSc axonal arbor in 74 wildtype animals and identified a prototypical "skeleton" comprised of 16 core branches occurring at >80% frequency for primary and secondary branches and >60% frequency for tertiary branches (**Figure 3.3f, g**). Axonal branches were considered ectopic if they occurred in less than 10% of wildtype flies and this was used as a cutoff for the definition of a targeting error (**Figure 3.4**). Variable branches were thus defined as occurring at greater than 10% and less than 60% frequency.

3.5.3 Loss of FMRP produces axonal targeting errors

Quantitative analysis of $dFmr^{null}$ axonal arbors revealed a significant increase in the cumulative branch length of the pSc arbor due to a significant increase in the number of ectopic

branches in the mutants (3.4 branches, $n = 99$, $p < 0.001$) compared to wildtype (1.6 branches, $n = 74$) (**Figure 3.5a**). These increases in axonal arbor sizes in Fragile X mutants were not due to non-specific overall growth, as the lengths of the branches that comprised the pSc "skeleton" were unaffected (**Figure 3.5b**). The sprouting of ectopic branches in the $dFmr^{null}$ animals was not random as they occurred at highly specific and identifiable locations in the prototypical pSc skeleton in the anterior, middle, and posterior regions of the central nervous system (**Figure 3.5**). However, Fragile X mutants had many more stereotyped targeting errors besides ectopic branches, including branch misrouting and midline crossing errors, and missing branches from the skeleton (**Figure 3.5**). As expected from a total loss of FMRP regulation of many RNA targets that could be involved in aspects of axon branching, more than 85% of $dFmr^{null}$ animals had targeting errors, with 59% also having multiple errors within their axonal arbors compared to only 2% of wildtype animals ($p < 0.001$).

Several controls were performed to confirm the validity of the observed phenotypes. We verified that these errors were due to loss of FMRP within mechanosensory neurons by using a specific Gal4 driver (455-Gal4) to express dsRNA against *dFmr* only within the four neurons on the scutellum of the fly (Neufeld et al., 2011; Hinz et al., 1994). Axonal targeting errors within these mosaic animals phenocopied the targeting errors observed in whole animal Fragile X mutants and immunostaining for FMRP protein in the neuron soma was 76% reduced compared to wildtype (**Figure 3.6a, b**). To minimize the effects of secondary mutations and to confirm that FMRP null phenotypes were not specific to any particular *dFmr* null allele, we used multiple null alleles in transheterozygous combinations and a deficiency line that has the entire *dFmr* gene deleted. By re-introducing a genomic copy of *dFmr* (*gdFmr*) in a FMRP null background we were able to rescue both the protein expression and the pSc axonal targeting errors (**Figure 3.7**).

3.5.4 Three copies of Dscam phenocopies axonal targeting errors of Fragile X mutants.

Dscam has previously been shown to have an essential function in axonal branch targeting of the pSc neuron, but not for the initial axon guidance into the central nervous system (Chen et al., 2006). We confirmed that loss of Dscam within pSc neurons collapsed the entire axonal arbor in 100% of animals, with axonal branches extending in single directions before curving back onto the primary branch (**Figure 3.6c**, also see **Figures 2.3b** and **2.5b,c**). Thus, because Dscam is critical for pSc axonal arbor formation and its protein expression is regulated by FMRP, we examined how axonal targeting is affected solely by increased Dscam protein levels rather than through loss of FMRP regulation. BAC transgenic flies containing the entire genomic locus of *Dscam* were used to express an exogenous copy of the *Dscam* gene (Venken et al, 2006). We analyzed the axonal arbors of flies that have three copies of the *Dscam* gene (Dscam X3), reflecting the Down syndrome trisomy 21 case. To control for any dominant phenotypes of the exogenous $Dscam^{BAC}$ that could be misinterpreted as being due to Dscam overexpression, we expressed $Dscam^{BAC}$ in a Dscam null background and found that the exogenous copy produces functional Dscam protein (demonstrated by rescuing the lethality of Dscam null animals), and that these animals had wildtype-looking pSc axons (**Figure 3.8**).

We found that more than 65% of Dscam X3 pSc neurons had axonal targeting errors, and 30% had multiple errors within their arbors ($n = 74$, $p < 0.001$ compared to wildtype). Similar to Fragile X mutants, Dscam X3 animals also had a significant increase in the number of ectopic branches in their pSc axonal arbors (3.2 ectopic branches per animal, $p < 0.001$ compared to wildtype) (**Figure 3.5**). Analysis of the axonal targeting phenotypes in Dscam X3 animals revealed that they were stereotyped and also similar to many of the errors observed in the Fragile X mutants (**Figure 3.5e**). To measure the degree of overlap in targeting error phenotypes among

different genotypes, we performed a blind analysis by shuffling the imaging data from the control and experimental groups. Twelve variability phenotypes occurring in wildtype and sixteen different error types were categorized among the data, occurring mostly within the *dFmr*^{null} genotype since Fragile X mutants had significantly higher occurrences of all error categories (**Figure 3.4**). Ten of these 16 errors were found to overlap between Dscam X3 and Fragile X mutants, and no targeting errors were observed in Dscam X3 animals that did not also occur in Fragile X mutants (**Figure 3.5g** and **Figure 3.4**). These targeting errors were specific for Dscam and Fragile X mutants, as overexpression of other neuronal receptors did not result in these error types and did not produce stereotyped errors (**Figure 3.9**). Thus, overexpression of Dscam from having three copies of the gene can reproduce a large majority of axonal targeting phenotypes present in Fragile X mutant animals.

3.5.4 Reducing Dscam levels in Fragile X mutants decreases targeting errors

To determine the contribution of elevated Dscam levels to the axonal targeting defects in *dFmr*^{null} animals, we examined double mutant animals that are heterozygous null for *Dscam* and homozygous null for *dFmr* (*Dscam*^{null}/+; *dFmr*^{null}/*dFmr*^{null}). Removing one copy of the *Dscam* gene reduced the Dscam overexpression in *dFmr*^{null} animals by approximately 40% (**Figure 3.1b**). Analysis of the axonal arbors of these *Dscam*^{null}/+; *dFmr*^{null} double mutant animals (n = 84) showed significant reductions in the number of animals with errors (75%) compared to *dFmr*^{null}, and fewer of the double mutants (44%) had multiple errors within their pSc arbors compared to *dFmr*^{null} ($p< 0.05$). We also observed significant reductions in five out of the ten phenocopied axonal targeting errors compared to *dFmr*^{null} animals ($p< 0.05$) (**Figure 3.5g**). However, we also observed a significant increase in one error phenotype from 4% in *dFmr*^{null}

animals to 12% in *Dscam*^{null}/+; *dFmr*^{null} double mutants. Thus, the significant changes observed in these targeting errors represent the axonal targeting decisions that are most sensitive to FMRP regulation of *Dscam*, as the loss of one *Dscam* allele in the Fragile X mutants did not reduce the Dscam expression completely to wildtype levels (**Figure 3.1b**).

3.5.5 Elevated Dscam levels impair sensory perception

Do these axonal targeting errors in single neurons affect the mechanosensory circuit's function? To measure the ability of a fly to perceive mechanical stimulation of its bristles, we stimulated only the left and right pSc bristles by applying a small amount of fluorescent dye to evoke a cleaning reflex from the rear legs (**Figure 3.10a,** also see **Figure 2.2c-e**) (Canal et al., 1998; Vandervorst and Ghysen, 1980; Corfas and Dudai, 1989; Philis et al., 1993). We examined how structural changes and axonal routing errors affect circuit function by matching behavioral responses with specific synaptic targeting patterns of the pSc neuron in individual animals (**Figure 3.10b**). We examined the cleaning responses in mosaic animals that lack FMRP in only the scutellar neurons (*455-Gal4*; *UAS-dsRNA-dFmr*) and in Dscam X3 animals, and found that the altered synaptic connectivity of the pSc neurons in both of these mutants significantly reduced their cleaning responses compared to control flies (**Figure 3.10c** and **Figure 3.11**). Furthermore, the changes in response rates in experimental animals were not due to interactions among genetic backgrounds (**Figure 3.11**). Analysis of double mutant Fragile X mosaic animals lacking one copy of *Dscam* (*Dscam*^{null}*/455-Gal4*; *UAS-dsRNA-dFmr*) returned the response rate to that of control animals, indicating that reduction of Dscam protein levels can not only rescue synaptic targeting errors, but can restore touch perception in *dFmr* mutant animals.

3.5.6 FMRP binds multiple Dscam isoforms

FMRP binds mRNAs in their untranslated regions through RNA secondary structures called "kissing complex RNA" (**Figure 3.12**) (Darnell et al., 2011; Darnell et al., 2005; Darnell et al., 2009). Alternative splicing of three large exon arrays in the *Drosophila Dscam* gene can produce different immunoglobulin domains to create 19,008 different protein isoforms that differ only in their extracellular region (**Figure 3.13a**) (Schmucker et al., 2000). Thus, to determine whether FMRP binds all *Dscam* mRNA isoforms, we performed high-throughput pyrosequencing of *Dscam* bound to FMRP after immunoprecipitation of the complex. Pyrosequencing of *Dscam* enabled deep coverage of more than 1.2 million reads and long base pair read lengths (Margulies et al., 2005). We confirmed that all possible *Dscam* isoforms expressed in the brain were also found bound to FMRP (**Figure 3.13b**), demonstrating that FMRP can regulate the translation of tens of thousands of different Dscam protein forms. Comparisons of isoform distributions between *Dscam* in the input fraction and *Dscam* immunoprecipitated with FMRP showed that there was no significant bias in the isoforms that FMRP bound (**Figure 3.13b**). These results demonstrate that FMRP regulation of *Dscam* is dependent on the splicing choices made in individual cells rather than through preferentially regulating specific mRNA isoforms. Interestingly, we observed that $dFmr^{null}$ animals had an altered *Dscam* isoform expression profile in the brain (**Figure 3.13b**). The frequency of some isoforms was either increased or reduced. This result implies that FMRP may have additional roles that affect *Dscam* isoform splicing.

3.5.7 Overexpression of FMRP impairs targeting that can be rescued by increasing Dscam levels.

When we increased the levels of FMRP, we observed a reduction in the protein levels of Dscam (**Figure 3.1b**) however overexpression of FMRP may suppress the expression of other proteins that are involved in normal neuronal function. Thus, when we overexpressed FMRP in the pSc neuron (*455-Gal4*; *UAS-dFmr*), this resulted in severe axon guidance and misrouting phenotypes, and also reduced the behavioral responses in these animals (**Figure 3.14**). Although the axon guidance and misrouting defects were suppressed when combined with Dscam overexpression (*455-Gal4*; *UAS-dFmr*/*Dscam*^{BAC}), the impaired behavioral response due to FMRP overexpression was not restored.

3.6 Discussion

In this study we found that an increase in Dscam protein levels due to either three copies of the *Dscam* gene or due to loss of translation suppression by FMRP impairs precise synaptic targeting and neural circuit function. Combining behavioral analysis of mechanical stimulation of the pSc neuron with pSc axonal targeting patterns we confirmed that aberrant axonal targeting degrades sensory circuit function enough to impact the animal's perception. The restoration of the *Dscam*^{null}/+; *dFmr*^{null} double mutants' cleaning response indicates that any other functions of Dscam independent of branch targeting that were impaired in the *dFmr*^{null} animals were also rescued. For example, *Aplysia* Dscam is required pre- and postsynaptically for synaptogenesis and synaptic plasticity induction, and Dscam signaling through trans-synaptic complexes leads to clustering of glutamate receptors (Li et al., 2009).

It is important to note that although the majority of the targeting errors that were phenocopied between Dscam X3 and *dFmr*^{null} mutants consisted of ectopic branches, four of the five targeting errors rescued in the double mutant *Dscam*^{null}/+; *dFmr*^{null} animals were branch misrouting and midline crossing problems (**Figure 3.5g**). It seems reasonable to assume that these particular mistargeting events contribute the most to the degradation of circuit function, since their rescue is sufficient to restore the animals' touch perception. However, correlating specific synaptic targeting decisions with an individual animal's behavioral output requires much larger data sets than obtained in this study, given that we condensed all behavioral positive responses together into "yes response" rather than separating the positive responses into levels of cleaning efficiency in removing the fluorescent dye from the scutellum.

It has been previously shown that the full isoform diversity of Dscam is required for establishing the precise arbor of the pSc neuron (Chen et al., 2006). Our results indicate that FMRP can bind and regulate all *Dscam* isoforms, so the mistargeting phenotypes we observe are not due to preferential overexpression of specific Dscam isoforms. Furthermore, the specificity and quantitative overlap of the synaptic targeting errors between Dscam X3 and Fragile X mutants suggest that the effects of Dscam protein overexpression are most likely independent of Dscam isoform choice. Isoform-specific homophilic interactions of the Dscam receptor have been shown to induce dendritic branch repulsion (Wang et al., 2003; Zhan et al., 2004; Hattori et al., 2007; Hughes et al., 2007; Soba et al., 2007; Matthews et al., 2007), but nearly all of the targeting error phenotypes we observed in the pSc axons of Dscam X3 and Fragile X mutants consisted of ectopic branches, routing errors, and midline crossing errors, indicating an attraction function for the Dscam receptor. An attractive homophilic interaction between Dscam isoforms has been previously described in laminar-specific targeting in the chick retina (Yamagata and

Sanes, 2008). Dscam has also been shown to bind Netrin, an attractive guidance cue (Andrews et al., 2008; Ly et al., 2008; Liu et al., 2009). It is possible that excessive Dscam protein levels in developing axonal branches induces erroneous targeting decisions through inappropriate attraction to cells expressing Dscam ligands.

Pyrosequencing of *Dscam* mRNA isoforms in $dFmr^{null}$ animals revealed specific differences in isoform splicing compared to wildtype (**Figure 3.13b**). This may be due to loss of FMRP's direct interaction with pre-mRNAs as an exonic splicing enhancer, or through unregulated expression of splicing proteins normally suppressed by FMRP (Didiot et al., 2008; Guruharsha et al., 2011). FMRP regulation of *Dscam* splicing may also be utilized in arthropod immune systems, as *Dscam* is expressed in insect and crustacean immune cells such as hemocytes (Watson et al., 2005; Watthanasurorot et al., 2011) , and FMRP is also expressed in hemocyte-derived S2 cells (Monzo et al., 2006; Stetler et al., 2006). In the arthropod immune system, the isoform diversity of Dscam receptor isoforms is used to recognize different pathogens and become preferentially spliced and upregulated for pathogen clearance (Watson et al., 2005; Watthanasurorot et al., 2011; Dong et al., 2006), but it remains unclear how the feedback to splicing and expression of Dscam isoforms occurs. FMRP might thus regulate *Dscam* isoform splicing in many different cell types for a wide range of functions.

This study has found that neural circuit development and function are sensitive to increases in Dscam protein amounts. Previous studies using *Dscam* null heterozygous mice and mouse models of Down syndrome revealed that Dscam dosage is crucial for proper sorting of retinal ganglion cell axons and dendritic development (Alves-Sampaio et al., 2010; Blank et al., 2011), but thus far it has not been clear how Dscam overexpression might contribute to neurological impairments like Down syndrome. *Dscam* has also been associated with the

congenital heart defects found in Down syndrome, which was identified using analysis of rare individuals with partial duplications of chromosome 21 (Barlow et al., 2001). Genetic interaction screens in *Drosophila* for congenital heart defect genes also identified *Dscam*, and overexpression of Dscam in the mouse produced physiological and morphological cardiac defects (Grossman et al., 2011). Given its evolutionarily-conserved widespread functions throughout cardiac and neural development (Schmucker and Chen, 2009), and its conserved interaction with FMRP (Brown et al., 2001; Darnell et al., 2011), Dscam expression levels are thus likely to be tightly regulated. Dysregulation of Dscam protein expression may therefore be a common molecular feature underlying a wide variety of neural developmental disorders such as in the dendritic spine pathologies found in Fragile X, Down, and Rett syndromes (Dierssen and Ramakers, 2006; Kaufmann and Moser, 2000; Nimchinski et al., 2001).

3.7 Figures

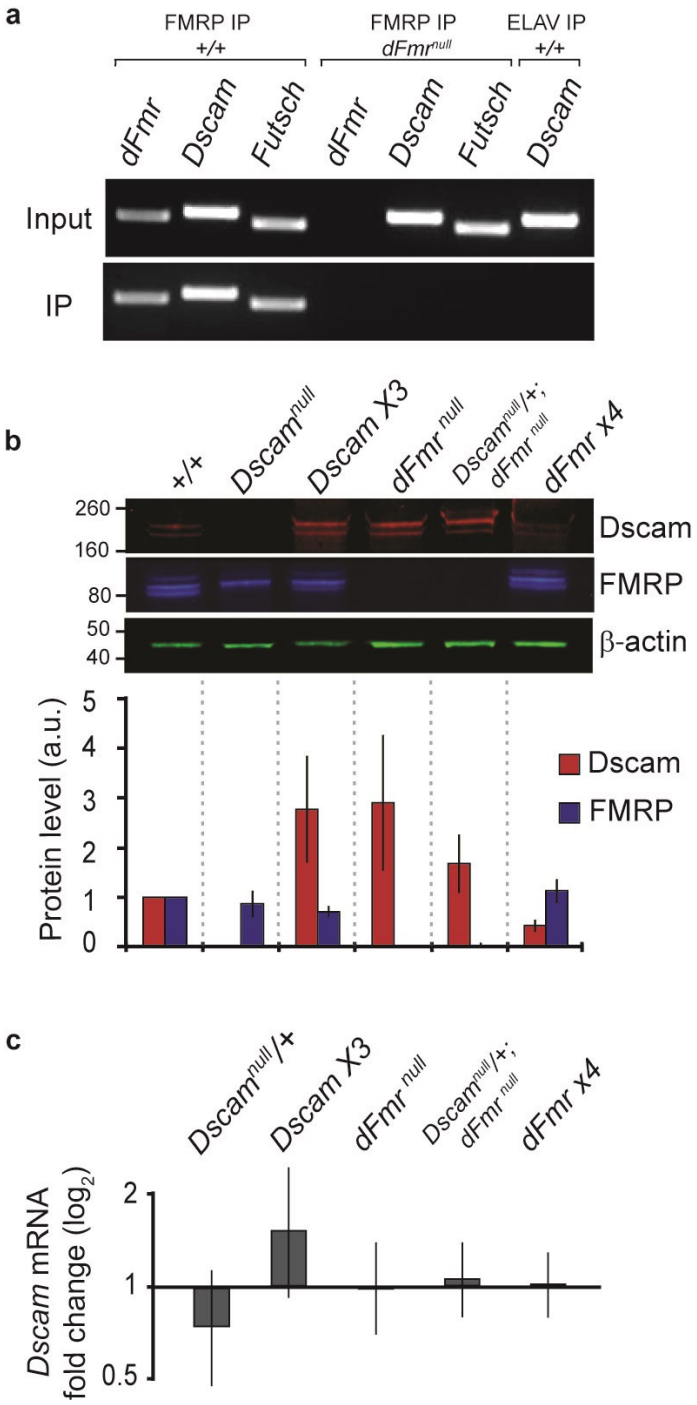

Figure 3.1 Fragile X Mental Retardation Protein (FMRP) suppresses Down syndrome cell adhesion molecule (Dscam) protein translation.

a, FMRP binds *Dscam* mRNA. FMRP-mRNA complexes were immunoprecipitated from *Drosophila* larval brains and specific targets were identified by RT-PCR. FMRP has been previously shown to bind its own mRNA and *Futsch*. No mRNAs were immunoprecipitated from Fragile X mutants ($dFmr^{null}$ IP), and *Dscam* mRNA did not immunoprecipitate with another neuronal RNA-binding protein, ELAV.

b, Loss of FMRP in Fragile X mutants increases neuronal Dscam protein amounts. Representative fluorescent immunoblots of Dscam, FMRP, and actin in different genotypes. Protein samples for $Dscam^{null}$ animals were prepared from embryos and showed restricted expression of FMRP isoforms. Dscam and FMRP protein intensities were normalized against actin (plotted in arbitrary units, a.u.), and the averages from 9 experiments are shown. Errors bars are standard error of the mean.

c, Quantitative real-time PCR analysis indicates that *Dscam* mRNA levels are not significantly altered in Fragile X mutants. *Dscam* mRNA for all experimental genotypes was measured as fold changes from wildtype levels. The averages from 6 experimental replicates are shown. Error bars are standard deviation of the mean.

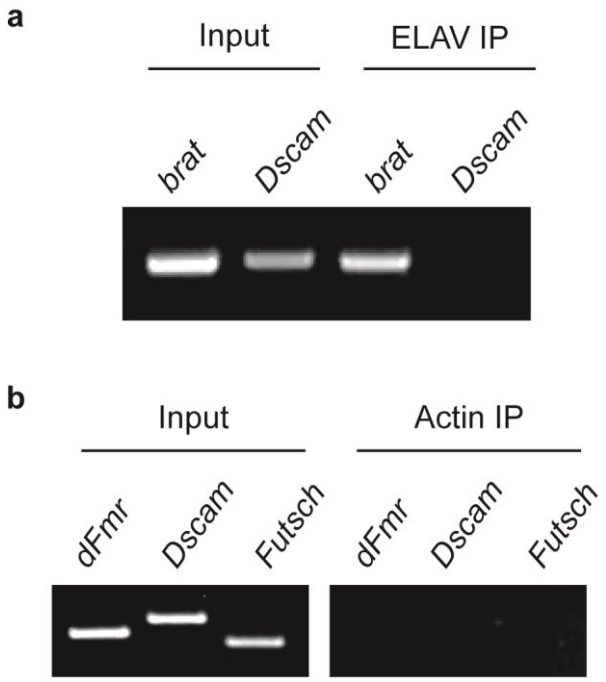

Figure 3.2 The neuronal RNA-binding protein ELAV does not bind *Dscam* mRNA.

a, Immunoprecipitation of Embryonic Lethal Abnormal Vision (ELAV) protein from adult fly brains pulls down *brain tumor (brat)* RNA, but not *Dscam*. Immunopreciptation of ELAV-mRNA complexes were used as negative controls for the specificity of the FMRP-*Dscam* mRNA interaction (Reeve et al, 2005). The neuron-specific RNA binding protein ELAV has been shown to extend the 3' untranslated region of *brat* mRNA (Hilgerset al, 2012), and this was used as a positive control of ELAV-mRNA complex precipitation.

b, *Dscam* mRNA does not immunoprecipitate non-specifically with other proteins. Immunoprecipitation of actin complexes from did not co-precipitate any mRNAs.

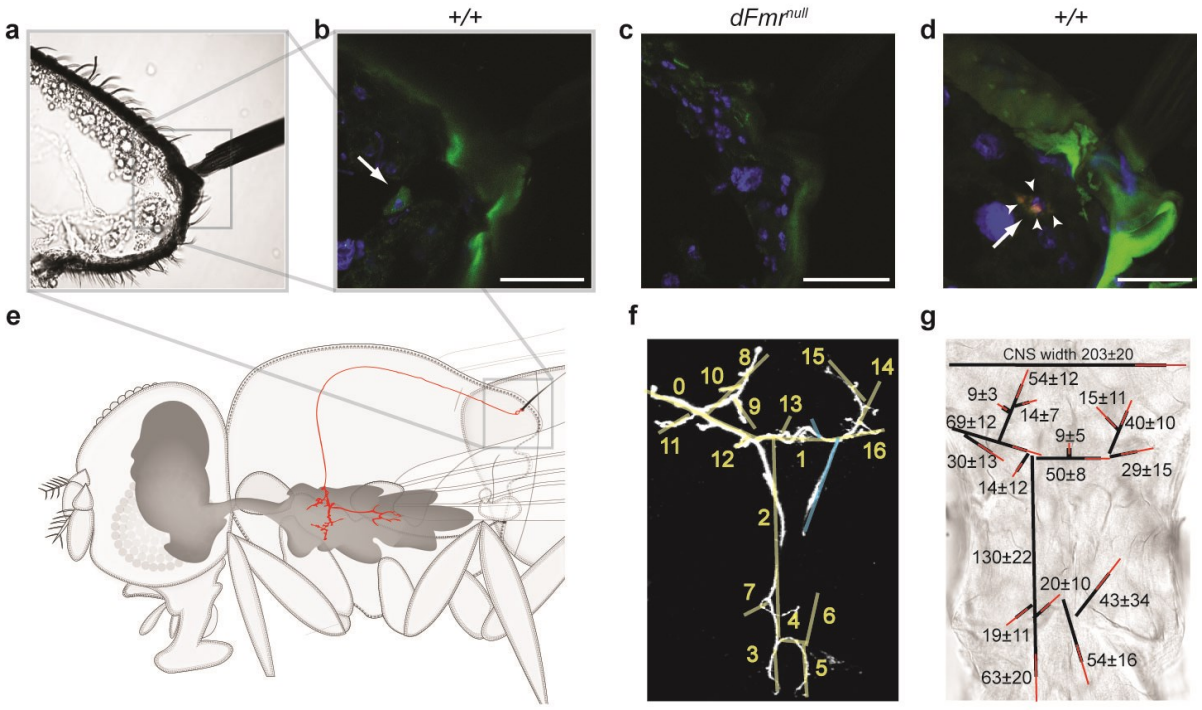

Figure 3.3 The posterior scutellar (pSc) mechanosensory neuron expresses FMRP and *Dscam*.

a-d, A cross section through a pSc bristle is shown in brightfield (**a**), and the corresponding FMRP immunofluorescence (green) within the pSc neuron (arrow) is shown in **b**. **c**, No detectable FMRP signal is observed in *dFmr*^{null} animals. **d**, Co-localization of FMRP and *Dscam* mRNA was observed in pSc neurons using fluorescence *in situ* hybridization for *Dscam* mRNA (magenta) combined with fluorescence immunohistochemistry for FMRP (green). Arrowheads point to *Dscam* mRNA puncta, arrow points to FMRP signal. Nuclei are stained in blue. Scale bars, 20µm.

e, A single mechanosensory neuron innervates a single bristle. The axonal projection into the central nervous system of the right posterior scutellar mechanosensory neuron is shown in red.

f, g, The stereotyped synaptic connectivity of the pSc neuron is used as a readout for synaptic targeting errors. **f**, The pSc axonal arbor has a complex and stereotyped branching pattern.

Quantitative analysis of wildtype pSc axons revealed 16 core branches (yellow lines) and 2 variable branches occurring in 50% of animals (blue lines). **g**, Individual branches of the pSc axonal arbor can be identified between animals, and their lengths and variance can be quantified. Black lines represent the average lengths of each branch, red lines represent the standard deviations, and values are in μm.

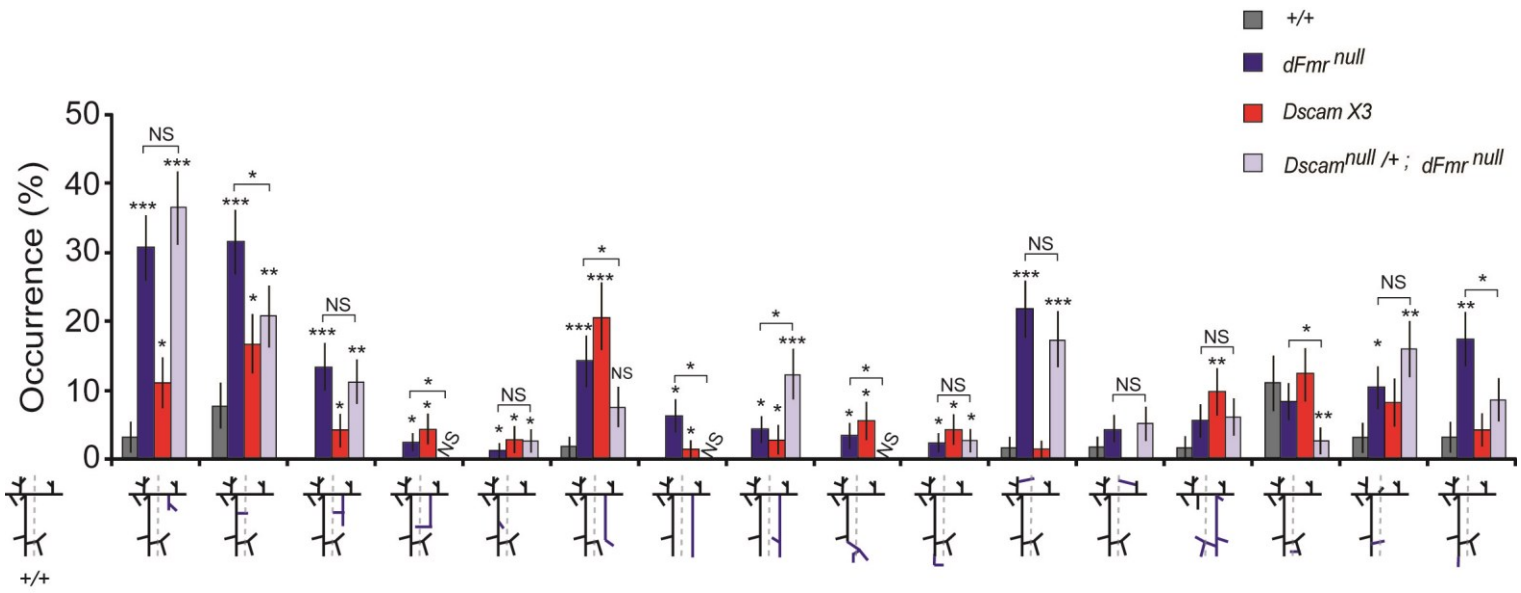

Figure 3.4 Fragile X mutants have a large number and frequency of axonal targeting errors.

The frequency distribution of 16 targeting error phenotypes categorized by blind analysis among the different genotypes is shown. Targeting errors are defined as those occurring at a frequency below 10% in wildtype animals. Fragile X mutants were found to have significantly higher occurrences of all error types. Animals with 3 copies of the Dscam gene (Dscam X3) had 15 error types, but only 10 were significantly higher than wildtype (categories 1-10). Thus, phenocopy between Fragile X mutants and Dscam X3 animals was defined as these error types that were both significantly higher than wildtype. Statistical significance comparisons to wildtype are indicated directly above the experimental genotypes' bar; the *Dscam*^{null}*/+; dFmr*^{null}*/dFmr*^{null} double mutant comparison to *dFmr*^{null} animals are indicated above a connecting line. Error bars are standard error of the mean. Statistical significance was determined using a two-tailed t test for proportions. * $p < 0.05$, ** $p < 0.01$, *** $p < 0.001$, and NS indicates not significant.

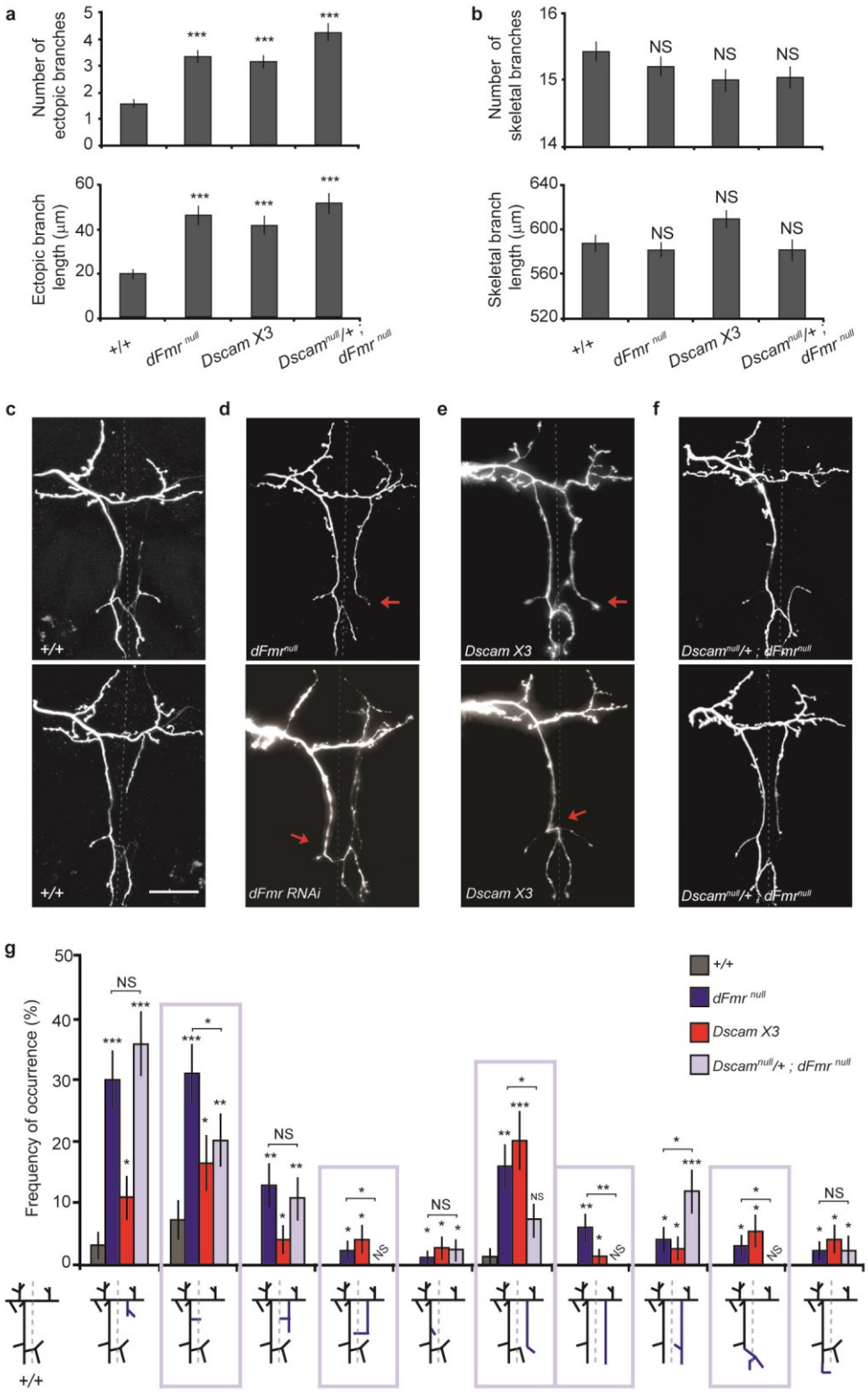

Figure 3.5 Elevated Dscam protein levels produce specific axonal targeting errors.

a, Ectopic branch number and length are increased in *dFmr*^{null} and Dscam X3 animals.

b, The core pSc skeleton does not change in branch number or lengths among different genotypes.

c, d, Axonal branch targeting is impaired in Fragile X mutants. Compared to the stereotyped axonal branching pattern of wildtype pSc neurons (**c**), animals lacking FMRP (**d**) have specific targeting errors, such as misrouting and aberrant midline crossing branches (arrows). Dotted line marks the midline of the central nervous system. Scale bar, 50μm.

e, Dscam X3 animals have targeting errors (arrows) similar to those observed in Fragile X mutants.

f, Reducing Dscam levels in Fragile X mutants decreases targeting errors. Double mutant animals have a single null allele of *Dscam* and are homozygous null for *dFmr*.

g, The frequency and type of targeting errors phenocopied between *dFmr*^{null} and Dscam X3 animals can be rescued by reducing Dscam protein levels. Frequency of occurrence for ten error types that are significantly greater than wildtype for both Fragile X mutants and Dscam X3 is shown. Double mutant animals have a significant reduction in five axonal targeting errors (purple rectangles). Statistical significance comparisons to wildtype are indicated directly above the experimental genotypes' bar; the double mutant comparison to *dFmr*^{null} animals are indicated above a connecting line. All error bars are standard error of the mean. * $p < 0.05$, ** $p < 0.01$, *** $p < 0.001$, and NS indicates not significant.

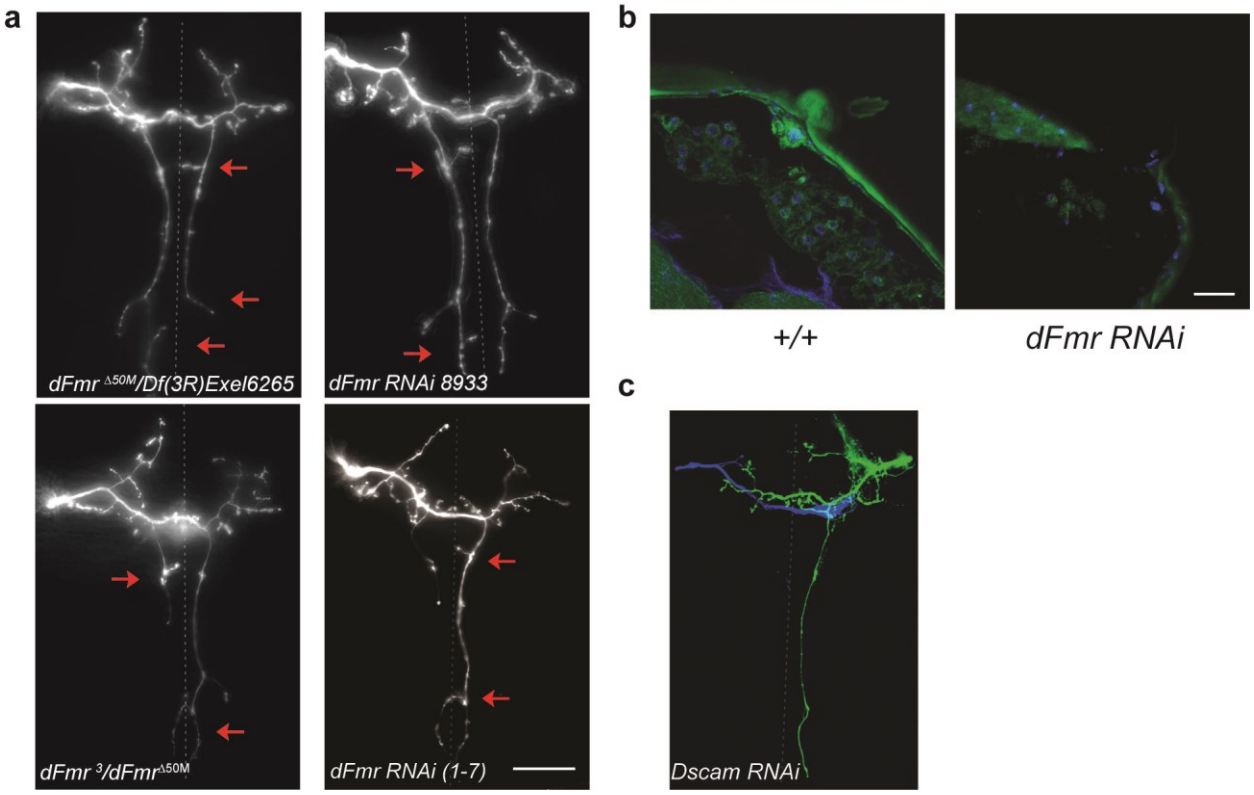

Figure 3.6 *Fmr1* RNAi is potent and specific.

a, Axonal targeting errors (arrows) in *455-Gal4; UAS-dsRNA-dFmr1* animals phenocopy the whole animal *dFmr1*^{null} mutant. Knockdown within only the scutellar neurons was achieved using the scutellum-specific *455-Gal4*. Dotted line marks the midline of the central nervous system. Scale bar, 50 µm.

b, Efficiency of the *dFmr1* RNAi knockdown was quantified using immunohistochemistry. FMRP (green) average intensity (arrow in wildtype, left panel) was quantified in a region of interest centered around the nucleus (blue) of the mechanosensory neuron directly underneath its corresponding scutellar bristle. FMRP expression was reduced by 76% in mechanosensory neurons (arrowhead) when driven by the pan-neuronal *elav-Gal4* driver, thus confirming the identity and specificity of FMRP within neurons (right panel, *elav-Gal4; UAS-dsRNA-Fmr1*, compare FMRP signal at arrowhead to non-neuronal FMRP signal at arrow). Scale bar, 20 µm.

c, Knockdown of Dscam in the scutellar mechanosensory neurons resulted in a *Dscam*^{null}-like axonal phenotype in the posterior scutellar neuron (left entry), but not the posterior dorsocentral neuron (right entry).

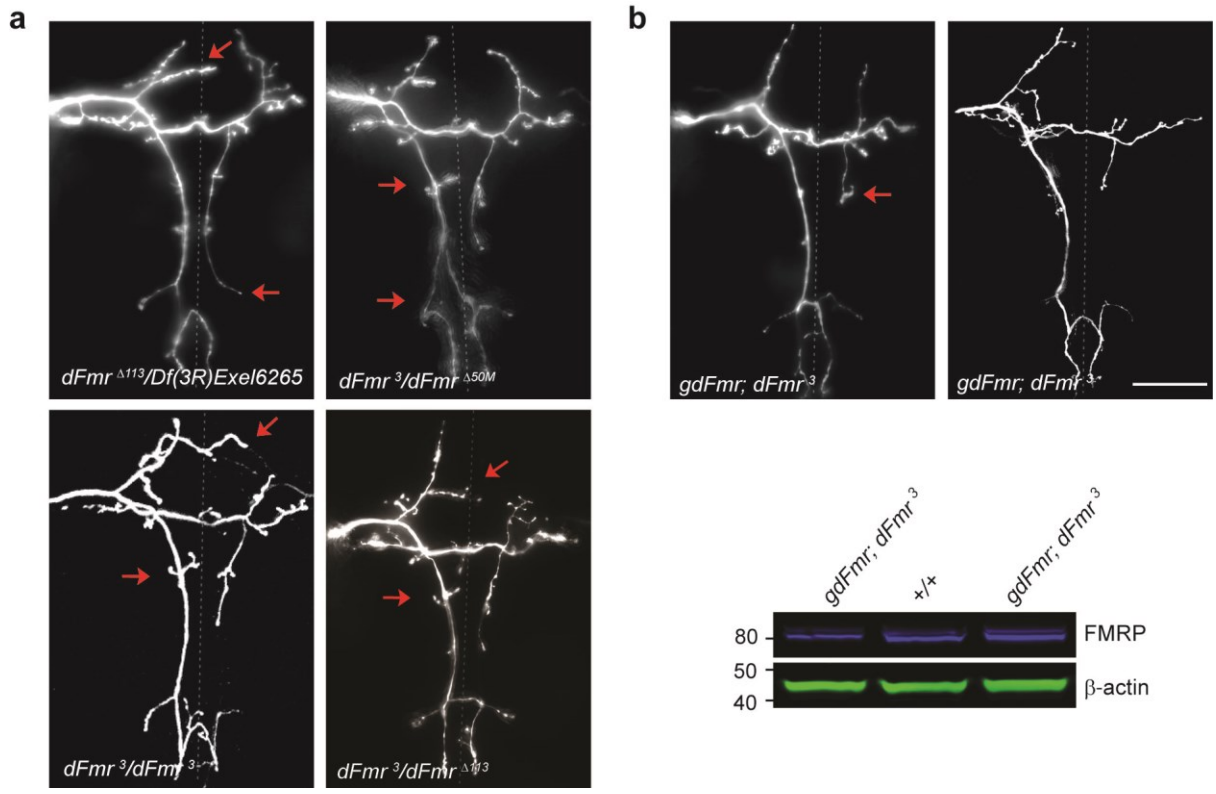

Figure 3.7 Different *Fmr1*^{null} alleles produce the same axonal targeting errors that can be rescued by reintroduction of genomic *Fmr1*.

a, Representative examples of transheterozygous combinations of *Fmr1*^{3}, *Fmr1*$^{\Delta 50M}$, *Fmr1*$^{\Delta 113}$ and *Df(3R)Exel6265* are shown. Arrows point to *Fmr1*^{null} targeting phenotypes.

b, Introduction of a genomic *Fmr1* transgene (*gdFmr1*) on a null background rescued axonal targeting phenotypes. Dotted line marks the midline of the central nervous system. Scale bar, 50µm. The *gdFmr1* transgene restores FMRP expression, but with variable levels of expression. Quantitation of fluorescence in immunoblots for FMRP and actin revealed FMRP levels in *gFmr1; Fmr1*^{null} flies ranging from 0.5 to 2.1 times that of wildtype (mean = 1.2 fold greater than wildtype, n = 8 experimental replicates).

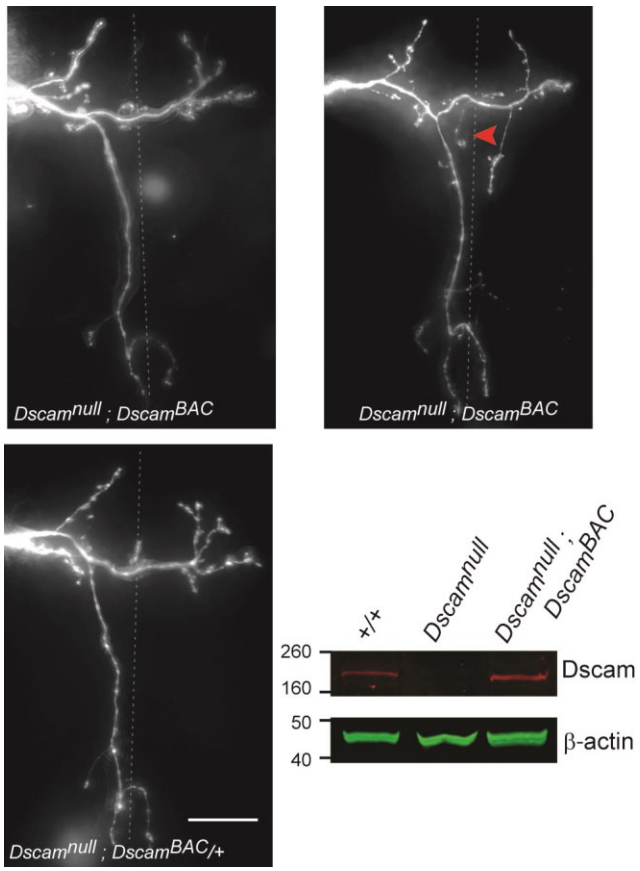

Figure 3.8 Animals expressing an exogenous *Dscam^{BAC}* on a *Dscam^{null}* background do not have pSc axonal targeting errors observed in Dscam X3 animals.

To determine whether the exogenous *Dscam^{BAC}* produced dominant phenotypes similar to those observed in *Dscam X3* animals, we analyzed the pSc axonal arbors of homozygous *Dscam^{null}; Dscam^{BAC}* animals. *Dscam^{21}/Dscam^{23}; 5-Dscam^{BAC}/33-Dscam^{BAC}, Dscam^{21}/Dscam^{23}; 7-Dscam^{BAC}/33-Dscam^{BAC}* and *Dscam^{21}/Dscam^{23}; 33-Dscam^{BAC}/+* are shown. Axonal targeting errors in *Dscam^{null}; Dscam^{BAC}* animals were infrequent, and those that were observed (arrowhead) were not seen in Dscam X3 animals. A representative fluorescent western blot of Dscam in wildtype, *Dscam^{null}* and *Dscam^{null}; Dscam^{BAC}* indicates that Dscam protein levels are restored in *Dscam^{null}; Dscam^{BAC}* animals. Dotted line marks the midline of the central nervous system. Scale bar, 50μm.

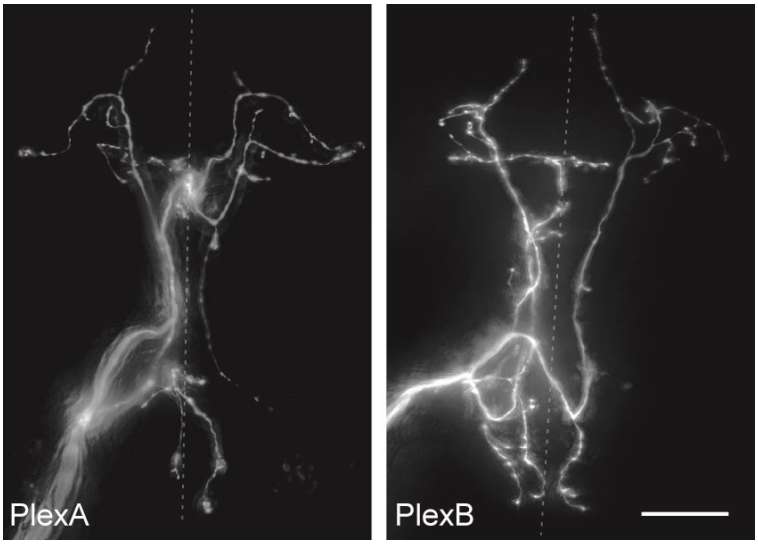

Figure 3.9 Overexpression of PlexinA and PlexinB neuronal receptors does not phenocopy the targeting errors observed in animals that overexpress Dscam.

PlexinA and PlexinB is overexpressed solely within the scutellar mechanosensory neurons using the 455-Gal4 driver (*455-Gal4; UAS-PlexA* and *455-Gal4; UAS-PlexB*). Overexpression of Plexin receptors typically caused axon guidance errors and branch growth and branch routing errors, and axonal targeting errors were not overtly stereotyped between animals (n = 19 for PlexinA, n = 5 for PlexinB). Dotted line marks the midline of the central nervous system. Scale bar, 50 μm.

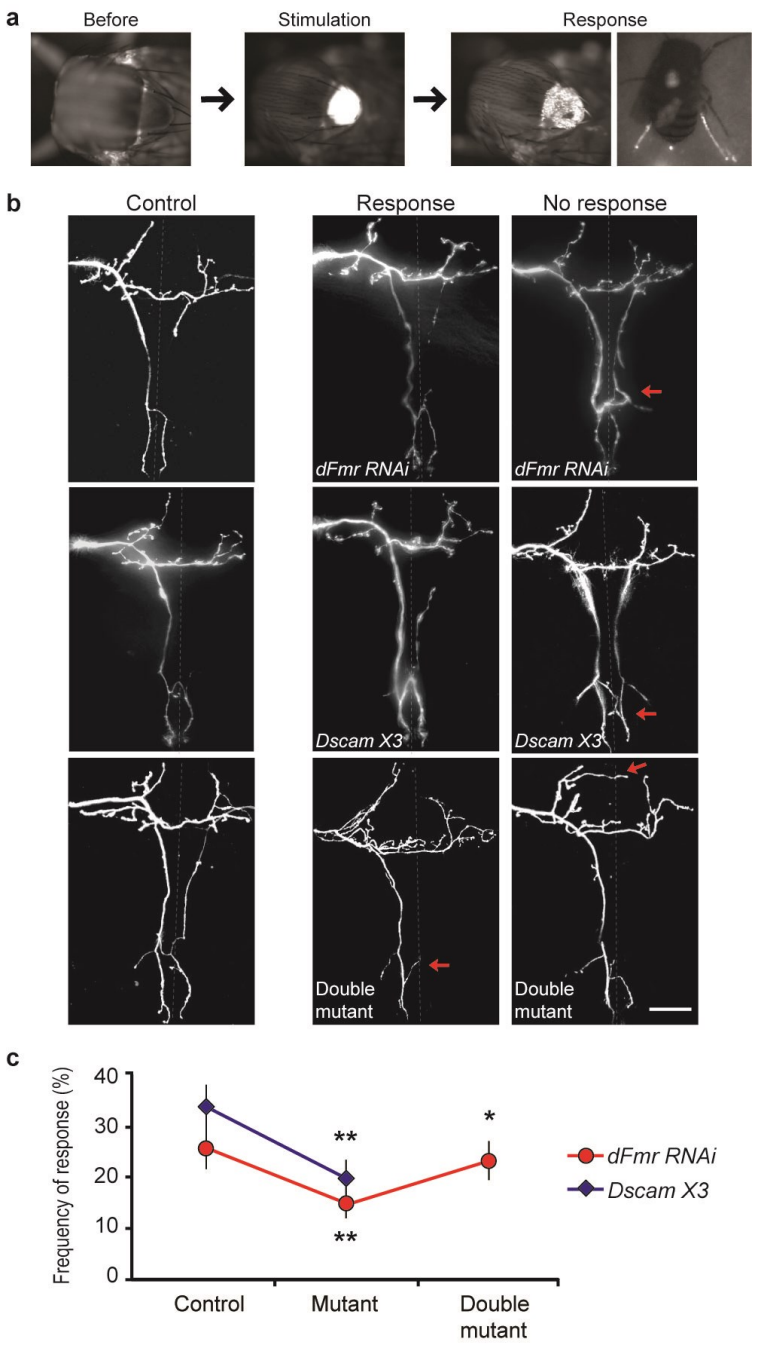

Figure 3.10 Errors in synaptic targeting impair touch perception in Fragile X and Dscam X3 animals.

a, Mechanical stimulation of the pSc bristles using a controlled amount of fluorescent dye elicits a cleaning reflex from the rear legs. Transfer of the fluorescent dye from the back of the fly onto the rear legs is used to confirm a positive response.

b, Synaptic targeting of a single, identified neuron can be matched to the specific behavioral output for each animal. Representative images of the axonal arbors of previously stimulated pSc neurons are shown. Axonal arbors of mutant animals that either succeeded or failed to respond to bristle stimulation are compared to control responding animals. Arrows indicate targeting errors. Dotted line marks the midline. Scale bar, 50μm.

c, Synaptic targeting errors in the pSc neuron impair touch perception in the Fragile X mutant and Dscam X3 flies, and can be restored in the double mutant. The frequency of response is shown for mosaic animals with FMRP knocked down only in the scutellar neurons and for animals with 3 copies of *Dscam*, compared to their specific genetic controls. The frequency of response to touch in mosaic double mutants, $Dscam^{null}$/*455-Gal4*; *UAS-dsRNA-dFmr*, was significantly higher (single asterisk) than mosaic Fragile X mutants, and was not significantly different from controls. $n > 120$ for each genotype. * $p < 0.05$, ** $p < 0.01$. Error bars are standard error of the mean.

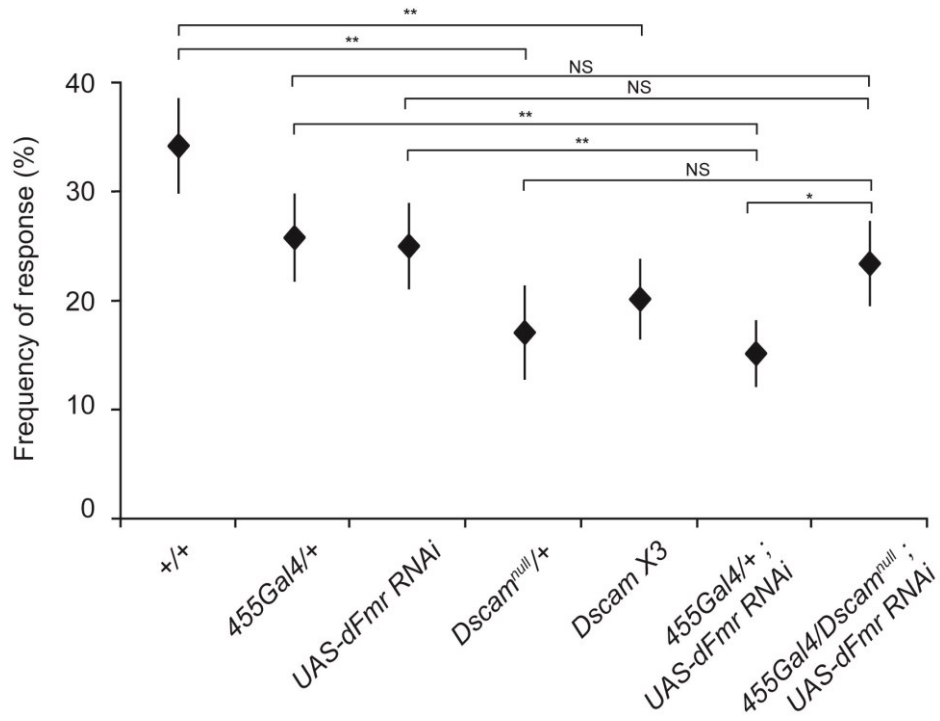

Figure 3.11 Differences in genetic background cannot account for changes in behavioral touch responses.

The touch response frequencies are shown for all control and experimental animals. Interactions among genetic backgrounds cannot account for the change in response rates in experimental animals. For example, the *455-Gal4/+* and *UAS-dsRNA-Fmr1* animals both had high touch response rates (26% response, $n = 121$; and 25% response, $n = 125$, respectively), but *455-Gal4/+; UAS-dsRNA-Fmr1* animals had a significantly lower response rate at 15%, $n = 139$, $p < 0.05$. Similarly, the heterozygous $Dscam^{null}$/+ mutant had a significantly lower response rate than +/+ controls (17% response, $n = 77$ compared to 34%, $n = 121$, respectively, $p < 0.01$), but when $Dscam^{null}$/+ is combined with *455-Gal4/+; UAS-dsRNA-Fmr1*, these double mutant animals ($Dscam^{null}$*/455-Gal4; UAS-dsRNA-Fmr1*) have much higher response rates at 23%, $n = 120$. Error bars are standard error of the mean. * $p < 0.05$, ** $p < 0.01$, and NS indicates not significant.

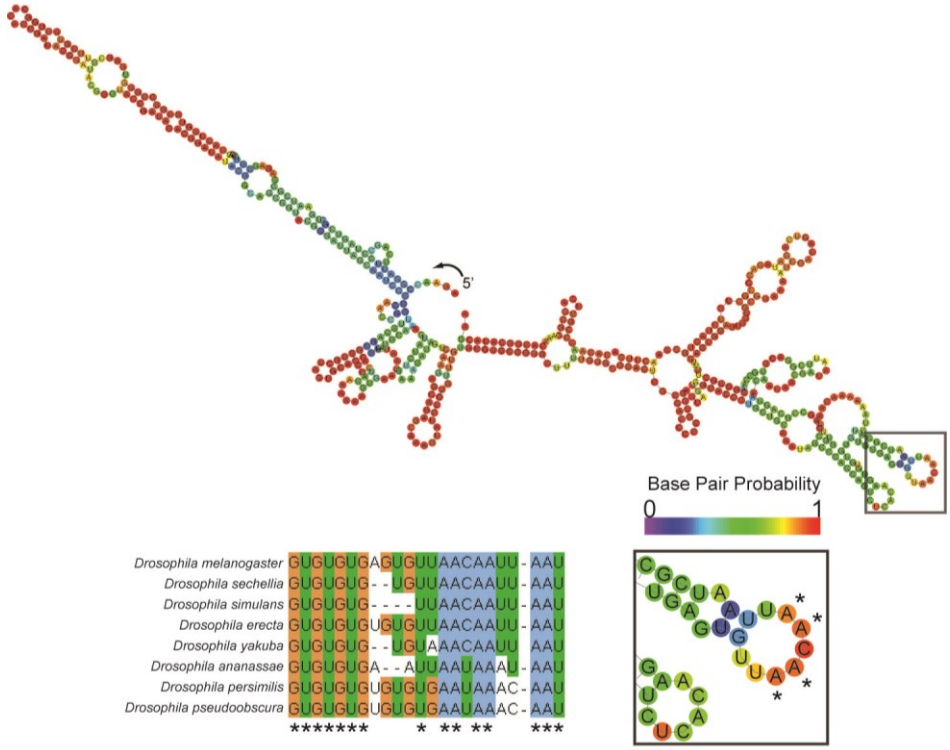

Figure 3.12 FMRP may bind Dscam mRNA at specific sites in the secondary RNA structure of the 5' untranslated region.

Predicted minimum free energy secondary structure of the 5' untranslated region in *Dscam* mRNA reveals several stem-loop structures and a unique kissing complex (boxed region) with internal reverse complementarity (i.e., palindromic). A 140 nucleotide sequence surrounding the putative kissing complex RNA in the 5' untranslated region of *Drosophila melanogaster Dscam* is highly conserved across Drosophilidae at greater than 74% similarity. Conserved RNA nucleotides are marked with asterisks, and conserved Adenine nucleotides in the kissing complex are marked. RNA fold predictions were performed using the Vienna RNA Website. Multiple sequence alignment of Drosophilid *Dscam* RNA was performed using ClustalW at EMBL-EBI.

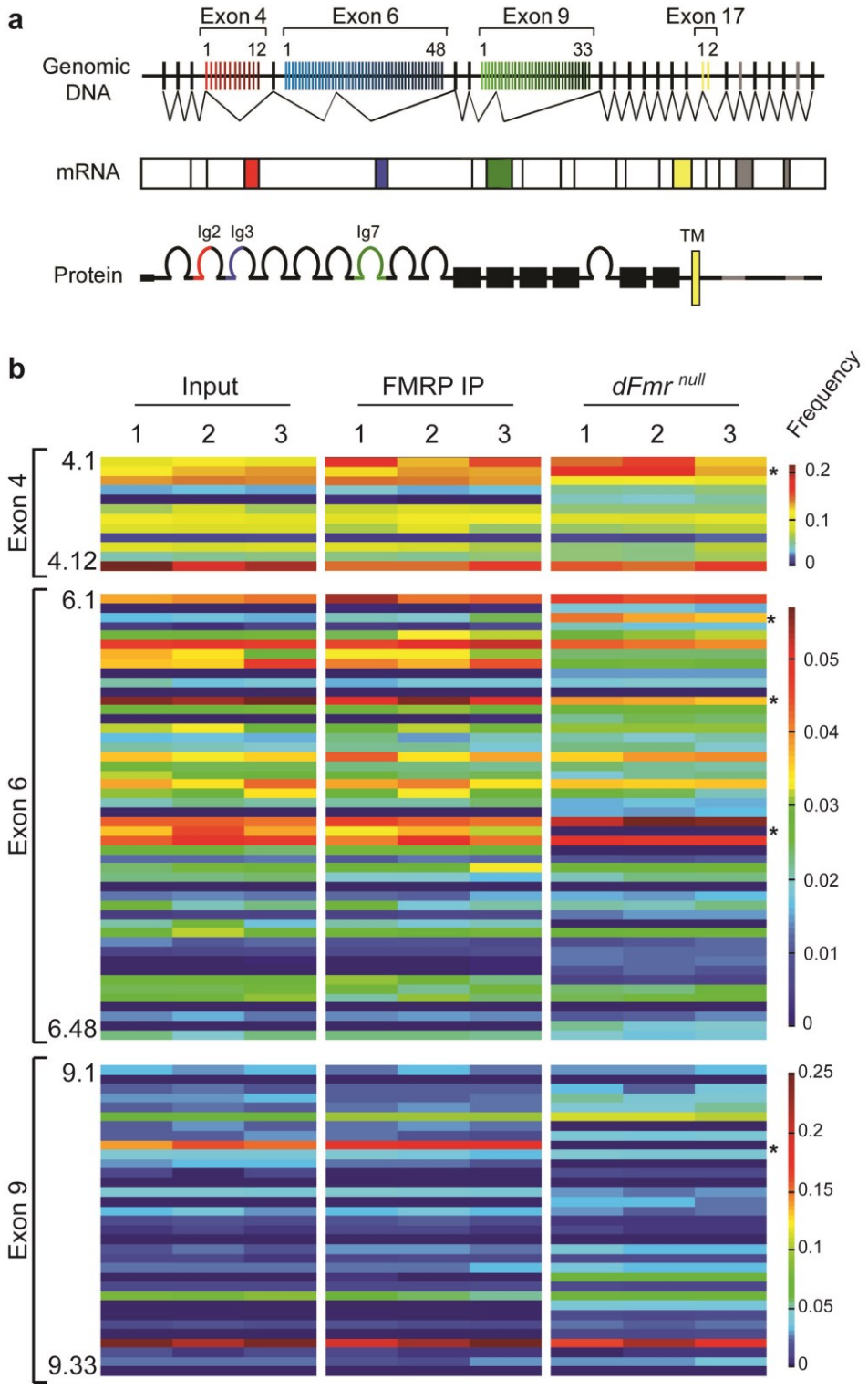

Figure 3.13 FMRP binds multiple *Dscam* isoforms.

a, Three large arrays of alternatively spliced exons in *Drosophila Dscam* (Exon 4, red; Exon 6, blue; Exon 9, green) encode for different extracellular immunoglobulin domains (Ig2, Ig3 and Ig7). Mutually exclusive splicing from each variable exon can produce 19,008 different extracellular domains. Exon 17 encodes for two alternate transmembrane domains (TM), and Exons 19 and 23 can be included or excluded in the intracellular domain.

b, High-throughput pyrosequencing of *Dscam* bound to FMRP identifies all possible *Dscam* isoforms. *Dscam* isoform distributions from a representative sequencing experiment of >1.2 million reads are shown as heatmaps for variable Exons 4, 6, and 9. Isoform distributions from the input and the FMRP IP from three separate experiments are shown. *Dscam* RNA isoforms immunoprecipitated with FMRP show no significant bias in representation compared to *Dscam* isoforms in the input fraction, indicating that FMRP binds all neuronal isoforms equally well. Loss of FMRP in Fragile X animals results in altered splicing of specific isoforms (indicated with asterisks).Relative isoform representations in Fragile X animals were found to both increase (e.g., Exons 4.2 and 6.3) and decrease (e.g., Exons 6.12, 6.26, and 9.9).

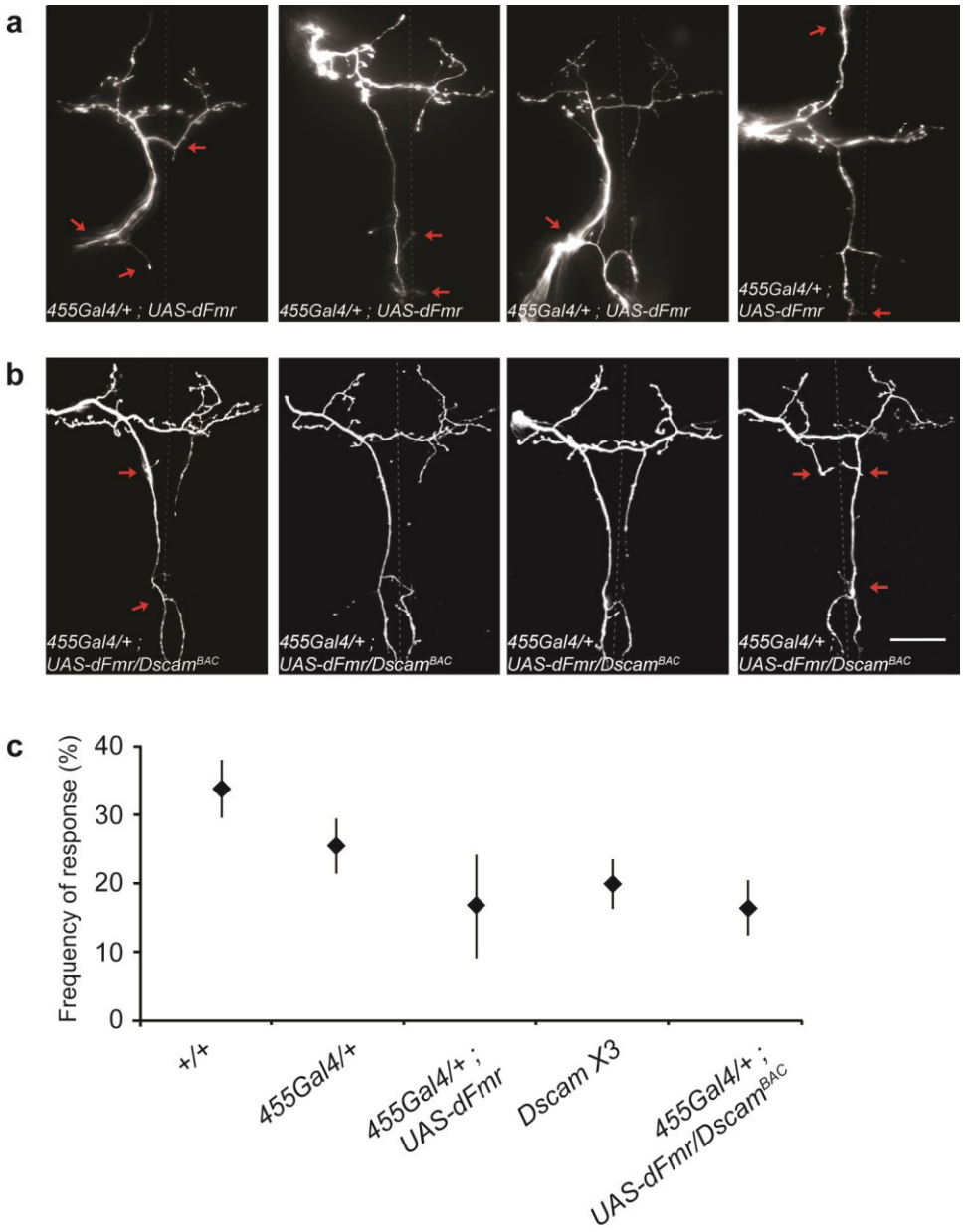

Figure 3.14 Increasing Dscam levels in FMRP overexpression animals rescues axonal targeting errors, but not circuit function.

a, Overexpression of FMRP in the pSc neurons (*455-Gal4; UAS-dFmr*) resulted in severe axon guidance and misrouting errors in addition to branch targeting errors. 46% of pSc axons in *455-Gal4; UAS-dFmr* animals (n = 28) had guidance and routing errors (arrowheads). Branch

targeting errors frequently consisted of midline-attracted ectopic branches (arrows). Most animals could also not be analyzed due to unformed pSc bristles.

b, Increasing Dscam expression in FMRP overexpression animals by introducing an exogenous *Dscam*^{BAC} (*455-Gal4; UAS-dFmr/Dscam*^{BAC}) restored the axon guidance and misrouting errors (n = 16). Thus, extra Dscam may compensate for a guidance or routing receptor that is suppressed in FMRP overexpression animals. Axonal targeting could also be partially rescued in *455-Gal4; UAS-dFmr/Dscam*^{BAC} animals.

c, Excess FMRP degrades sensory circuit function, which increased Dscam levels cannot restore. Dotted line marks the midline of the central nervous system. Scale bar, 50μm.

Chapter 4

RNA interference screen identifies a role for Teneurin-m in precise synaptic targeting

4.1 Relation to overall project

Neurons in hard-wired circuits use genetically encoded information to establish a wiring diagram that is invariable between animals. As demonstrated in the experiments in **Chapters 2** and **3**, the mechanosensory system in *Drosophila* can be studied at the level of a single neuron that is identifiable between animals, and we can use the neuron's precise connectivity to investigate genes that the specific neuron uses for wiring. Therefore, if we identify the molecular code that results in the formation of a stereotyped arbor we could better understand how a neuron utilizes these molecular instructions for decision-making. This chapter describes an RNA interference (RNAi) knockdown approach to screen for genes involved in pSc mechanosensory axon targeting. Identification and systematic characterization of axonal targeting phenotypes, which we have done for Teneurin-m loss of function, can ultimately reveal the wiring code that instructs fine-scale targeting of a single neuron.

4.2 Abstract

The *Drosophila* mechanosensory circuit is a useful system for performing RNAi screens for genes that are involved in the synaptic targeting of the mechanosensory neuron. In one such screen for genes that impair the axonal targeting of the pSc neuron, we found that knockdown of *Teneurin-m* (*Ten-m*) produced stereotyped axonal branching phenotypes. Ten-m belongs to the highly conserved teneurin family of cell surface receptors that have important roles during nervous system development for axon guidance, cell adhesion, and synaptic specificity. We investigated how Ten-m regulates axonal targeting decisions at the level of single neurons and its effect on circuit function. Characterization of the stereotyped targeting errors in *Ten-m* RNAi animals revealed inappropriate branch extensions in the anterior CNS in contrast to premature

branch terminations in the posterior CNS, frequently co-occurring within the same axon. These structural defects in *Ten-m* knockdown neurons reduced the ability of the animal to detect and respond to a mechanical stimulus. These results suggest that Ten-m may have a dual attractive and repulsive targeting role within the same axon and that proper expression of Ten-m is important for correct connectivity and mechanosensory circuit function.

4.3 Introduction

Since the discovery that double stranded RNA (dsRNA) can result in potent sequence-specific gene silencing in the nematode *C. elegans* (Fire et al., 1998) RNA interference has become a standard method for manipulating gene expression (Kennerdell and Carthew, 1998; Elbashir et al., 2001; Angelini et al., 2005; Zimmermann et al., 2006). RNAi is mediated by an enzymatic RNA-induced silencing complex that recognizes and processes dsRNA into small interfering RNAs to target complementary mRNA for degradation (Hutvagner and Zamore, 2002). Genetic tractability of *Drosophila* has allowed insertion of transgenes encoding hairpin dsRNAs under the control of the Gal4/UAS system (Kennerdell and Carthew, 1998). The creation of collections of *Drosophila* lines encoding UAS-driven dsRNA (Dietzl et al, 2007; Ni et al., 2009) has been a valuable resource to help bridge the gap between gene function and phenotype. Genome-wide, targeted, or small scale RNAi screens can be performed to systematically dissect the roles of genes involved in biological processes (Sharma and Rao, 2009). The *Drosophila* mechanosensory circuit is a good system for investigating genes involved in precise synaptic targeting. We have previously developed a fast and reliable method to assess synaptic targeting structural defects combined with behavioral analysis of circuit function (**Chapter 2**) (Kays et al., 2014). Here, we expand the utility of this system by demonstrating that

RNAi screens can be used to identify novel genes involved in the targeting of mechanosensory axons.

A single neuron expresses a repertoire of molecules that it uses to target its axon to appropriate postsynaptic partners. We sought to perform a small scale RNAi screen to determine if axonal targeting of the pSc neuron is regulated by genes previously implicated in circuit development of other systems. We used the *455-Gal4* driver that is specific to the four scutellar mechanosensory neurons to drive the expression of dsRNA against specific genes and looked at the effect on the targeting of axonal branches of the pSc neuron. In this kind of forward genetic screen we expected that if the gene was used for axonal targeting, then its knockdown will produce targeting errors within the axonal arbor. Focusing our screen on seven genes involved in circuit development, we identified Teneurin-m being required for correct mechanosensory axon targeting (**Figure 4.1**). The teneurins are a conserved family of cell surface molecules. Originally discovered in *Drosophila* as *Ten-m* and *Ten-a*, four homologs named *Ten-m1−4* have been described in vertebrates (Baumgarthner and Chiquet-Ehrismann, 1993; Baumgarthner et al., 1994; Rubin et al., 1999; Minet et al., 1999, Oohashi et al., 2000). The intracellular domains of invertebrate and vertebrate teneurins are different in size and sequence, however the extracellular domains of all teneurins consist of eight epidermal growth factor (EGF)-like domains, a conserved stretch of cysteines, and unique tyrosine-aspartate (YD) repeats (Tucker and Chiquet-Ehrismann, 2006). Teneurins have widespread expression in the developing nervous system of invertebrates and vertebrates and functions in axon guidance, cell adhesion, synapse organization and maintenance (Zheng et al, 2011; Rubin et al., 2002; Mosca et al., 2012). In the avian and mammalian brain teneurins are expressed in non-overlapping populations of cells (Kenzelmann et al., 2008; Zhou et al., 2003) and expression gradients have also been reported in the mouse

cortex and developing visual pathway (Li et al., 2006; Leamey et al., 2007). In *Drosophila*, Ten-m and Ten-a have been shown to be important in regulating synaptic partner matching between classes of olfactory neurons and at the larval neuromuscular junction (Hong et al., 2012; Mosca et al., 2012). Since they can form homo- and heterodimers *in vitro* and *in vivo* (Feng et al., 2002; Mosca et al., 2012; Hong et al., 2012), these studies proposed a trans-synaptic binding mechanism between teneurins, but it is not known if other ligands can bind them heterophilically. Recently it was shown that alternative splice forms of latrophilins can bind mammalian teneurins in a heterophilic fashion, forming stable trans-synaptic cell contacts (Boucard et al., 2014). Consistent with a role in cytoskeleton organization (Mosca et al., 2012), several studies in vertebrates have also implicated teneurins as positive regulators of neurite outgrowth (Minet et al.,1999; Al Chawaf et al., 2007; Suzuki et al., 2014).

In this study we identify the involvement of Ten-m and rule out roles of dSema1a, dSema2a, dSema5c, Nervy, Sidekick, and Ten-a in axonal targeting of the pSc neuron. We further characterize how loss of Ten-m expression affects axonal targeting decisions and circuit function. This study emphasizes the utility of the mechanosensory system in screening for novel targeting molecules and demonstrates the stereotypy of axonal targeting phenotypes upon knockdown of a single targeting molecule.

4.4 Material and methods

4.4.1 *Drosophila* Strains

The following RNAi fly stocks from the Vienna *Drosophila* RNAi Centre (Vienna, Austria) were used for screening: *UAS- dsRNA Sidekick* lines 9437 and 106217; *UAS-dsRNA*

dSema1a lines 36147 and 36148; *UAS-dsRNA dSema2a* line 15810; UAS-dsRNA dSema5c line 9429; *UAS-dsRNA Ten-a* lines 8322, 32482, 39244, 39245, 40134 and 103298; and *UAS-dsRNA Ten-m* line 51173. Multiple RNAi lines from the GD and KK collections against the same target gene were tested to control for RNAi knockdown efficiency and off-target effects. Gal4 expression within only the scutellar neurons was achieved by mating the *UAS-dsRNA* flies with the 455-Gal4 driver line (Neufeld et al., 2011; Cvetkovska et al., 2013; Kays et al., 2014). The phenotypes observed in *455-Gal4/+; UAS-dsRNA Ten-m* ^{VDRC51173}/+ animals were confirmed by testing another line, *UAS-dsRNA Ten-m JF03323* (L. Luo, Howard Hughes Medical Institute, Stanford University). The two lines had identical phenotypes and were used in all experiments. *455-Gal4/+* animals were used as controls and were generated by mating *455-Gal4/CyO* with w^- wildtype animals.

Transheterozygous animals carrying one copy of *UAS-dsRNA Ten-m* and one *Ten-m* null allele were generated by crossing *455-Gal4/CyO; UAS-dsRNA Ten-m* ^{VDRC51173} animals with *Ten-m* ^{KG00101}*/ TM3, Sb, Ser* or *Df(3L)Ten-m-AL1/TM3, Sb, Ser* (Bloomington *Drosophila* Stock Center, Bloomington, IN).

Teneurin overexpression was achieved by crossing *455-Gal4/CyO* animals to *P{GSV6} Ten-m*^{GS9267} for Ten-m, and *P{EP}Ten-a*^{GE1914} or *UAS-Ten-a (86Fb)* for Ten-a (L. Luo, Howard Hughes Medical Institute, Stanford University).

4.4.2 Single mechanosensory neuron microdissection and RT-PCR

Single mechanosensory neuron RT-PCR experiments were performed in triplicate. Female flies were collected immediately after eclosion, anesthetized with CO_2 and frozen on dry ice. A single pSc neuron was isolated by carefully cutting around the bristle socket with a

surgical blade under a standard stereomicroscope. Since the pSc socket is at the tip of the scutellum and is separated from other bristles, this dissection method includes a single neuron. Total RNA in the microdissected sample was extracted using Trizol reagent (Life Technologies, Carlsbad, CA) and was used as template for RT-PCR using the following gene-specific reverse transcription primers: *Ten-m* GTGCTGCTTTGAGAACTTAATCTTG, *Ten-a* GTTCGCTCTTGTCGTTTTTATTTTA, α*Tubulin* CGTACCAGTGGACGAAGGCA, *Repo* GTGTAGTGCTGATGATGTTGATGAT. *αTubulin* was used as a positive control to verify that the dissection was successful, and the glial gene *Repo* was used to control for glial cell contamination. Two rounds of PCR amplification, 25 and 35 cycles, were performed using Q5 High Fidelity Polymerase (New England Biolabs, Ipswich, MA) using the following forward and reverse primers, respectively, for each gene:

Ten-m ATCAGGCAGCGAATGATACC, GGTCCCAGCTCAATCACAAT;

Ten-a CTCAGCGATAACCTCCGTTC, TCTGCGTCGAAATCCCTATC;

α*Tubulin* CTACGGCAAGAAGTCCAAGC, CCAATCAGACGGTTCAGGTT;

Repo GCTGTTACTGTGCGTTCCAA, CATTCGGCAGTATGGTGTTG.

4.4.3 Carbocyanine dye labeling and imaging

Lipophilic dye labeling of single mechanosensory axons was performed as described in the detailed protocol in **Chapter 2**.

4.4.4 Image Analysis

Image analysis, branch measurements, and statistical analysis were performed as described in **Chapter 2.** *455-Gal4/+* control animals have pSc axon branching patterns that are not different from wildtype, therefore for qualitative analysis of pSc axon phenotypes the prototypical skeleton of the wildtype pSc axonal arbor was used. Axon guidance errors of the primary axon entry point were occasionally observed in *455-Gal4/+* controls that were never observed in wildtypes, but these were not counted as axon targeting errors. A total of 52 *455-Gal4/+*control, and 106 *455-Gal4/; UAS-dsRNA Ten-m/+* animals were analyzed for axonal targeting errors, branch number and lengths. Qualitative analysis of axonal targeting errors was performed by classifying *Ten-m* RNAi phenotypes in 4 specific categories that were occurring at frequencies below 10% in control animals.

4.4.5 Behavioral Analysis

The behavioral assay was performed as described in the detailed protocol in **Chapter 2**. The scutellum-specific *455-Gal4* driver was used to drive *UAS-dsRNA Ten-m* only in the four scutellar mechanosensory neurons to ensure that the postsynaptic neural circuitry was left unperturbed by the gene manipulations. Experiments were performed on two day old female flies with the experimenter blind to genotype. A total of 162 *455-Gal4*/+ controls, 101 UAS-*dsRNA Ten-m* controls, 155 *455-Gal4*/+; UAS-*dsRNA Ten-m*, 110 *Ten-m*^{null}/+, 83 *455-Gal4*/+; UAS-*dsRNA Ten-m/Ten-m*^{null}, and 151 *455-Gal4*/+; UAS-*dsRNA Ten-m/UAS-Ten-a* were analyzed using DiD stimulation.. Statistical significance in response rate between genotypes was determined using a two tailed *t*-test for proportions set at $p < 0.05$.

4.5 Results

4.5.1 Small scale RNAi screens can identify genes involved in targeting of the pSc axon

We took a targeted approach to look for genes that have been previously shown to be involved in branch repulsion, attraction, and synaptic target selection. Using RNAi we screened three of the five *Drosophila* semaphorins. dSema1a is a transmembrane semaphorin that can act by forward signaling as a ligand to PlexinA or by reverse signaling as a receptor (Winberg et al., 1998; Komuyama et al., 2007). dSema1a has been shown to regulate dendritic and axonal targeting in the *Drosophila* olfactory system (Komiyama et al., 2007; Latterman et al., 2007; Sweeney et al., 2007). We found that *dSema1a* RNAi did not affect pSc branching (**Figure 4.1b**). This result was not surprising, since it has been previously shown that its receptor PlexinA regulates correct targeting of the pSc neuron by restricting branch overgrowth (Neufeld et al., 2011). Nervy, an A kinase anchoring protein, has been suggested to couple Protein Kinase A (PKA) signaling to PlexinA-Sema1a-mediated repulsion (Terman and Kolodkin, 2004). We tested whether Nervy is also involved in pSc axon targeting through this pathway. We found that knockdown of *Nervy* does not affect axonal targeting, suggesting that the previously reported role of PlexinA might not involve the PKA-regulated pathway (**Figure 4.1e**). We also tested the knockdown of *dSema2b*, a secreted semaphorin that is a ligand for PlexinB (Ayoob et al., 2006), and *dSema5c* which has been suggested to be involved in olfactory system development (Rollmann et al., 2007). Neither *dSema2a* nor *dSema5c* RNAi produced obvious branching phenotypes (**Figure 4.1c,d**).

Because we have previously demonstrated critical roles for Dscam, we wanted to test if its most closely related immunoglobulin superfamily member Sidekick (Yamagata et al., 2002) is similarly involved in targeting of the pSc axon. However, *Sidekick* RNAi did not impair pSc

axonal targeting (**Figure 4.1f**). Next, we tested the two *Drosophila* teneurins, Ten-a and Ten-m, which have been implicated in target selection in the olfactory and neuromuscular systems (Hong et al., 2012; Mosca et al., 2012). We found that knockdown of *Ten-a* had no effect on the pSc branching pattern, however knockdown of *Ten-m* produced obvious phenotypes, notably truncated arbors (**Figure 4.1g,h**). We focus on characterizing this phenotype in the rest of this study.

4.5.2 Loss of Ten-m produces stereotyped targeting errors and reduces arbor size

To confirm that *Ten-m* is indeed expressed in the pSc neuron, we detected the presence of *Ten-m* RNA in a single pSc neuron by RT-PCR. A single pSc soma was microdissected from the periphery by carefully cutting around the bristle socket with a fine scalpel. This captures a large number of surrounding cells, but only the single pSc neuron because it is well isolated from other bristles. Other RNA can come from the hair, socket, sheath and glial cell of the sensory organ and approximately 50-100 surrounding epithelial cells that are captured. Out of all these cells the glial cell of the sensory organ originates from a precursor cell that adopted a neural fate and might be expressing molecules shared by neurons (Gho et al., 1999). The glial cell migrates away from the neuron during development and whether the dissection captures the glial cell can be tested using the glial marker *Repo* (Gho et al., 1999) (**Figure 4.2a**). Our RT-PCR results supported both the negative and positive RNAi phenotypes by identifying *Ten-m*, but not *Ten-a*, mRNA expressed in the pSc neuron (**Figure 4.2a**).

In order to characterize the *Ten-m* RNAi phenotypes, we first verified that *455-Gal4/+* and *UAS-dsRNA Ten-m* control animals had wildtype axonal arbors (**Figure 4.2b,c**). Errors in

axonal targeting were defined as mistargeting events that occur with less than 10% frequency in wildtype animals, and control animals did not have targeting errors in their arbors (*n* = 52 *455-Gal4/+* and *n* = 17 *UAS-dsRNA Ten-m*). In contrast, 42% of *455-Gal4/+; UAS-dsRNA Ten-m/+* animals (*n* = 106) had axonal targeting errors within their arbors. The most common error occurring in 38% of animals was that the axon did not terminate in the anterior CNS and instead followed another nerve fiber leaving the CNS (**Figure 4.2d**, all panels). Multiple errors co-occurred within the same axon and were observed in 33% of animals. These involved posterior truncations and stereotyped midline crossing errors (**Figure 4.2d**). In severe cases (9.5% of animals) the axons had an undeveloped arbor consisting of only few short branches (**Figure 4.2d,** bottom right panel**)**.

Since *Ten-m* null mutants are homozygous lethal at the early embryonic stage (Zheng et al., 2011) and a MARCM line is currently not available, we were not able to confirm these knockdown phenotypes with a complete knockout. Instead we further reduced the levels of Ten-m in RNAi animals by creating animals that carry one copy of *UAS-dsRNA Ten-m* and one *Ten-m* null allele. We found that these transheterozygous Ten-m mutant animals had the same severe targeting errors as only *Ten-m* RNAi (**Figure 4.2e**). Although we did not observe an increase in the occurrence of targeting errors, no new errors were introduced by reducing the levels of Ten-m with a null allele, suggesting that the targeting errors that we observed were due to a reduction in *Ten-m* and not non-specific effects of the RNAi.

We categorized the stereotyped errors into four non-mutually exclusive categories by measuring the frequency of occurrence of specific branching defects in *Ten-m* RNAi axons (**Figure 4.3a**). These targeting error categories were rarely (< 10% occurrence) or never seen in *455-Gal4/+* controls (*n* = 52), and were significantly more frequent in *455-Gal4/+; UAS-dsRNA*

Ten-m/+ animals ($p < 0.05$, $n = 106$). By categorizing the types of errors we found that they either involved inappropriate branch extension in the anterior CNS (**Figure 4.3a**, categories 1 and 2), or failure to elaborate the posterior arbor (**Figure 4.3a**, categories 3 and 4). Overall, *Ten-m* RNAi resulted in a significant reduction in the number of branches ($p < 0.01$) and their cumulative branch length compared to axons in control animals ($p < 0.05$) (**Figure 4.3b**).

The expression of dsRNA and its processing into small interfering RNAs can sometimes lead to non-specific downregulation of other non-target mRNA, through degradation or translational silencing, which could lead to false-positive results (Kulkarni et al., 2006; Sharma and Rao, 2009). Furthermore, insertion of UAS- driven dsRNA transgenes into the *Drosophila* genome can have a positional effect on expression or cause dominant phenotypes (Green et al., 2014). To control for off-target effects of RNAi we compared the phenotypes of two independent RNAi lines: the VDRC51173 line created by P-element insertion by the Vienna *Drosophila* Resource Center, and JF03323 line created by phiC31 site-directed insertion by the Transgenic RNAi Project. We found that each category was equally represented by both RNAi lines, strengthening the conclusion that the observed phenotypes were indeed due to loss of Ten-m (**Figure 4.4**). Furthermore, driving dsRNA against *Ten-a* does not produce targeting errors **(Figure 4.1g)** and control *UAS-dsRNA Ten-m* flies, in which no dsRNA expression is driven, have wildtype axonal arbors (**Figure 4.2b)**.

4.5.3 Loss of Ten-m impairs mechanosensory circuit function

To investigate if the structural defects that we observed in *Ten-m* mutant pSc axons affected the downstream function of the circuit, we tested the ability of the animals to respond to

mechanical stimulation of the pSc bristles. We observed that *Ten-m* knockdown resulted in a significant reduction in the ability of the animal to respond to bristle stimulation by brushing its scutellum (from 22% response rate in *455-Gal4/+* controls and 20% response rate in *UAS-dsRNA Ten-m* controls to 12% response rate in *455-Gal4/+; UAS-dsRNA Ten-m/+*, $p < 0.05$, $n > 100$ for all genotypes), presumably due to the inability of the pSc axon to target to its postsynaptic targets (**Figure 4.5**). We also found that *455-Gal4/+; UAS-dsRNA Ten-m/Ten-m^{null}* animals had similar cleaning reflex response rate as *455-Gal4/+; UAS-dsRNA Ten-m/+* (14%, $p > 0.05$, n = 83), and this was presumably because of the low levels of Ten-m and not due to an effect of the genetic background of *Ten-m^{null}/+* (**Figure 4.5a**).

4.5.4 Expression of Ten-a can compensate for loss of Ten-m in the mechanosensory neuron

Previous studies that demonstrated that Ten-m is involved in synaptic partner matching in the *Drosophila* olfactory system and neuromuscular junction suggested that at basal levels Ten-a and Ten-m interact heterophilically across synapses. However homophilic interaction between Ten-m proteins on pre- and postsynaptic cells instructs axonal targeting, where cells with high Ten-m levels target to other cells with high Ten-m levels (Hong et al., 2012; Mosca et al., 2012),. Since we did not detect *Ten-a* mRNA expression in the pSc neuron (**Figure 4.2a**) we were interested if ectopic expression of Ten-a will perturb the targeting of the pSc axon. Interestingly, we found that ectopic expression of Ten-a restored correct synaptic targeting in *Ten-m* knockdown neurons (**Figure 4.6a**). In addition, the behavioral response in these animals was rescued to control levels (**Figure 4.5a**), implying that there is functional redundancy between the two teneurins for the wiring and function of the mechanosensory circuit. Nevertheless, when the

levels of Ten-m were normal and we ectopically expressed Ten-a, the synaptic targeting of the pSc axon was not impaired (**Figure 4.6b**).

Next, we overexpressed Ten-m solely within scutellar neurons using a construct that inserts a UAS binding site in front of the endogenous *Ten-m* promoter, *P{GSV6} Ten-m*^{GS9267}. Similar to previously published results (Mosca el al., 2012), we observed no major defects in the targeting of the pSc axon (**Figure 4.6c**). Thus, it is possible that the pSc neuron targets to postsynaptic cells that also have high teneurin expression levels. Unfortunately, one disadvantage of the mechanosensory system is that we do not know the identity of postsynaptic targets and therefore we cannot directly vary the postsynaptic levels of Ten-m.

4.6 Discussion

Genetic and RNAi screens have been used successfully to identify synaptic targeting roles of leucine-rich repeat proteins Tartan and Capricious (Kurusu et al., 2008) and RNA-binding proteins with roles in dendritic patterning (Olesnicky et al., 2013). In this study we knocked down seven genes that have been previously implicated in circuit development and tested for structural defects in pSc axonal branching. The observations from the small scale RNAi screen were two-fold. First, we found that out of seven screened genes only one was expressed and utilized for pSc axon targeting. This suggests that the repertoire of targeting molecules expressed by this neuron may be rather limited. Second, by characterizing the Ten-m phenotype, we observed that the targeting phenotypes were extremely stereotyped and very different from previously reported pSc branching defects (see **Chapter 2** and Chen et al., 2006 for Dscam loss of function, **Chapter 3** for Dscam overexpression and Plexin overexpression,

Neufeld et al., 2011 for PlexinA and PlexinB loss of function). Therefore, the mechanosensory axon is a good system to confirm and to discover novel genes involved in pSc axonal targeting. If we identify the specific targeting contribution of each gene through analysis of stereotyped errors, we could dissect the cellular mechanisms that these wiring instructions employ.

We identified Ten-m in a screen for structural changes in axonal branching, and we subsequently showed that mechanosensory circuit function is also compromised in *Ten-m* RNAi animals. A reverse screening strategy is also possible: screening for changes in behavior and then determining if the gene is involved in synaptic targeting by examining the morphology of the axonal arbor. The key difference between structural and behavioral screens is that a change in behavior is not restricted to genes that affect synaptic target recognition, but also neural and bristle development, synapse formation, maintenance or transmission. Therefore, impairment or potentiation of sensory perception might not necessarily predict a change in the structure of the neuron. This is illustrated in our experiments in **Chapter 3** where overexpression of FMRP in mechanosensory neurons impaired both behavioral output and the axonal targeting, however structurally restoring branch targeting by increasing the levels of Dscam did not rescue the behavioral deficits (Cvetkovska et al., 2013). This example clearly illustrates the need for assessing both structure and function when evaluating the effects of genetic manipulation on synaptic targeting. If we assume that every axonal branch in the invariable "core" arbor forms functional contacts with postsynaptic partners, then branching defects will result in loss of these synapses. In this case, phenotypes that deviate from wildtype arbors in morphological screens are expected to produce a change in behavioral response. Conversely, specific structural phenotypes may reveal if specific branches are dispensable for eliciting a grooming reflex.

Characterization of the *Ten-m* knockdown phenotype raised several interesting points. The stereotypy of the phenotypes indicates that Ten-m has very specific roles in the development of the axonal arbor and these were dependent on the location within the CNS. Consistent with previously suggested functions (Minet et al.,1999; Al Chawaf et al., 2007; Suzuki et al., 2014), Ten-m seems to be involved in neurite outgrowth in the mechanosensory neuron, as loss of Ten-m prevented the projection of the pSc axon into the posterior regions of the CNS (**Figure 4.1h**, **Figure 4.2d, e** and **Figure 4.3a**). Interestingly, the opposite effect was observed in the anterior CNS where branches failed to terminate or projected inappropriately across the midline (**Figure 4.1h, Figure 4.2d, e** and **Figure 4.3a**). These conflicting observations in the same axonal arbor suggest a possible dual attractive and repulsive function. Ten-m may be interacting with different postsynaptic ligands, or other, unknown mechanisms could be contributing to differential downstream signaling depending on whether the branch projects to anterior or posterior areas in the CNS. A strict distinction between posterior attraction and anterior repulsion suggests that gradients of Ten-m levels may contribute to our observations. A gradient of mouse Ten-m3 expression has been described in the dorso-ventral axis of the retina and lateral geniculate nucleus (LGN), where high Ten-m3 expressing retinal ganglion cells originating from the ventral retina project to high Ten-m3 expressing regions of the dorsal LGN (Leamey et al., 2007). This study also found that loss of Ten-m3 gradients in knockout animals disrupted the retinotopic map by mistargeting retinal ganglion cells along the dorso-ventral axis of the LGN. If this mechanism is conserved in *Drosophila*, and there is an increasing Ten-m gradient along the anterior-posterior axis of the CNS, this could explain how wildtype axons that normally express high levels of Ten-m project posteriorly and do not extend too far anteriorly. Thus *Ten-m* RNAi axons, in which expression of Ten-m is low, would not be able to project to the posterior of the

CNS anymore, and would preferentially match with lower Ten-m expressing cells in the anterior CNS (**Figure 4.2d** and **Figure 4.3a**). Nevertheless, an anterior-posterior gradient might not fully account for the contralaterally projecting branching errors that we observed (**Figure 4.3a**, categories 2 and 3). Immunohistochemical staining and *in situ* hybridization for *Ten-m* transcripts may reveal the existence of discrete Ten-m gradients within the CNS, and so establish a mechanism that could explain our observations.

Another interesting observation on the *Ten-m* RNAi phenotype was the range of severity of axonal mistargeting. Axonal mistargeting was 42% penetrant in these animals, and those that presented a phenotype ranged from inappropriate branch extension to severely truncated pSc axons (**Figure 4.2d, e**). Variability in dsRNA expression or *Ten-m* gene expression, or redundancy with other cell surface receptors may account for this (Raj et al., 2010). We also observed that the errors in the anterior portion of the arbor were represented in a higher proportion of animals (**Figure 4.3a)**. The reduced penetrance of truncation errors may suggest a differential sensitivity to Ten-m levels in the anterior versus posterior regions of the CNS. In such a model, a critical level of Ten-m would be required to prevent midline crossing or to terminate the axonal anterior extension. Therefore reduction in Ten-m levels would result in the increased frequency of these errors. Conversely, the attractive function of Ten-m in the posterior arbor may be less sensitive to Ten-m levels, and so the truncation errors would occur less often. Additional experiments are required to confirm this model, such as examining the phenotypes in MARCM mosaic loss-of-function animals.

Ten-a and Ten-m are known to interact both homophilically and heterophilically *in vivo* (Mosca et al., 2012). In the *Drosophila* neuromuscular junction it has been shown that correct targeting of motor neurons to their target muscles depends on high Ten-m expression in both

tissues (Mosca et al., 2012). If the mechanism of axonal targeting uses strictly homophilic Ten-m interactions it is not clear how Ten-a could compensate for loss of Ten-m in mechanosensory neurons (**Figure 4.5a** and **Figure 4.6a**). One possibility is that targeting specificity switches to a heterophilic interaction between the ectopically expressed Ten-a protein and postsynaptic Ten-m. Overexpression of teneurins, either by ectopically expressing Ten-a or by overexpressing Ten-m in the mechanosensory neuron, does not lead to impairment of the axonal targeting because the targeting choice is already determined by high teneurin expression in pre- and postsynaptic cells. The mechanism that could allow teneurin heterophilic interaction to assume a targeting role remains to be investigated.

Not much is known about how teneurins signal in the cell. The intracellular domains of vertebrate teneurins are relatively conserved in size and sequence, however the intracellular domains of invertebrate teneurins are not conserved with vertebrates, or between themselves (Tucker and Chiquet-Ehrismann, 2006; Tucker et al., 2011). Some similar features in all teneurins include proline-rich stretches predicted to be docking sites for SH3 adaptor proteins, and tyrosine residues that could be phosphorylated (Tucker and Chiquet-Ehrismann, 2006; Tucker et al., 2011). While these features are indicative of signaling initiation, there is evidence that some teneurins can be cleaved and translocated to the nucleus where they could regulate transcription. For example, the intracellular domains of *C. elegans* Ten-1 and vertebrate Ten-m1 and Ten-m2 have been localized in nuclear puncta (Drabikowski et al., 2005; Nunes et al., 2005; Bagutti et al., 2003), and some studies have shown interactions between vertebrate teneurins with the transcription factor Zic-1 and the transcriptional repressor MBD1. (Bagutti et al., 2003; Nunes et al., 2005). Interestingly, there is some evidence that homophilic interaction between the extracellular domains can cause cleavage of Ten-m2 and translocation into the nucleus (Bagutti

et al., 2003), suggesting that contact mediated proteolysis could potentially modify gene transcription. It is not known if the intracellular domains of *Drosophila* Ten-m or Ten-a can translocate to the nucleus, although both contain at least one putative nuclear localization signal (Tucker et al., 2011). Generating antibodies specific for Ten-m and Ten-a intracellular domains and mutants that lack intracellular or extracellular domains are needed to investigate the interesting possibility that *Drosophila* teneurins regulate synaptic partner matching and targeting not through their extracellular domains, but rather through transcription factor activity.

Drosophila RNAi experiments must be heavily controlled. In addition to off-target effects of the dsRNA down-regulating unrelated mRNAs, the methods of generating *UAS-dsRNA* animals carry risks for unintended genetic effects. Both P-element and site-directed insertions can result in multiple insertions that may cause dominant phenotypes (Green et al., 2014). Without a loss-of-function mutant in the present study it is hard to provide definitive proof that *Ten-m* knockdown phenotypes are due to loss of *Ten-m* expression. Nevertheless, for all experiments, we used two independently created RNAi lines, one created by random P-element insertion (VDRC51173) and another by phiC31 integrase site-directed insertion (JF03323). If any phenotypes were dominant, it seems unlikely that they would be observed in both RNAi lines, and indeed the phenotypic representation in all categories was indistinguishable between the two lines. Observing no dominant phenotypes in *UAS-dsRNA* animals that do not express Gal4 is an additional control that confirms the validity of the knockdown phenotype. The level of scrutiny and genetic controls required should not undermine results from RNAi-based experiments or screens, rather it points out to a general principle of how good experimental conclusions should be reached.

4.7 Figures

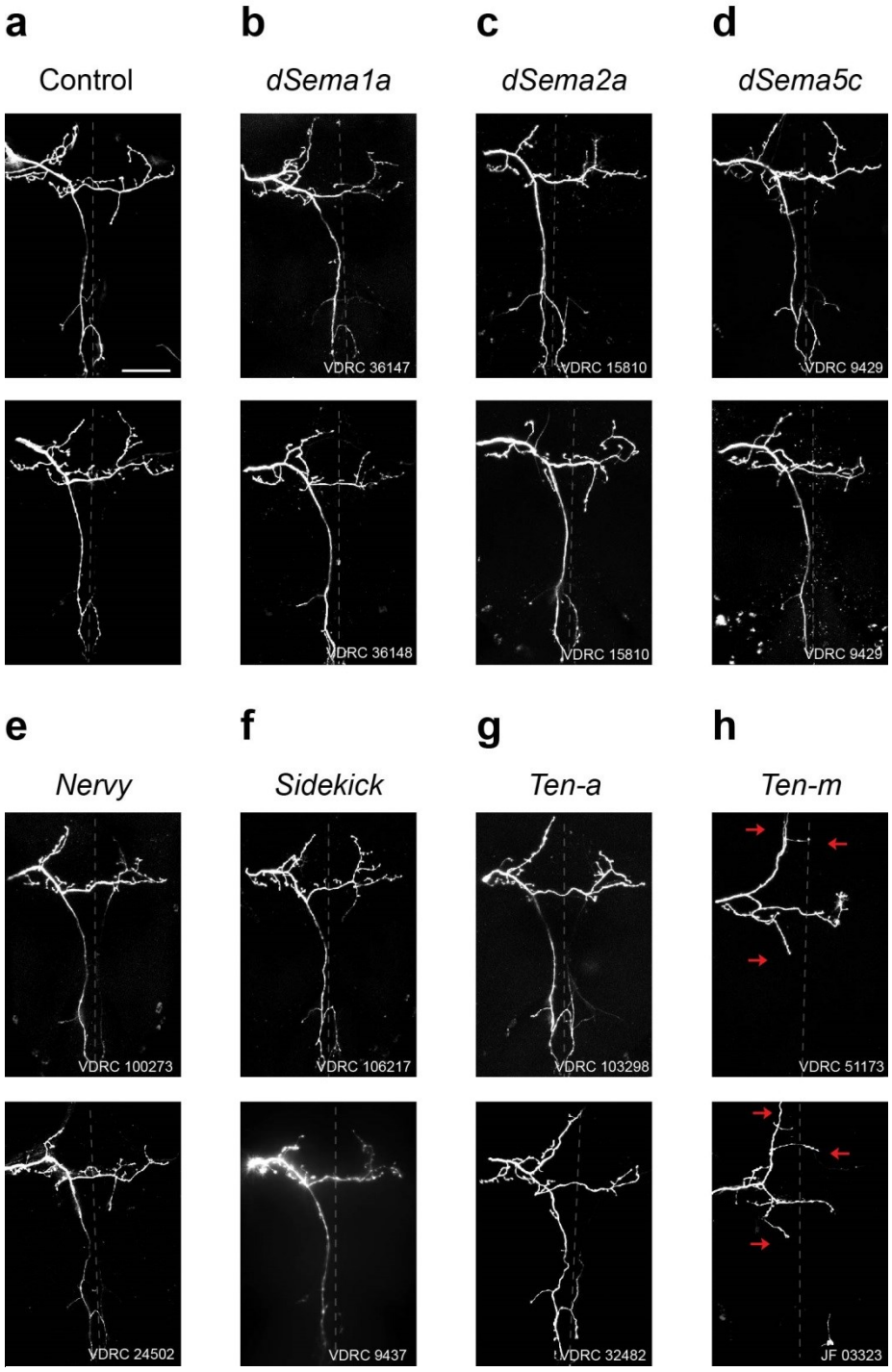

Figure 4.1 Scutellar-specific knockdown of genes implicated in circuit development reveals their role in targeting of the posterior scutellar (pSc) axon.

a, Representative images of the wildtype branching pattern of the pSc axon are shown for control *455-Gal4/+* animals.

b-g, dsRNA-mediated knockdown of three Semaphorins *dSema1a*, *dSema2a*, *dSema5c*, the potential downstream mediator *Nervy*, immunoglobulin cell adhesion receptor *Sidekick* and EGF-like *Ten-a* did not produce noticeable impairment of axonal targeting. Multiple RNAi lines were used when available, except for *dSema2a* and *dSema5c*. Representative images are shown for each gene, with the specific RNAi line used shown in the bottom right corner of each image.

h, dsRNA-mediated knockdown of the second teneurin gene in *Drosophila, Ten-m* produced an obvious targeting phenotype in the pSc axon. Deviations from the wildtype branching pattern are indicated by red arrows. These involved truncation of the arbor, inappropriate midline crossing of a specific branch and inappropriate extension into the anterior CNS. Similar phenotypes were observed in two RNAi lines, indicated in the bottom right corner of each representative image.

The midline of the CNS is indicated by a dotted line. Scale bar is 50μm.

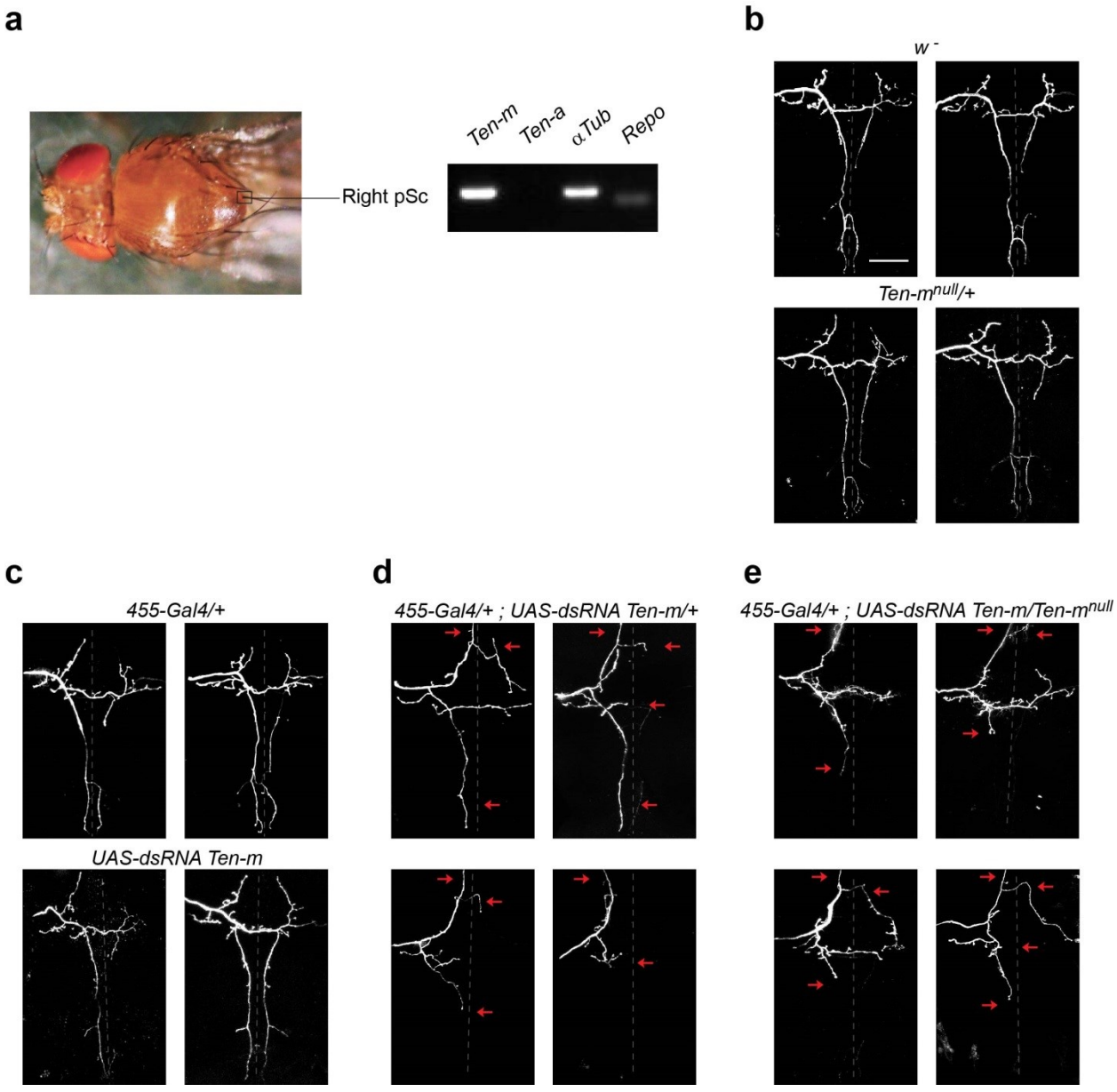

Figure 4.2 Loss of *Ten-m* impairs pSc axonal targeting.

a, *Ten-m* is expressed in the pSc neuron. *Ten-m*, but not *Ten-a,* mRNA is detected in a single pSc neuron preparation. *αTubulin* is used as a positive control and the glial marker *Repo* is used to control for glial cell contamination.

b, Wildtype pSc axons have characteristic branching patterns. The pSc axon forms an invariant and stereotyped arbor that extends contralaterally across the midline of the CNS and into the

posterior of the CNS. Two representative images of wildtype w^- pSc axons are shown in the top panels. Two representative images of *Ten-m*^{null}/+ heterozygotes (bottom panels) show wildtype pSc axonal branching.

c, *455-Gal4/+* (top panel) and *UAS-dsRNA Ten-m* control animals (bottom panel) have wildtype pSc axonal branching.

d, Four representative images are shown for *Ten-m* knockdown pSc axons. The same stereotyped errors were observed in phenotypes that varied in severity. The top panels show axons that extend into the posterior CNS however fail to elaborate contralateral projections, and also have inappropriate extensions in the anterior CNS. The bottom panels show axons that fail to extend in the posterior CNS but share the other stereotyped errors as the top panel examples. Targeting errors are indicated by red arrows.

e, Four representative images are shown for transheterozygous Ten-m mutant animals that carry one copy of *UAS-dsRNA Ten-m* and one copy of a *Ten-m* null allele. The same errors were observed as in animals that only have *UAS-dsRNA Ten-m* (red arrows). The midline of the CNS is indicated by a dotted line. Scale bar is 50μm.

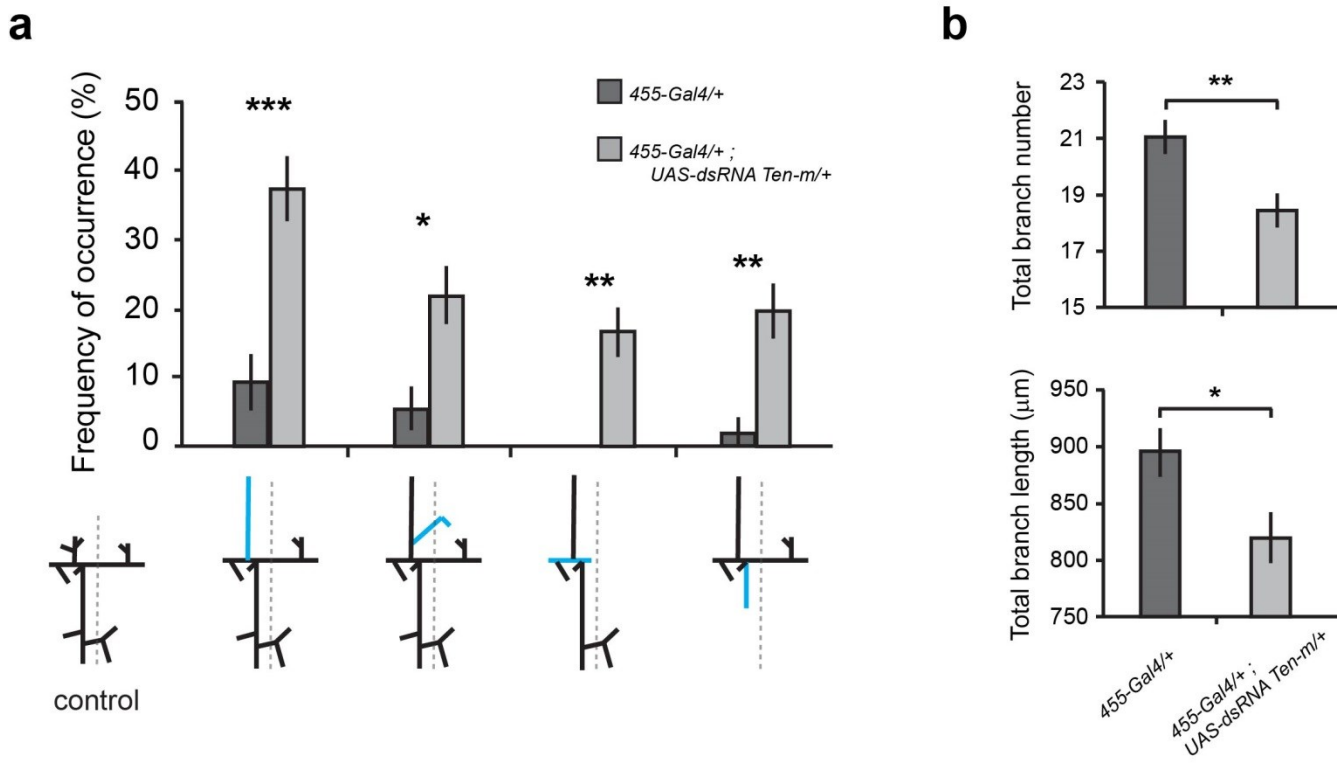

Figure 4.3 Four non-mutually exclusive targeting error categories constitute the *Ten-m* knockdown phenotype.

a, The frequency of occurrence of the four stereotyped targeting errors observed in *Ten-m* knockdown axons is shown compared to *455-Gal4/+* controls. Each category is displayed as a schematic, with the blue branches indicating the targeting error. All errors were significantly more frequent in *455-Gal4/+; UAS-dsRNA Ten-m/+* animals ($p < 0.05$, $n = 106$) than in *455-Gal4/+*controls ($n = 52$). 42% of *Ten-m* knockdown animals had at least one of these errors, and 38% involved failure to terminate in the anterior CNS (first category). 22% of animals also extended a contralateral branch in the anterior part of the arbor that inappropriately crossed the midline (second category). Contralateral and posterior truncations (third and fourth categories) were observed at 17% and 20%, respectively. Error categories are displayed as schematics, with the blue branches indicating the targeting error.

b, *455-Gal4/+; UAS-dsRNA Ten-m/+* animals had a significant reduction in the average number of branches in the axonal arbor ($p < 0.01$), which resulted in a significant reduction in the average cumulative branch lengths ($p < 0.05$), compared to *455-Gal4/+* controls.

All error bars are standard error of the mean. * $p < 0.05$, ** $p < 0.01$, *** $p < 0.001$

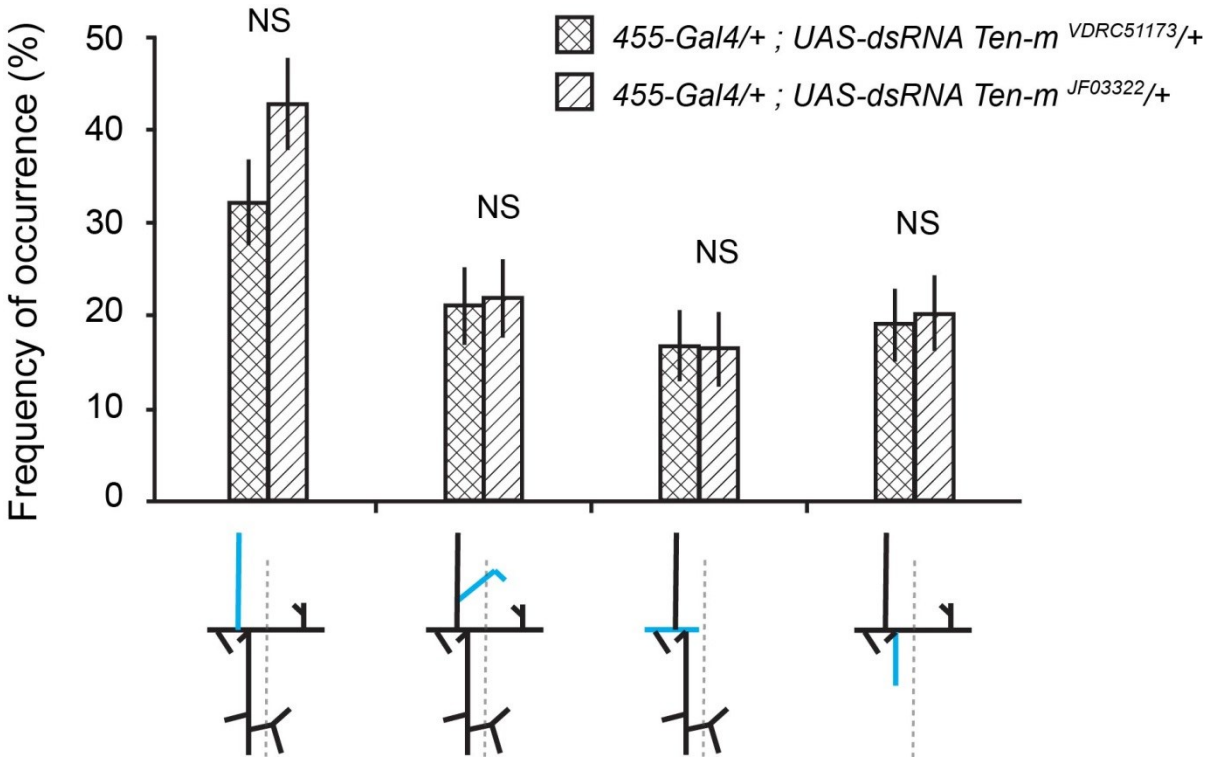

Figure 4.4 Two independent RNAi lines contribute equally to the observed *Ten-m* knockdown phenotypes.

The frequency of occurrence for the stereotyped targeting errors is compared between *455-Gal4/+; UAS-dsRNA Ten-m VDRC51173/+* (n = 47) and *455-Gal4/+; UAS-dsRNA Ten-m JF03322/+* animals (n = 59). Neither RNAi line contributed significantly more than the other to any targeting error.

Error categories are displayed as schematics, with the blue branches indicating the targeting error. All error bars are standard error of the mean. NS indicates not significant.

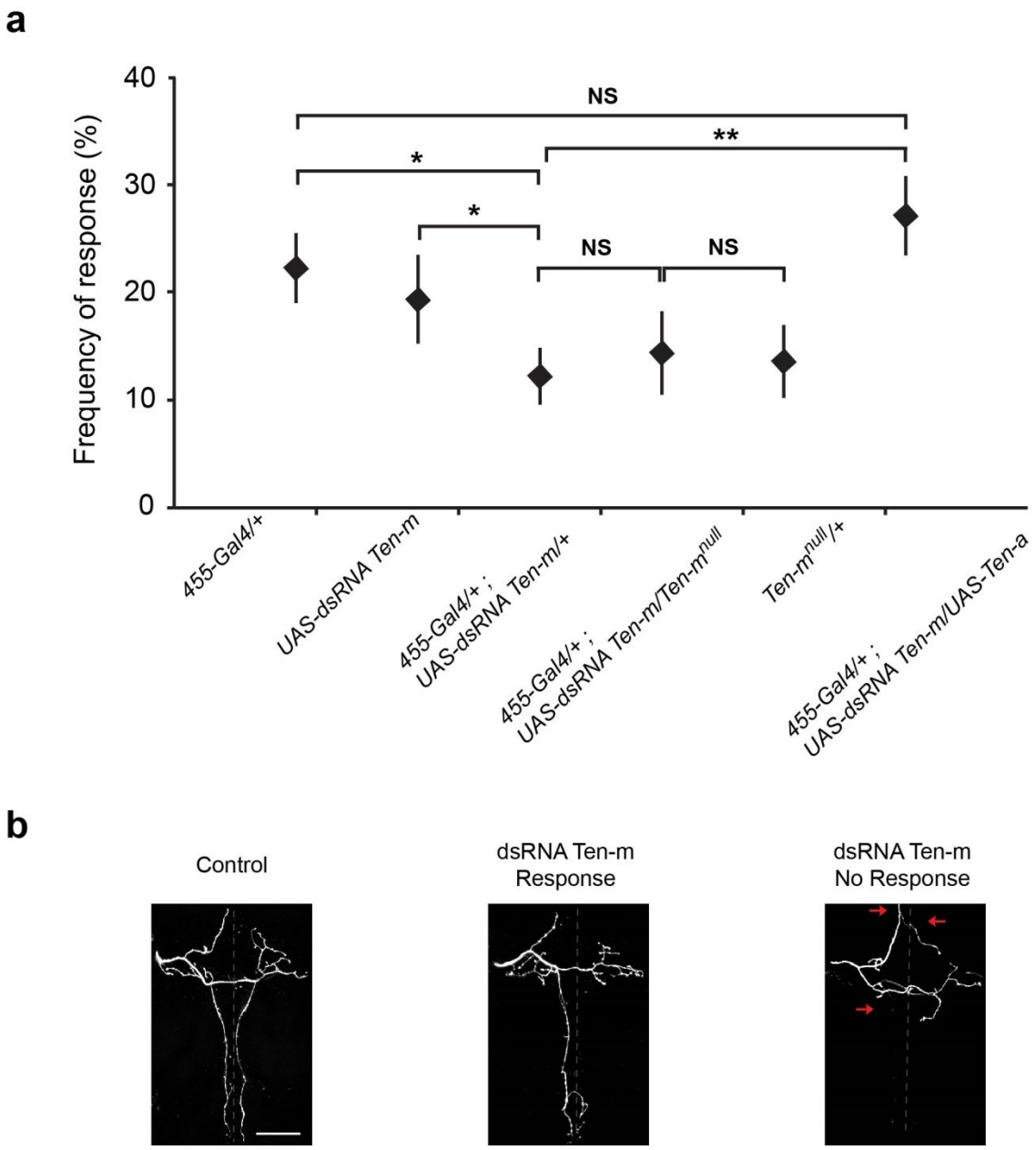

Figure 4.5 *Ten-m* knockdown in the pSc neurons impairs the function of the mechanosensory circuit.

a, The frequency of eliciting a grooming reflex upon mechanical stimulation of pSc bristles was compared between different genotypes. *Ten-m* knockdown in the scutellar neurons in *455-Gal4/+; UAS-dsRNA Ten-m/+* animals significantly reduced the ability of the animals to respond to bristle stimulation compared to *455-Gal4/+* and *UAS-dsRNA Ten-m* controls ($p < 0.05$, $n >$

100 for all genotypes). Transheterozygous *Ten-m* mutant animals *455-Gal4/+; UAS-dsRNA Ten-m/Ten-m*^{null} (n = 83) had a similar response rate as just *Ten-m* knockdown. Driving the expression of *Ten-a* in *Ten-m* knockdown animals (*455-Gal4/+; UAS-dsRNA Ten-m/UAS-Ten-a,* n = 151) restored the response rate to control levels. Error bars are standard error of the mean. * $p < 0.05$, ** $p < 0.01$, NS indicates non-significant.

b, Representative images are shown for a control pSc axon and *Ten-m* knockdown axons that either succeeded or failed to respond to pSc bristle stimulation. Targeting errors in *Ten-m* knockdown axons are indicated by red arrows. The midline of the CNS is indicated by a dotted line. Scale bar is 50μm.

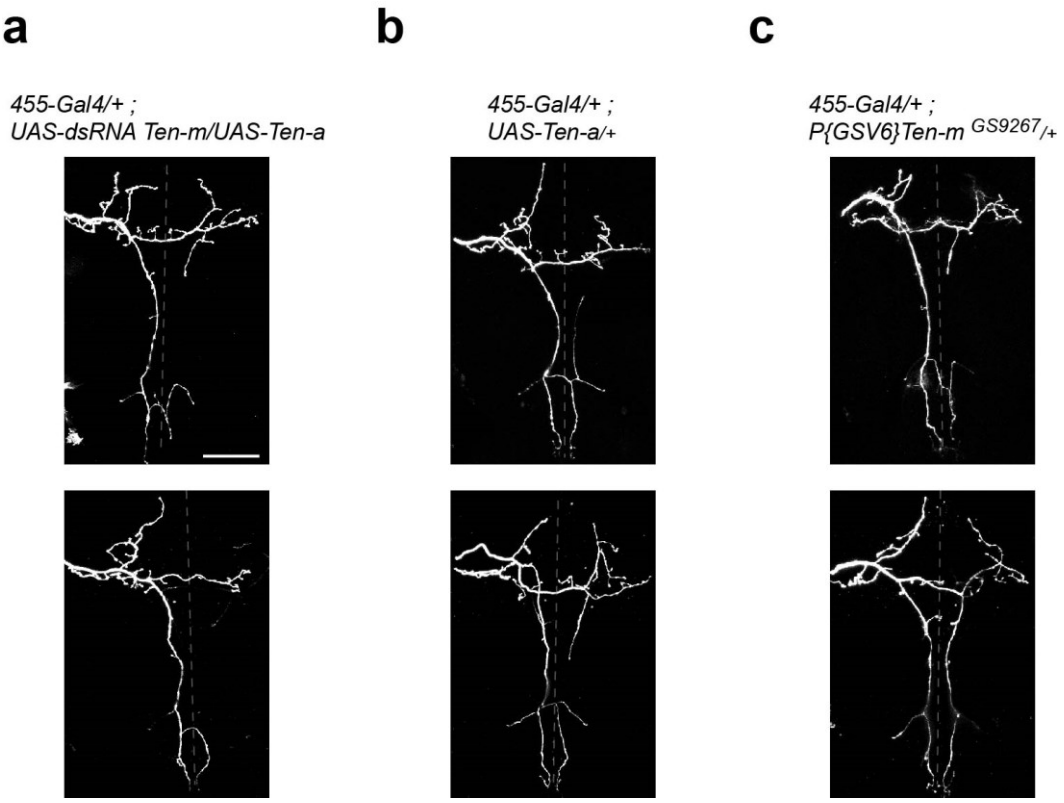

Figure 4.6 Ectopic expression of *Ten-a* can rescue the axonal targeting defects in *Ten-m* knockdown animals.

a, Animals in which *Ten-m* is knocked-down and that have *Ten-a* ectopically expressed in the scutellar neurons (*455-Gal4/+ ; UAS-dsRNA Ten-m/UAS-Ten-a*) do not have targeting errors characteristic of *Ten-m* knockdown and show a normal axonal branching pattern (n = 22).

b, Ectopic expression of *Ten-a* in the scutellar neurons in *455-Gal4/+ ; UAS-Ten-a/+* animals does not impair the targeting of axonal branches (n = 8).

e, Overexpression of Ten-m by driving the endogenous promoter in *P{GSV6} Ten-m*^{GS9267} animals only in the scutellar neurons does not impair the axonal arbor (n = 17).

Two representative images for each genotype are shown. The midline of the CNS is indicated by a dotted line. Scale bar is 50μm.

Chapter 5

General conclusions and future directions

Billions of neurons provide us with the ability to experience our surroundings by forming organized networks dedicated to efficient processing of information. We still understand very little about how wiring precision is achieved at the level of single neurons. Complex orchestrations of different molecular and cellular mechanisms act together to achieve this complex task. Hard-wired circuits, such as the *Drosophila* mechanosensory circuit, form precise connections independent of experience and therefore must follow strict wiring rules. The intricate axonal branching patterns of different mechanosensory neurons (**Figure 1.3**) allow them to appropriately respond to spatially defined stimuli. In these neurons very little variability in connectivity is allowed, and indeed this can be observed in the high level of stereotypy of a particular axonal arbor between individual animals. Thus, the targeting mechanisms employed by mechanosensory axons are most likely predominantly genetically encoded in each neuron. Taking advantage of the tight genetic control of axonal branch targeting, the studies in this dissertation have demonstrated that we can assess both structure and function of the primary sensory neuron in the circuit, and that we can identify genes and their specific mechanisms that contribute to establishing an invariant wiring scheme.

While the study of invertebrate model organisms is invaluable in learning the basic mechanisms developed by biological systems, an ultimate goal of neuroscience is to understand ourselves. It remains to be determined whether the same rules that apply in a *Drosophila* hard-wired circuit apply to mammalian systems. It is clear that different systems have evolved independent mechanisms for using the same proteins for synaptic specificity and there is likely no single molecular "holy grail" of neuronal wiring. Dscam and Ten-m are good examples. Dscam homophilic binding has been shown to function as a repulsive cue in self-avoidance (Hattori et al., 2007; Hughes et al., 2007; Soba et al., 2007; Matthews et al., 2007; Fuerst et al.,

2008), as well as an attractive one in targeting (Yamagata and Sanes, 2008; Zhan et al., 2004). In our model for targeting of the mechanosensory axon, Dscam is absolutely necessary for branch extension, illustrated by the collapsed arbors of Dscam null axons, and likely functions through attractive interactions. The necessity for the full molecular diversity of Dscam for correct targeting has previously suggested that isoform-specific interactions may be responsible for the fine-scale targeting (Chen et al., 2006). Nevertheless, it remains to be seen if single identifiable neurons express pre-determined sets of Dscam isoforms and if isoform matching is truly responsible for instructing specific branches to complementary postsynaptic targets. Similarly, the targeting of olfactory neurons in *Drosophila* is regulated by homophilic Ten-m binding, however in the neuromuscular junction Ten-m is largely absent from the presynaptic neuron (Hong et al., 2012; Mosca et al., 2012). My results suggest that presynaptic Ten-m can have dual attractive and repulsive functions, which could arise from target area-specific interactions with different ligands. Therefore, even within the same axon, different mechanisms using the same protein can add to the complexity of achieving fine-scale circuitry precision.

A conceptual problem that our current techniques have not been able to address is how targeting molecules are localized to decision points along the axon. Furthermore, what defines a decision point? The complex arbor of the pSc axon creates many junctions, bifurcations, and positions where some branch occurrence variability is tolerated. Analysis of mutants that affect the invariant branching pattern could offer some insight into where branching decisions are made. Stereotyped targeting errors in Dscam overexpressing or Ten-m knockdown animals suggest that these proteins may be localized to decision points that generate these errors. Therefore, by mapping positions in mutant arbors that sprout ectopic branches or lose invariable branches we could learn about the attractive or repulsive forces that act at these positions. This

could explain why we observed a greater variability in the Dscam overexpression phenotypes, consisting of 15 categories (**Figure 3.4**). Over-clustering of Dscam in local domains may perturb decision-making and contribute to inappropriate responses to other ligands. Hence, some of the stereotyped misrouting errors could have resulted due to a competition between correct and incorrect targets. Conversely, localization to decision points where Dscam is normally not found may have caused stereotyped ectopic branches to sprout because Dscam was being attracted to an inappropriate target. In comparison, loss of Ten-m phenotypes were much less variable and could reflect a sparse localization of Ten-m to only four key decision points (**Figure 4.3**). Several fundamental questions remain to be answered in future studies: how are decision points specified within the axonal membrane, what mechanisms target specific subsets of proteins to them, and how is presentation at the cell surface regulated For example, identification of scaffolding protein complexes that organize synaptic targeting proteins to specific domains could provide evidence for the existence of local decision points. Intracellular proteins could be identified that regulate local translation or membrane trafficking of cell surface receptors. Tightly regulated interactions that control surface presentation, such as the well characterized regulation of Robo receptor by the transient expression of the sorting protein Commissureless, could also be regulating many other targeting molecules (Keleman et al., 2002).

A large part of the work presented here was performed to identify genes that are crucial for the correct targeting of the pSc axon. Previous studies in this system have shown that PlexinA and PlexinB have opposing roles in branch restriction and branch elongation, respectively, in the pSc neuron (Neufeld et al., 2011). It is clear even from small scale screens that the pSc neuron expresses a defined repertoire of proteins that it utilizes for targeting its axon to distinct postsynaptic targets. For example, in **Chapter 4** out of the seven genes that were

investigated based on previously reported roles in other systems, only one was found to be involved in correct wiring of the pSc axon. Therefore, if we can identify all the cell surface molecules that the pSc neuron expresses and utilizes for targeting, this defined set could be considered the molecular wiring code of the neuron. Future studies taking advantage of tagging and isolating cell-type specific mRNA (Miller et al., 2009) and advances in single cell next generation mRNA sequencing (Ramskold et al., 2012) could allow a complete transcriptome analysis of single identifiable mechanosensory neurons. A reasonable hypothesis is that identical neurons would have identical wiring codes, and a high level of arbor similarity between two different mechanosensory neurons (for example, the aSc and pSc neuron, see **Figure 1.3m,n**) would predict a high degree of overlap between the targeting molecules expressed by those two neurons. In contrast, two mechanosensory neurons with very different arbors (for example, the Hu and pSc neuron, see **Figure 1.3c, m**) would be expected to have very different cell surface molecule expression profiles. If this assumption proves to be correct, then it is possible that by changing the expression of key cell surface molecules we could change the wiring decisions that the neuron makes. Re-programming a Hu neuron to assume the axonal branching pattern of a pSc neuron would effectively change the behavioral output of the circuit, so that stimulation of the Hu bristle will elicit a cleaning reflex using the third pair of legs, as opposed to the first pair of legs. Being able to reprogram circuit wiring has important implications, from learning about the genetic control in circuits that mediate innate behaviors to potentially correcting miswiring that occurs in neurodevelopmental disorders.

There is much to be learned before we can achieve the goal of precise and predictable re-wiring of an entire circuit. The molecular mechanisms of synaptic targeting are clearly regulated on multiple levels. On one level, expressing a repertoire of genetically-encoded targeting

instructions imparts a neuron with an identity that allows it to match to appropriate targets through homophilic or heterophilic interactions. On another level, the expression of these targeting molecules has to be tightly regulated at the level of gene transcription and, as we have demonstrated, protein translation for correct dosage, and spatial and temporal expression. While we have shown that FMRP binds all isoforms of *Dscam*, this does not exclude the possibility that other RNA binding proteins may also regulate *Dscam* expression, RNA stability and localization. Furthermore, even all of the cell surface molecules that provide wiring instructions to a neuron are identified, they would likely have inter-coordinated roles. Molecules used for guiding primary branch extension along the anterior-posterior axis of the CNS might also be involved in other aspects of branching, such as proper midline crossing or targeting small tertiary branches to their termination points. It is also not known how these events unfold temporally, whether branches of the axonal arbor are first formed, followed by specification of decision points and elongation, or via simultaneous splitting of two sister branches. As an added consideration, most cell surface molecules may have co-receptors that refine the mechanism of their action (Kirkbride et al., 2005).

This thesis work strongly supports the model that proper development and fine-scale synaptic targeting of mechanosensory neurons is governed by an intrinsic molecular code; nonetheless the contribution of the extrinsic codes, such as the target-derived signals and cellular scaffolds, remain to be determined. Taking a reductionist approach to untangling a complex idea such as brain wiring is important, however it should always relate back to "big picture" concepts. From my studies it is evident that in a hard-wired circuit in the fruit fly the molecular mechanisms that dictate synaptic specificity can be reduced to contributions of specific proteins, but it is essential to keep in mind that for a neuron these molecules are not isolated instructions

but part of a coordinated developmental program that continuously interacts with other cells. Future work in this field will certainly be as exciting as reaching our current state of knowledge has been, and I believe that it will establish a solid framework for understanding the basic mechanisms that allow a developing brain to achieve the extraordinary task of properly wiring complex circuits.

Bibliography

Adams JC. (1977) Technical considerations on the use of horseradish peroxidase as a neuronal marker. *Neuroscience.* 2:141-5.

Agarwala KL, Nakamura S, Tsutsumi Y, Yamakawa K (2000) Down syndrome cell adhesion molecule DSCAM mediates homophilic intercellular adhesion. *Brain Res. Mol. Brain Res.*, 79: 118-26.

Agmon A, Yang LT, Jones EG, O'Dowd DK. (1995) Topological precision in the thalamic projection to neonatal mouse barrel cortex. *J Neurosci.*15:549-61.

Al Chawaf A, St Amant K, Belsham D, Lovejoy DA (2007) Regulation of neurite growth in immortalized mouse hypothalamic neurons and rat hippocampal primary cultures by teneurin C-terminal-associated peptide-1. *Neuroscience*.144:1241-54.

Alves-Sampaio A, Troca-Marín JA, Montesinos ML. (2010) NMDA-mediated regulation of DSCAM dendritic local translation is lost in a mouse model of Down's syndrome. *J Neurosci*. 30:13537-48.

Andrews GL, Tanglao S, Farmer WT, Morin S, Brotman S, Berberoglu MA, Price H, Fernandez GC, Mastick GS, Charron F, Kidd T. (2008) Dscam guides embryonic axons by Netrin-dependent and -independent functions. *Development*, 135: 3839-48.

Angelini DR, Liu PZ, Hughes CL, Kaufman TC. (2005) Hox gene function and interaction in the milkweed bug Oncopeltus fasciatus (Hemiptera). *Dev Biol*. 287:440-55.

Antonarakis SE (1998) 10 years of Genomics,chromosome 21 and Down syndrome. *Genomics* 51:1-16.

Ascano M Jr, Mukherjee N, Bandaru P, Miller JB, Nusbaum JD, Corcoran DL, Langlois C, Munschauer M, Dewell S, Hafner M, Williams Z, Ohler U, Tuschl T (2012) FMRP targets distinct mRNA sequence elements to regulate protein expression.

Nature. 492:382-6.

Ashley CT, Jr., Wilkinson KD, Reines D, Warren ST (1993) FMR1 protein: conserved RNP family domains and selective RNA binding. *Science,* 262: 563-566.

Ayoob JC, Terman JR, Kolodkin AL (2006) *Drosophila* Plexin B is a Sema-2a receptor required for axon guidance. *Development.* 133:2125-35

Bagutti C, Forro G, Ferralli J, Rubin B, Chiquet-Ehrismann R (2003) The intracellular domain of teneurin-2 has a nuclear function and represses zic-1-mediated transcription. *J. Cell Sci.*, 116: 2957–2966

Baker BS et al. (2001) Are complex behaviors specified by dedicated regulatory genes? Reasoning from *Drosophila*. *Cell*, 105: 13–24

Barallobre MJ, Del Río JA, Alcántara S, Borrell V, Aguado F, Ruiz M, Carmona MA, Martín M, Fabre M, Yuste R, Tessier-Lavigne M, Soriano E (2000) Aberrant development of hippocampal circuits and altered neural activity in netrin 1-deficient mice. *Development*, 127: 4797-810.

Barlow GM, Chen XN, Shi ZY, Lyons GE, Kurnit DM, Celle L, Spinner NB, Zackai E, Pettenati MJ, Van Riper AJ, Vekemans MJ, Mjaatvedt CH, Korenberg JR (2001) Down syndrome congenital heart disease: a narrowed region and a candidate gene. *Genet Med* 3:91-101.

Bassell GJ, Warren ST. (2008) Fragile X syndrome: loss of local mRNA regulation alters synaptic development and function. *Neuron.* 60:201-14.

Baumgartner S, Chiquet-Ehrismann R. (1993) Tena, a *Drosophila* gene related to tenascin, shows selective transcript localization. *Mech Dev.* 40:165-76

Baumgartner S, Martin D, Hagios C, Chiquet-Ehrismann R. (1994) Tenm, a *Drosophila* gene related to tenascin, is a new pair-rule gene. *EMBO J.* 13:3728-40.

Bishop KM, Goudreau G, O'Leary DD (2000) Regulation of area identity in the mammalian neocortex by Emx2 and Pax6. *Science.* 288:344-9.

Blank M, Fuerst PG, Stevens B, Nouri N, Kirkby L, Warrier D, Barres BA, Feller MB, Huberman AD, Burgess RW, Garner CC (2011) The Down syndrome critical region regulates retinogeniculate refinement. *J Neurosci.*31:5764-76

Blankenship AG, Feller MB (2010) Mechanisms underlying spontaneous patterned activity in developing neural circuits. *Nat Rev Neurosci*, 11:18-29

Boucard AA, Chubykin AA, Comoletti D, Taylor P, Südhof TC. (2005) A splice code for trans-synaptic cell adhesion mediated by binding of neuroligin 1 to alpha- and beta-neurexins. *Neuron*.48:229-36.

Boucard AA, Maxeiner S, Südhof TC (2014) Latrophilins function as heterophilic cell-adhesion molecules by binding to teneurins: regulation by alternative splicing. *J Biol Chem*. 289:387-402

Brieher WM, Gumbiner BM. (1994) Regulation of C-cadherin function during activin induced morphogenesis of Xenopus animal caps. *J Cell Biol*. 126:519-27.

Brown V, Jin P, Ceman S, Darnell JC, O'Donnell WT et al. (2001) Microarray identification of FMRP-associated brain mRNAs and altered mRNA translational profiles in fragile X syndrome. *Cell,* 107:477-487

Cajal SR (1888). Estructura del cerebelo. *Gac. Med. Catalana* 11:449–457.

Cajal SR (1896). Les épine collarérales des cellules du cerveau colorées au bleu de méthylène. *Rev Trimestr. Micrograf*. 1: 5–19.

Canal I, Acebes A, Ferrús A. (1998) Single neuron mosaics of the *Drosophila* gigas mutant project beyond normal targets and modify behaviour. *J Neurosci.* 18:999-1008.

Celotto AM, Graveley BR (2001) Alternative splicing of the *Drosophila* Dscam pre-mRNA is both temporally and spatially regulated. *Genetics* 159:599-608.

Certel SJ, Clyne PJ, Carlson JR, Johnson WA (2000) Regulation of central neuron synaptic targeting by the *Drosophila* POU protein, Acj6. *Development,* 127:2395-405.

Chen BE, Kondo M, Garnier A, Watson FL, Puettmann-Holgado R, et al. (2006) The molecular diversity of Dscam is functionally required for neuronal wiring specificity in *Drosophila*. *Cell* 125: 607-620.

Chiba A, Snow P, Keshishian H, Hotta Y (1995) Fasciclin III as a synaptic target recognition molecule in *Drosophila*. *Nature*, 374:166-8.

Chiba A, Keshishian H (1996) Neuronal pathfinding and recognition: roles of cell adhesion molecules. *Dev Biol*, 108: 424-32

Chih B, Gollan L, Scheiffele P. (2006) Alternative splicing controls selective trans-synaptic interactions of the neuroligin-neurexin complex. *Neuron*. 51:171-8.

Chotard C and Salecker I (2004) Neurons and glia: team players in axon guidance. *Trends in Neurosci* 27:655-661

Cloutier JF, Sahay A, Chang EC, Tessier-Lavigne M, Dulac C, Kolodkin AL, Ginty DD (2004) Differential requirements for semaphorin 3F and Slit-1 in axonal targeting, fasciculation, and segregation of olfactory sensory neuron projections. *J Neurosci*, 24:9087-96.

Corfas G, Dudai Y. (1989) Habituation and dishabituation of a cleaning reflex in normal and mutant *Drosophila*. *J Neurosci*. 9:56-62.

Corfas G, Dudai Y. (1990) Adaptation and fatigue of a mechanosensory neuron in wild-type *Drosophila* and in memory mutants. *J Neurosci.* 10:491-9.

Cvetkovska V, Hibbert AD, Emran F, Chen BE (2013) Overexpression of Down syndrome cell

adhesion molecule impairs precise synaptic targeting. *Nat Neurosci,* 16: 677-682

Darnell JC, Jensen KB, Jin P, Brown V, Warren ST, et al. (2001) Fragile X mental retardation protein targets G quartet mRNAs important for neuronal function. *Cell*, 107: 489-499.

Darnell JC, Mostovetsky O, Darnell RB (2005) FMRP RNA targets: identification and validation. *Genes Brain Behav*. 4:341-9

Darnell JC, Fraser CE, Mostovetsky O, Darnell RB (2009) Discrimination of common and unique RNA-binding activities among Fragile X mental retardation protein paralogs. *Hum Mol Genet*.18:3164-77.

Darnell JC, Van Driesche SJ, Zhang C, Hung KY, Mele A, Fraser CE, Stone EF, Chen C, Fak JJ, Chi SW, Licatalosi DD, Richter JD, Darnell RB (2011) FMRP stalls ribosomal translocation on mRNAs linked to synaptic function and autism. *Cell.*146:247-61.

de Wit J, Sylwestrak E, O'Sullivan ML, Otto S, Tiglio K, Savas JN, Yates 3rd JR, Comoletti D, Taylor P, Ghosh A (2009) LRRTM2 interacts with Neurexin1 and regulates excitatory synapse formation, *Neuron*, 64: 799–806

Didiot, MC, Tian Z, Schaeffer C, Subramanian M, Mandel JL, Moine H (2008) The G-quartet containing FMRP binding site in FMR1 mRNA is a potent exonic splicing enhancer. *Nucleic Acids Res* 36, 4902-4912

Dierssen M, Ramakers GJ (2006) Dendritic pathology in mental retardation: from molecular genetics to neurobiology.*Genes Brain Behav.* 5 Suppl 2:48-60

Dietzl G, Chen D, Schnorrer F, Su KC, Barinova Y, Fellner M, Gasser B, Kinsey K, Oppel S, Scheiblauer S, Couto A, Marra V, Keleman K, Dickson BJ. (2007) A genome-wide transgenic RNAi library for conditional gene inactivation in *Drosophila*. *Nature*, 448:151-6.

Dong Y, Taylor H, Dimopoulos G (2006) AgDscam, a Hypervariable Immunoglobulin Domain-Containing Receptor of the Anopheles gambiae Innate Immune System. *Plos Biol* 4: e229

Drabikowski K, Trzebiatowska A, Chiquet-Ehrismann R (2005) ten-1, an essential gene for germ cell development, epidermal morphogenesis, gonad migration, and neuronal pathfinding in *Caenorhabditis elegans*. *Dev. Biol.*, 282: 27–38

Elbashir SM, Harborth J, Lendeckel W, Yalcin A, Weber K, Tuschl T (2001) Duplexes of 21-nucleotide RNAs mediate RNA interference in cultured mammalian cells. *Nature* 411:494-8.

Esumi S, Kakazu N, Taguchi Y, Hirayama T, Sasaki A, Hirabayashi T, Koide T, Kitsukawa T, Hamada S, Yagi T. (2005) Monoallelic yet combinatorial expression of variable exons of the protocadherin-alpha gene cluster in single neurons. *Nat Genet.* 37:171-6

Evrony GD, Cai X, Lee E, Hills LB, Elhosary PC, Lehmann HS, Parker JJ, Atabay KD, Gilmore EC, Poduri A, Park PJ, Walsh CA (2012) Single-neuron sequencing analysis of L1 retrotransposition and somatic mutation in the human brain. *Cell*. 151:483-96.

Feng K, Zhou XH, Oohashi T, Morgelin M, Lustig A, Hirakawa S, Ninomiya Y, Engel J, Rauch U, Fassler R (2002)All four members of the Ten-m/Odz family of transmembrane proteins form dimers. *J Biol Chem*, 277: 26128–26135

Fire A, Xu S, Montgomery MK, Kostas SA, Driver SE, Mello CC (1998) Potent and specific genetic interference by double-stranded RNA in Caenorhabditis elegans. *Nature*, 391:806-11.

Fu YH, Kuhl DP, Pizzuti A, Pieretti M, Sutcliffe JS, Richards S, Verkerk AJ, Holden JJ, Fenwick RG Jr, Warren ST, et al. (1991) Variation of the CGG repeat at the fragile X site results in genetic instability: resolution of the Sherman paradox. *Cell*. 67:1047-58.

Fuerst PG, Koizumi A, Masland RH, Burgess RW. (2008) Neurite arborisation and mosaic spacing in the mouse retina require DSCAM. Nature 451:470-4.

Garcia-Garcia MJ, Ramain P, Simpson P, Modolell J (1999) Different contributions of pannier and wingless to the patterning of the dorsal mesothorax of *Drosophila*. *Development* 126: 3523-3532

Gho M, Bellaïche Y, Schweisguth F (1999) Revisiting the Drosophila microchaete lineage: a novel intrinsically asymmetric cell division generates a glial cell. *Development,* 126:3573-84.

Ghysen, A. (1980) The projection of sensory neurons in the central nervous system of *Drosophila*: choice of the appropriate pathway. *Dev Biol* 78, 521-541

Godement P, Vanselow J, Thanos S, Bonhoeffer F (1987) A study in developing visual systems with a new method of staining neurones and their processes in fixed tissue. *Development.* 101:697-713.

Goyret J, Pfaff M, Raguso RA, Kelber A (2008) Why do Manduca sexta feed from white flowers? Innate and learnt colour preferences in a hawkmoth. *Naturwissenschaften*, 95: 569–576

Graf ER, Zhang X, Jin SX, Linhoff MW, Craig AM (2004) Neurexins induce differentiation of GABA and glutamate postsynaptic specializations via neuroligins. *Cell*, 119:1013-1026

Green EW, Fedele G, Giorgini F, Kyriacou CP (2014) A *Drosophila* RNAi collection is subject to dominant phenotypic effects. *Nat Methods.*11:222-3

Grossman TR, Gamliel A, Wessells RJ, Taghli-Lamallem O, Jepsen K, Ocorr K, Korenberg JR, Peterson KL, Rosenfeld MG, Bodmer R, Bier E (2011) Over-expression of DSCAM and COL6A2 cooperatively generates congenital heart defects. *PLoS Genet*. 7:e1002344.

Gumbiner BM (1996) Cell adhesion: the molecular basis of tissue architecture and morphogenesis. *Cell*, 84: 345–357

Guruharsha, K. G. et al. (2011) A protein complex network of *Drosophila* melanogaster. *Cell* , 147:690-703

Haase G, Dessaud E, Garcès A, de Bovis B, Birling M, Filippi P, Schmalbruch H, Arber S, deLapeyrière O (2002) GDNF acts through PEA3 to regulate cell body positioning and muscle innervation of specific motor neuron pools. *Neuron*, 35: 893-905.

Hattori D, Chen Y, Matthews BJ, Salwinski L, Sabatti C, Grueber WB, Zipursky SL. (2009) Robust discrimination between self and non-self neurites requires thousands of Dscam1 isoforms. *Nature*. 461: 644-8

Hiesinger PR, Zhai RG, Zhou Y, Koh TW, Mehta SQ, Schulze KL, Cao Y, Verstreken P, Clandinin TR, Fischbach KF, Meinertzhagen IA, Bellen HJ (2006) Activity-independent prespecification of synaptic partners in the visual map of *Drosophila*. *Curr Biol*. 16:1835-43.

Hildmann T, Kong X, O'Brien J, Riesselman L, Christensen HM, Dagand E, Lehrach H, Yaspo ML (1999) A contiguous 3-Mb sequence-ready map in the S3-MX region on 21q22.2 based on high- throughput nonisotopic library screenings. *Genome Res*. 9:360-72.

Hilgers V, Lemke SB, Levine M (2012) ELAV mediates 3' UTR extension in the *Drosophila* nervous system.*Genes Dev*. 26:2259-64.

Hinz U, Giebel B, Campos-Ortega JA. (1994) The basic-helix-loop-helix domain of *Drosophila* lethal of scute protein is sufficient for proneural function and activates neurogenic genes. *Cell*. 76:77-87.

Hiromi Y, Chédotal A, Mitchell KJ, Manabe T, Fujisawa H (2007) Interactionsbetween plexin-

A2, plexin-A4, and semaphorin 6A control lamina-restricted projection of hippocampal mossy fibers. *Neuron*, 53: 535-47.

Hong W, Mosca TJ, Luo L (2012) Teneurins instruct synaptic partner matching in an olfactory map. *Nature*, 484:201-7.

Honig MG, Hume RI (1986) Fluorescent carbocyanine dyes allow living neurons of identified origin to be studied in long-term cultures.*J. Cell Biol.,* 103:171–187

Hubel DH, Wiesel TN (1962) Binocular interaction in striate cortex of kittens reared with artificial squint. *J Physiol* 160:106-154

Hubel DH, Wiesel TN (1970) The period of susceptibility to the physiological effects of unilateral eye closure in kittens. *J Physiol* 206: 419-436

Huber AB, Kolodkin AL, Ginty DD, Cloutier JF (2003) Signaling at the growth cone: ligand-receptor complexes and the control of axon growth and guidance. *Annu Rev Neurosci*.26:509-63

Hughes ME, Bortnick R, Tsubouchi A, Bäumer P, Kondo M, Uemura T, Schmucker D (2007) Homophilic Dscam interactions control complex dendrite morphogenesis. *Neuron*, 54: 417-27.

Hutvágner G, Zamore PD. (2002) RNAi: nature abhors a double-strand. Curr Opin Genet Dev.12:225-32

Ichtchenko K, Nguyen T, Südhof TC. (1996) Structures, alternative splicing, and neurexin binding of multiple neuroligins. *J Biol Chem*. 271:2676-82.

Inatani M, Irie F, Plump AS, Tessier-Lavigne M, Yamaguchi Y (2003) Mammalian brain morphogenesis and midline axon guidance require heparan sulfate.*Science*. 302:1044-6.

Jamain S, Quach H, Betancur C, Rastam M, Colineaux C, Gillberg IC, Soderstrom H, Giros B,

Leboyer M, Gillberg C et al. (2003) Mutations of the X-linked genes encoding neuroligins NLGN3 and NLGN4 are associated with autism. *Nat Genet,* 34: 27–29

Jefferis GS, Marin EC, Stocker RF, Luo L (2001) Target neuron prespecification in the olfactory map of *Drosophila*. *Nature*, 414 414: 204–208

Jin L, Han Z, Platisa J, Wooltorton JR, Cohen LB, Pieribone VA (2012) Single action potentials and subthreshold electrical events imaged in neurons with a fluorescent protein voltage probe. *Neuron*.75:779-85

Kamiguchi H (2007) The role of cell adhesion molecules in axon growth and guidance. *Adv Exp Med Biol*, 621: 95-103

Kaneko R, Kato H, Kawamura Y, Esumi S, Hirayama T, Hirabayashi T, Yagi T. (2006) Allelic gene regulation of Pcdh-alpha and Pcdh-gamma clusters involving both monoallelic and biallelic expression in single Purkinje cells. *J Biol Chem*. 281: 30551-60.

Karuppudurai T, Lin TY, Ting CY, Pursley R, Melnattur KV, Diao F, White BH, Macpherson LJ, Gallio M, Pohida T, Lee CH. (2014) A hard-wired glutamatergic circuit pools and relays UV signals to mediate spectral preference in *Drosophila*. *Neuron*. 81:603-15.

Katz LC (1993) Coordinate activity in retinal and cortical development. *Curr Opin Neurobiol*, 3:93-99

Katz LC, Shatz JC (1996) Synaptic activity and the construction of cortical circuits. *Science* 247:1133-8

Kaufmann WE, Moser HW (2000) Dendritic anomalies in disorders associated with mental retardation. *Cereb Cortex*. 10:981-91

Kays I, Cvetkovska V, Chen BE (2014) Structural and functional analysis of single sensory

neurons in *Drosophila* melanogaster using lipophilic dye labeling and behavior for hard-wired neural connectivity analysis. *Nature Protocols.* 9: 1-14.

Keleman K, Rajagopalan S, Cleppien D, Teis D, Paiha K, Huber LA, Technau GM, Dickson BJ (2002) Comm sorts robo to control axon guidance at the *Drosophila* midline. *Cell* 110: 415–27

Kennerdell JR, Carthew RW (1998) Use of dsRNA-mediated genetic interference to demonstrate that frizzled and frizzled 2 act in the wingless pathway. *Cell* 95:1017-26.

Kenzelmann D, Chiquet-Ehrismann R, Leachman NT, Tucker RP. (2008) Teneurin-1 is expressed in interconnected regions of the developing brain and is processed in vivo. *BMC Dev Biol*. 8:30

Kernan M, Zuker C. (1995) Genetic approaches to mechanosensory transduction. *Curr Opin Neurobiol*.5:443-8.

Kirkbride KC, Ray BN, Blobe GC. (2005) Cell-surface co-receptors: emerging roles in signaling and human disease. *Trends Biochem Sci*. 30:611-21

Ko J, Fuccillo MV, Malenka RC, Sudhof TC (2009) LRRTM2 functions as a neurexin ligand in promoting excitatory synapse formation, *Neuron*, 64 : 791–798

Kohmura N, Senzaki K, Hamada S, Kai N, Yasuda R, Watanabe M, Ishii H, Yasuda M, Mishina M, Yagi T (1998) Diversity revealed by a novel family of cadherins expressed in neurons at a synaptic complex.*Neuron.*20: 1137-51.

Kolb B, Whishaw IQ (1998) Brain plasticity and behavior. *Annu Rev Psychol*, 49:43-64

Komiyama T, Johnson WA, Luo L, Jefferis GS (2003) From lineage to wiring specificity. POU domain transcription factors control precise connections of *Drosophila* olfactory projection neurons. *Cell*, 112: 157-67.

Komiyama T, Carlson JR, Luo L (2004) Olfactory receptor neuron axon targeting: intrinsic transcriptional control and hierarchical interactions. *Nat Neurosci*. 7:819-25.

Komiyama T, Sweeney LB, Schuldiner O, Garcia KC, Luo L (2007) Graded expression of semaphorin-1a cell-autonomously directs dendritic targeting of olfactory projection neurons. *Cell*, 128:399-410.

Korenberg, JR, Chen XN, Schipper R, Sun Z, Gonsky R, Gerwehr S, Carpenter N, Daumer C, Dignan P, Disteche C, et al. (1994) Down syndrome phenotypes: the consequences of chromosomal imbalance. *Proc Natl Acad Sci U S A*, 91: 4997-5001

Kulkarni MM, Booker M, Silver SJ, Friedman A, Hong P, Perrimon N, Mathey-Prevot B (2006) Evidence of off-target effects associated with long dsRNAs in *Drosophila melanogaster* cell-based assays. *Nature Methods,* 3:833-838 Kurusu M, Cording A, Taniguchi M, Menon K, Suzuki E, Zinn K. (2008) A screen of cell-surface molecules identifies leucine-rich repeat proteins as key mediators of synaptic target selection. *Neuron.*59:972-85.

Laggerbauer B, Ostareck D, Keidel EM, Ostareck-Lederer A, Fischer U (2001) Evidence that fragile X mental retardation protein is a negative regulator of translation. *Hum Mol Genet,* 10: 329-338.

Lattermann M, Zierau A, Schulte C, Seidl S, Kuhlmann B, Hummel T (2007) Semaphorin-1a controls receptor neuron-specific axonal convergence in the primary olfactory center of *Drosophila. Neuron*, 53:169–84

Lauren J, Airaksinen MS, Saarma M, Timmusk T (2003) A novel gene family encoding leucine-rich repeat transmembrane proteins differentially expressed in the nervous system. *Genomics*, 81: 411–421

Leamey CA, Merlin S, Lattouf P, Sawatari A, Zhou X, Demel N, Glendining KA, Oohashi T, Sur M, Fässler R. (2007) Ten_m3 regulates eye-specific patterning in the mammalian visual pathway and is required for binocular vision. *PLoS Biol.* 5:e241.

Lee G, Foss M, Goodwin SF, Carlo T, Taylor BJ, Hall JC. (2000) Spatial, temporal,and sexually dimorphic expression patterns of the fruitless gene in the *Drosophila* central nervous system. *J Neurobiol*. 43:404-26.

Lee CH, Herman T, Clandinin TR, Lee R, Zipursky SL (2001) N-cadherin regulates target specificity in the *Drosophila* visual system. *Neuron*, 30: 437-50

Lee RC, Clandinin TR, Lee CH, Chen PL, Meinertzhagen IA, Zipursky SL (2003) The protocadherin Flamingo is required for axon target selection in the *Drosophila* visual system. *Nat Neurosci*, 6:557-63

Lefebvre JL, Kostadinov D, Chen WV, Maniatis T, Sanes JR. (2012) Protocadherins mediate dendritic self-avoidance in the mammalian nervous system. *Nature*.488: 517-21.

Lejeune J, Gautier M, Turpin R (1959) Les chromosomes humains en culture de tissus. *C R Acad Sci* 248:602–603

Li Z, Zhang Y, Ku L, Wilkinson KD, Warren ST, et al. (2001) The fragile X mental retardation protein inhibits translation via interacting with mRNA. *Nucleic Acids Res,* 29: 2276-2283.

Li W, Guan KL (2004) The Down syndrome cell adhesion molecule (DSCAM) interacts with and activates Pak. *J Biol Chem,* 279: 32824-31.

Li HL, Huang BS, Vishwasrao H, Sutedja N, Chen W, Jin I, Hawkins RD, Bailey CH, Kandel ER (2009) Dscam mediates remodeling of glutamate receptors in Aplysia during de novo and learning-related synapse formation. *Neuron,* 61:527-40

Li H, Bishop KM, O'Leary DD. (2006) Potential target genes of EMX2 include Odz/Ten-M and other gene families with implications for cortical patterning. *Mol Cell Neurosci.* 33:136-49

Lin JH, Saito T, Anderson DJ, Lance-Jones C, Jessell TM, Arber S (1998) Functionally related motor neuron pool and muscle sensory afferent subtypes defined by coordinate ETS gene expression. *Cell*, 95:393-407.

Livet J, Sigrist M, Stroebel S, De Paola V, Price SR, Henderson CE, Jessell TM, Arber S (2002) ETS gene Pea3 controls the central position and terminal arborization of specific motor neuron pools. *Neuron*, 35: 877-92.

Livet J, Weissman TA, Kang H, Draft RW, Lu J, Bennis RA, Sanes JR, Lichtman JW. (2007) Transgenic strategies for combinatorial expression of fluorescent proteins in the nervous system. *Nature*.450:56-62.

Ly A, Nikolaev A, Suresh G, Zheng Y, Tessier-Lavigne M, Stein E (2008) DSCAM is a netrin receptor that collaborates with DCC in mediating turning responses to netrin-1. *Cell*, 133: 1241-54.

Manoli DS, Meissner GW, Baker BS. (2006) Blueprints for behavior: genetic specification of neural circuitry for innate behaviors. *Trends Neurosci*.29: 444-51.

Margulies M et al. (2005) Genome sequencing in microfabricated high-density picolitre reactors. *Nature*. 437: 376-80.

Matthes DJ, Sink H, Kolodkin AL, Goodman CS (1995) Semaphorin II can function as a selective inhibitor of specific synaptic arborizations. *Cell*, 81: 631-9.

Matthews BJ, Kim ME, Flanagan JJ, Hattori D, Clemens JC, Zipursky SL, Grueber WB. (2007) Dendrite self-avoidance is controlled by Dscam. *Cell*.129:593-604.

Melzig J, Buchner S, Wiebel F, Wolf R, Burg M, Pak WL, Buchner E. (1996) Genetic depletion of histamine from the nervous system of *Drosophila* eliminates specific visual and mechanosensory behavior. *J Comp Physiol A*. 179:763-73.

Miller MR, Robinson KJ, Cleary MD, Doe CQ. (2009) TU-tagging: cell type-specific RNA isolation from intact complex tissues. *Nat Methods.*6:439-41.

Minet AD, Rubin BP, Tucker RP, Baumgartner S, Chiquet-Ehrismann R. (1999)Teneurin-1, a vertebrate homologue of the *Drosophila* pair-rule gene ten-m, is a neuronal protein with a novel type of heparin-binding domain. *J Cell Sci.* 112:2019-32.

Missler M, Südhof TC. (1998) Neurexins: three genes and 1001 products. *Trends Genet*.14:20-6

Mitchell KJ, Doyle JL, Serafini T, Kennedy TE, Tessier-Lavigne M, Goodman CS, Dickson BJ (1996) Genetic analysis of Netrin genes in *Drosophila*: Netrins guide CNS commissural axons and peripheral motor axons. *Neuron*, 17: 203-15.

Miyashiro KY, Beckel-Mitchener A, Purk TP, Becker KG, Barret T, et al. (2003) RNA cargoes associating with FMRP reveal deficits in cellular functioning in Fmr1 null mice. *Neuron,* 37: 417-431.

Monzo K, Papoulas O, Cantin GT, Wang Y, Yates JR 3rd, Sisson JC (2006) Fragile X mental retardation protein controls trailer hitch expression and cleavage furrow formation in *Drosophila* embryos. *Proc Natl Acad Sci U S A* 103, 18160-18165

Mosca TJ, Hong W, Dani VS, Favaloro V, Luo L (2012) Trans-synaptic Teneurin signalling in neuromuscular synapse organization and target choice. *Nature*. 484:237-41

Myers PZ, Bastiani MJ. (1993) Growth cone dynamics during the migration of an identified commissural growth cone. *J Neurosci.*13:127-43.

Nern A, Zhu Y, Zipursky SL. (2008)Local N-cadherin interactions mediate distinct steps in the

targeting of lamina neurons. *Neuron*, 58: 34-41.

Neufeld SQ, Hibbert AD, Chen BE (2011) Opposing roles of PlexinA and PlexinB in axonal branch and varicosity formation. *Molecular brain*, 4:15

Neves G, Zucker J, Daly M, Chess A. (2004) Stochastic yet biased expression of multiple Dscam splice variants by individual cells. *Nature Genetics*. 36: 240 - 246

Nguyen T, Südhof TC.(1997) Binding properties of neuroligin 1 and neurexin 1beta reveal function as heterophilic cell adhesion molecules. *J Biol Chem.* 272:26032-9.

Ni JQ, Liu LP, Binari R, Hardy R, Shim HS, Cavallaro A, Booker M, Pfeiffer BD, Markstein M, Wang H, Villalta C, Laverty TR, Perkins LA, Perrimon N. (2009) A *Drosophila* resource of transgenic RNAi lines for neurogenetics. *Genetics*.182:1089-100.

Nimchinsky EA, Oberlander AM, Svoboda K. (2001) Abnormal development of dendritic spines in FMR1 knock-out mice. *J Neurosci* 21: 5139-5146

Nose A, Takeichi M, Goodman CS. (1994) Ectopic expression of connectin reveals a repulsive function during growth cone guidance and synapse formation. Neuron, 13: 525-39.

Nunes SM, Ferralli J, Choi K, Brown-Luedi M, Minet AD, Chiquet-Ehrismann R (2005) The intracellular domain of teneurin-1 interacts with MBD1 and CAP/ponsin resulting in subcellular codistribution and translocation to the nuclear matrix. *Exp. Cell Res.*, 305: 122–132

Olesnicky EC, Killian DJ, Garcia E, Morton MC, Rathjen AR, Sola IE, Gavis ER. (2014) Extensive use of RNA-binding proteins in *Drosophila* sensory neuron morphogenesis. *G3 (Bethesda)*, 4:297-306

Oohashi T, Zhou XH, Feng K, Richter B, Mörgelin M, Perez MT, Su WD, Chiquet-Ehrismann

R, Rauch U, Fässler R. (1999) Mouse ten-m/Odz is a new family of dimeric type II transmembrane proteins expressed in many tissues. *J Cell Biol.*145:563-77.

Palka J, Witlock KE, Murray MA (1992) Guidepost cells. *Curr Opin Neurobiol* 2:48-54

Phillis RW, Bramlage AT, Wotus C, Whittaker A, Gramates LS, Seppala D, Farahanchi F, Caruccio P, Murphey RK. (1993) Isolation of mutations affecting neural circuitry required for grooming behavior in *Drosophila* melanogaster. *Genetics,* 133:581-92.

Pieretti M, Zhang FP, Fu YH, Warren ST, Oostra BA, Caskey CT, Nelson DL. (1991) Absence of expression of the FMR-1 gene in fragile X syndrome. *Cell,* 66:817-22.

Ragnarson B, Bengtsson L, Haegerstrand A. (1992) Labeling with fluorescent carbocyanine dyes of cultured endothelial and smooth muscle cells by growth in dye-containing medium. *Histochemistry.* 97:329-33.

Raj A, van den Bogaard P, Rifkin SA, van Oudenaarden A, Tyagi S.(2008) Imaging individual mRNA molecules using multiple singly labeled probes. Nat Methods. 5::877-9

Raj A, Rifkin SA, Andersen E, van Oudenaarden A. (2010) Variability in gene expression underlies incomplete penetrance. Nature. 463:913-8.

Ramsköld D, Luo S, Wang YC, Li R, Deng Q, Faridani OR, Daniels GA, Khrebtukova I, Loring JF, Laurent LC, Schroth GP, Sandberg R. (2012) Full-length mRNA-Seq from single-cell levels of RNA and individual circulating tumor cells. *Nat Biotechnol.* 30::777-82.

Reeve SP, Bassetto L, Genova GK, Kleyner Y, Leyssen M, Jackson FR, Hassan BA (2005) The *Drosophila* fragile X mental retardation protein controls actin dynamics by directly regulating profilin in the brain. *Curr Biol*.15:1156-63

Roegiers F, Younger-Shepherd S, Jan LY, Jan YN (2001) Two types of asymmetric divisions in the *Drosophila* sensory organ precursor cell lineage. *Nat Cell Biol.* 3:58-67.

Rolf B, Bastmeyer M, Schachner M, Bartsch U (2003) Pathfinding errors in corticospinal axons in neural cell adhesion molecule-deficient mice. *J Neurosci,* 22:8357-62

Rollmann SM, Yamamoto A, Goossens T, Zwarts L, Callaerts-Végh Z, Callaerts P, Norga K, Mackay TF, Anholt RR. (2007) The early developmental gene Semaphorin 5c contributes to olfactory behavior in adult *Drosophila*.*Genetics*.176:947-56.

Rowen L, Young J, Birditt B, Kaur A, Madan A, Philipps DL, Qin S, Minx P, Wilson RK, Hood L, Graveley BR. (2002) Analysis of the human neurexin genes: alternative splicing and the generation of protein diversity. *Genomics.*79:587-97

Rubin BP, Tucker RP, Martin D, Chiquet-Ehrismann R. (1999) Teneurins: a novel family of neuronal cell surface proteins in vertebrates, homologous to the *Drosophila* pair-rule gene product Ten-m. *Dev Biol*. 216:195-209.

Rubin BP, Tucker RP, Brown-Luedi M, Martin D, Chiquet-Ehrismann R. (2002) Teneurin 2 is expressed by the neurons of the thalamofugal visual system in situ and promotes homophilic cell-cell adhesion in vitro. *Development.* 129:4697-705.

Ryner LC, Goodwin SF, Castrillon DH, Anand A, Villella A, Baker BS, Hall JC, Taylor BJ, Wasserman SA. (1996) Control of male sexual behavior and sexual orientation in *Drosophila* by the fruitless gene. *Cell.* 87:1079-89.

Scheiffele P, Fan J, Choih J, Fetter R, Serafini T (2000) Neuroligin expressed in nonneuronal cells triggers presynaptic development in contacting axons. *Cell*, 101:657-669

Shinza-Kameda M, Takasu E, Sakurai K, Hayashi S, Nose A (2006) Regulation of layer-specific targeting by reciprocal expression of a cell adhesion molecule, capricious. *Neuron*, 49: 205-13.

Schmucker D, Clemens JC, Shu H, Worby CA, Xiao J, Muda M, Dixon JE, Zipursky SL. (2000)

Drosophila Dscam is an axon guidance receptor exhibiting extraordinary molecular diversity. *Cell,* 101:671-84.

Schmucker D, Flanagan JG. (2004) Generation of recognition diversity in the nervous system. *Neuron*.44:219-22.

Schmucker D. (2007) Molecular diversity of Dscam: recognition of molecular identity in neuronal wiring. *Nat Rev Neurosci*.8:915-20

Schmucker D, Chen B. (2009) Dscam and DSCAM: complex genes in simple animals, complex animals yet simple genes. *Genes Dev*. 23:147-56.

Schramm RD, Li S, Harris BS, Rounds RP, Burgess RW, Ytreberg FM, Fuerst PG (2012) A novel mouse Dscam mutation inhibits localization and shedding of DSCAM. *PLoS One*.7:e526-52.

Schreiner D, Weiner JA. (2010) Combinatorial homophilic interaction between gamma-protocadherin multimers greatly expands the molecular diversity of cell adhesion. *Proc Natl Acad Sci U S A* 107:14893-8.

Schroeder HW Jr, Cavacini L. (2010) Structure and function of immunoglobulins. *J Allergy Clin Immunol*. 125(2 Suppl 2):S41-52.

Semmelhack JL, Wang JW. (2009) Select *Drosophila* glomeruli mediate innate olfactory attraction and aversion. *Nature*. 459:218-23.

Senti KA, Usui T, Boucke K, Greber U, Uemura T, Dickson BJ (2003) Flamingo regulates R8 axon-axon and axon-target interactions in the *Drosophila* visual system. *Curr Biol*, 13: 828-32.

Shapiro L, Love J, Colman DR (2007) Adhesion molecules in the nervous system: structural insights into function and diversity. *Annu Rev Neurosci*, 30:451-74

Sharma S, Rao A. (2009) RNAi screening: tips and techniques. *Nat Immunol.*10:799-804

Shen K (2004) Molecular mechanisms of target specificity during synapse formation. *Current opinion in neurobiology*, 14: 83-88

Shen K, Scheiffele P (2010) Genetics and cell biology of building specific synaptic connectivity. *Annu Rev Neurosci*, 33:473-507.

Siddiqui TJ, Pancaroglu R, Kang Y, Rooyakkers A, Craig AM (2010) LRRTMs and neuroligins bind neurexins with a differential code to cooperate in glutamate synapse development. *J Neurosci*, 30: 7495–7506

Soba P, Zhu S, Emoto K, Younger S, Yang SJ, Yu HH, Lee T, Jan LY, Jan YN. (2007) *Drosophila* sensory neurons require Dscam for dendritic self-avoidance and proper dendritic field organization. *Neuron.* 54:403-16.

Song JY, Ichtchenko K, Südhof TC, Brose N. (1999) Neuroligin 1 is a postsynaptic cell-adhesion molecule of excitatory synapses. *Proc Natl Acad Sci U S A.* 96:1100-5.

Sperry RW (1963) Chemoaffinity in the Orderly Growth of Nerve Fiber Patterns and Connections. *Proc Natl Acad Sci U S A,* 50, 703–710.

Stetler A, Winograd C, Sayegh J, Cheever A, Patton E, Zhang X, Clarke S, Ceman S (2006) Identification and characterization of the methyl arginines in the fragile X mental retardation protein Fmrp. *Hum Mol Genet* 15:87-96

Stockinger P, Kvitsiani D, Rotkopf S, Tirián L, Dickson BJ. (2005) Neural circuitry that governs *Drosophila* male courtship behavior. *Cell*.121:795-807.

Suh GS, Ben-Tabou de Leon S, Tanimoto H, Fiala A, Benzer S, Anderson DJ. (2007) Light activation of an innate olfactory avoidance response in *Drosophila*. *Curr Biol.*17:905-8.

Suto F, Tsuboi M, Kamiya H, Mizuno H, Kiyama Y, Komai S, Shimizu M, Sanbo M, Yagi T,

Suzuki N, Numakawa T, Chou J, de Vega S, Mizuniwa C, Sekimoto K, Adachi N, Kunugi H, Arikawa-Hirasawa E, Yamada Y, Akazawa C (2014) Teneurin-4 promotes cellular protrusion formation and neurite outgrowth through focal adhesion kinase signaling. *FASEB J*. 28:1386-97.

Sweeney LB, Couto A, Chou YH, Berdnik D, Dickson BJ, Luo L, Komiyama T (2007) Temporal target restriction of olfactory receptor neurons by Semaphorin-1a/PlexinA-mediated axon-axon interactions. *Neuron*, 53:185-200.

Tabuchi K, Sudhof TC (2002) Structure and evolution of neurexin genes: insight into the mechanism of alternative splicing. *Genomics*. 79: 849-78

Takashima S, Becker LE, Armstrong DL, Chan F (1981) Abnormal neuronal development in the visual cortex of the human fetus and infant with down's syndrome. A quantitative and qualitative Golgi study. *Brain Res.* 225:1-21.

Terman JR, Kolodkin AL (2004) Nervy links protein kinase a to plexin-mediated semaphorin repulsion.*Science*.303:1204-7.

Tessier-Lavigne M and Goodman CS (1996) The molecular biology of axon guidance. *Science*, 274: 1123 -33

Thurm U. (1965) An insect mechanoreceptor. I. Fine structure and adequate stimulus. *Cold Spring Harb Symp Quant Biol.* 30:75-82

Tissot M, Gendre N, Hawken A, Storkulh KF, Stocker RF (1997) Larval chemosensory projections and invasion of adult afferents in the antennal lobe of *Drosophila*. J Neurobiol, 32:281-97

Treutlein B, Gokce O, Quake SR, Südhof TC. (2014) Cartography of neurexin alternative

splicing mapped by single-molecule long-read mRNA sequencing. *Proc Natl Acad Sci U S A.* 111: E1291-9.

Tucker RP, Chiquet-Ehrismann R (2006) Teneurins: a conserved family of transmembrane proteins involved in intercellular signaling during development. *Dev Biol.* 290:237-45.

Ushkaryov YA, Petrenko AG, Geppert M, Sudhof TC (1992) Neurexins: synaptic cell surface related to alpha-latrotoxin receptor and laminin. *Science*, 257: 50-6

Vandervorst P, Ghysen A. (1980) Genetic control of sensory connections in *Drosophila*. *Nature.* 286: 65-7.

Varoqueaux F, Jamain S, Brose N (2004) Neuroligin 2 is exclusively localized to inhibitory synapses. *Eur J Cell Biol*, 83: 449-56

Venken KJ, He Y, Hoskins RA, Bellen HJ. (2006) P[acman]: a BAC transgenic platform for targeted insertion of large DNA fragments in D. melanogaster. *Science.* 314:1747-51.

Verheij C, Bakker CE, de Graaff E, Keulemans J, Willemsen R, et al. (1993) Characterization and localization of the FMR-1 gene product associated with fragile X syndrome. *Nature* 363: 722-724.

Verkerk AJ, Pieretti M, Sutcliffe JS, Fu YH, Kuhl DP, et al. (1991) Identification of a gene (FMR-1) containing a CGG repeat coincident with a breakpoint cluster region exhibiting length variation in fragile X syndrome. *Cell,* 65: 905-914.

Vrieseling E, Arber S (2006) Target-induced transcriptional control of dendritic patterning and connectivity in motor neurons by the ETS gene Pea3. *Cell*, 127:1439-52.

Walker RG, Willingham AT, Zuker CS. (2000) A *Drosophila* mechanosensory transduction channel. *Science*. 287:2229-34.

Wang J, Ma X, Yang JS, Zheng X, Zugates CT, Lee CH, Lee T (2004)

Transmembrane/juxtamembrane domain-dependent Dscam distribution and function during mushroom body neuronal morphogenesis. *Neuron* 43:663-72.

Watson FL, Püttmann-Holgado R, Thomas F, Lamar DL, Hughes M, Kondo M, Rebel VI, Schmucker D (2005) Extensive diversity of Ig-superfamily proteins in the immune system of insects. *Science.*309:1874-8.

Watthanasurorot A, Jiravanichpaisal P, Liu H, Soderhall I, Soderhall K. (2011)Bacteria-Induced Dscam Isoforms of the Crustacean, Pacifastacus leniusculus. *PLoS pathogens,* 7: e1002062

Weiss MR (1997) Innate colour preferences and flexible colour learning in the pipevine swallowtail, *Anim. Behav*., 53: 1043–1052

Williams DW, Shepherd D. (2002) Persistent larval sensory neurones are required for the normal development of the adult sensory afferent projections in *Drosophila*. *Development,* 129: 617-624

Williams ME, de Wit J, Gnosh A (2010) Molecular mechanisms of synaptic specificity in developing neural circuits. *Neuron* 68: 9-18

Winberg ML, Mitchell KJ, Goodman CS (1998) Genetic analysis of the mechanisms controlling target selection: complementary and combinatorial functions of netrins, semaphorins, and IgCAMs. *Cell*, 93: 581-91.

Wine JJ (1984) The Structural Basis of an Innate Behavioural Pattern. *J Exp Biol* 112: 283-319.

Wojtowicz WM, Flanagan JJ, Millard SS, Zipursky SL, Clemens JC (2004) Alternative splicing of *Drosophila* Dscam generates axon guidance receptors that exhibit isoform-specific homophilic binding. *Cell*, 118:619-33.

Wu Q, Zhang T, Cheng JF, Kim Y, Grimwood J, Schmutz J, Dickson M, Noonan JP, Zhang MQ,

Myers RM, Maniatis T (2001) Comparative DNA sequence analysis of mouse and human protocadherin gene clusters. *Genome Res.* 11: 389-404.

Xu X et al. (2012) Single-cell exome sequencing reveals single-nucleotide mutation characteristics of a kidney tumor. *Cell*. 148:886-95.

Yamagata M, Weiner JA, Sanes JR (2002) Sidekicks: synapic adhesion molecules that promote lamina-specific connectivity in the retina. *Cell*, 110: 649-60

Yamagata M, Sanes JR and Weiner JA (2003) Synaptic adhesion molecules. *Curr Op Cell Biol*, 15(5):621-632

Yamagata M, Sanes JR. (2008) Dscam and Sidekick proteins direct lamina-specific synaptic connections in vertebrate retina. *Nature*. 451(7177):465-9.

Yamagata M, Sanes JR (2012) Expanding the Ig superamily code for laminar specificity in retina: expression and role of contactins. *J Neurosci*, 32: 14402-14

Yamaguchi S, Desplan C, Heisenberg M (2010) Contribution of photoreceptor subtypes to spectral wavelength preference in *Drosophila*. *Proc Natl Acad Sci U S A*, 107: 5634–5639

Yamakawa K, Huot YK, Haendelt MA, Hubert R, Chen XN, Lyons GE, Korenberg JR. Hum (1998) DSCAM: a novel member of the immunoglobulin superfamily maps in a Down syndrome region and is involved in the development of the nervous system. *Mol Genet.* 7:227-37.

Yu HH, Yang JS, Wang J, Huang Y, Lee T. (2009) Endodomain diversity in the *Drosophila* Dscam and its roles in neuronal morphogenesis. *J Neurosci*. 29:1904-14.

Zhan XL, Clemens JC, Neves G, Hattori D, Flanagan JJ, Hummel T, Vasconcelos ML, Chess A,

Zipursky SL (2004) Analysis of Dscam diversity in regulating axon guidance in *Drosophila* mushroom bodies. *Neuron*. 43:673-86

Zheng L, Michelson Y, Freger V, Avraham Z, Venken KJ, Bellen HJ, Justice MJ, Wides R. (2011) *Drosophila* Ten-m and filamin affect motor neuron growth cone guidance. *PLoS One*. 6:e22956.

Zhou XH, Brandau O, Feng K, Oohashi T, Ninomiya Y, Rauch U, Fässler R. (2003) The murine Ten-m/Odz genes show distinct but overlapping expression patterns during development and in adult brain. *Gene Expr Patterns*. 3:397-405.

Zill NS, Frazier SF, Macfarland DL, Fish SE (1993) Characterization of insect sense organs and optical clearing of whole-mount preparations using diI in fixed tissues. *J Exp Biol* 175, 299-303.

Zimmermann TS et al. (2002) RNAi-mediated gene silencing in non-human primates. *Nature*. 441:111-4

Zipursky SL, Sanes JR. (2010) Chemoaffinity revisited: dscams, protocadherins, and neural circuit assembly. *Cell.* 143:343-53